CHARACTERIZATION OF ELASTIN-CONTAINING POLYMER BLENDS USING SOLID-STATE NMR SPECTROSCOPY

A THESIS SUBMITTED TO THE GRADUATE DIVISION OF

THE UNIVERSITY OF HAWAIʻI AT MĀNOA IN PARTIAL FULFILLMENT OF THE

REQUIREMENTS FOR THE DEGREE OF

MASTER OF SCIENCE

IN

CHEMISTRY

DECEMBER 2017

By

David Tadashi Shinsato

Thesis Committee:

Kristin Kumashiro, Chairperson
Thomas Apple
Thomas Hemscheidt

DEDICATION

I dedicate this thesis to my family,

who have been a constant source of support, discernment,

counsel, encouragement, and inspiration my whole life.

ACKNOWLEDGMENTS

First, I would like to express my gratitude to my research advisor, Professor Kristin Kumashiro, for the many opportunities and support she has provided for me during my graduate studies.

I would also like to thank the other members of my thesis committee, Professor Thomas Apple and Professor Thomas Hemscheidt, for their helpful feedback and suggestions over the years.

I am grateful for the support and assistance provided by faculty members, staff, graduate students and other individuals who have helped me over the years. I am especially thankful for all the technical help and philosophical discussions provided by Dr. Kosuke Ohgo, and the camaraderie and encouragement from Dr. Chester Dabalos and Dr. Jhonsen Djajamuliadi. Also, I would like to thank Dr. Walter Niemczura for NMR support and hosting many gatherings.

I am also appreciative for the teaching assistantships provided by the Department of Chemistry. Whether it was teaching the lab classes, or working with undergraduate students in our research lab, I felt very privileged to be given the opportunity to help others in their own academic journeys.

Finally, I would like to thank all of the teachers and professors that I have encountered throughout my life. Your time and dedication to education helped to not only to mold my academic interests, but also helped me develop as a person.

ABSTRACT

Elastin is the polymeric extracellular matrix protein that confers the ability to stretch and recoil to vertebrate connective tissues such as blood vessels and skin. Due to its unique mechanical and biological properties, elastin is an attractive candidate for the fabrication of biomaterials. Therefore, elastin and elastin-based hybrid constructs have been the focus of investigation for their potential use in tissue engineering, repair, and replacement. Electrospinning is a common method for the production of nanofibers, and has been used to fabricate elastin-based materials. Most studies usually describe the morphological features, mechanical properties, and cell- and bio-compatibility of these materials, but very few focus on the molecular-level characterization.

Solid-state NMR (SSNMR) provides a means to probe the structure and dynamics of these solid biomaterials, and thus seems to be a promising tool for their molecular-level characterization. In this study, electrospun samples of elastin and two synthetic polymer-elastin blends were prepared. First, blends were compared to the individual components using one-dimensional SSNMR spectra. NMR relaxation experiments were then used to probe for molecular motions, inter-polymer interactions, and the effects of hydration on the system.

TABLE OF CONTENTS

LIST OF TABLES

LIST OF FIGURES

LIST OF ABBREVIATIONS AND SYMBOLS

^{13}C	carbon-13 isotope
1D	one-dimensional
3D	three-dimensional
^{1}H	proton
Å	Angstrom
Ala	alanine
Arg	arginine
Asx	asparagine or aspartic acid
B_0	external magnetic field
B_1	transverse magnetic field
BNL	bovine nuchal ligament
CNBr	cyanogen bromide
CO	carbonyl carbon
CP	cross-polarization
CSA	chemical shift anisotropy
Cys	cysteine
Cα	carbon-alpha
Cβ	carbon-beta
Cγ	carbon-gamma
Cδ	carbon-delta
Da	dalton
Des	desmosine
DCM	dichloromethane
DP	direct polarization

DTT	dithiothreitol
ECM	extracellular matrix
ELP	elastin-like peptide(s)
FID	free-induction decay
FT	Fourier transformation
FWHM	full-width at half maximum or linewidth
Gly	glycine
Glx	glutamine or glutamic acid
HCl	hydrochloric acid
HFIP	1,1,1,3,3,3-hexafluoro-2-propanol
His	histidine
Hyp	hydroxyproline
Hz	hertz
Ile	isoleucine
Ides	isodesmosine
K	Kelvin
kDa	kilodalton
kHz	kilohertz
L/G	Lorentzian/Gaussian
Leu	leucine
Lys	lysine
MAS	magic-angle spinning
Met	methionine
mg	milligram
MHz	megahertz
mL	milliliter
mm	millimeter

ms	millisecond
M	molarity
NMR	nuclear magnetic resonance
PCL	poly(caprolactone)
PGC	poliglecaprone
Phe	phenylalanine
ppm	parts per million
PVA	poly(vinyl alcohol)
PVAc	poly(vinyl acetate)
Pro	proline
rf	radio frequency
RMS	root mean square
RPTR	repeat per thousand residues
s	second
S/N	signal-to-noise ratio
Ser	serine
SDS-PAGE	sodium dodecyl sulfate-polyacrylamide gel electrophoresis
SPORT	Separating Peaks for Obtaining Relaxation Times (NMR processing method)
SSNMR	solid-state nuclear magnetic resonance
T	temperature
t	time
T_1	longitudinal spin-lattice relaxation time constant
$T_{1\rho}$	longitudinal spin-lattice relaxation time constant in the rotating frame
T_{CH}	carbon-proton cross-polarization time constant
Thr	threonine
TPPM	two-pulse phase modulation
Tyr	tyrosine

Val	valine
wt%	weight percent
°C	degree Celsius
$\Delta\delta$	difference in chemical shifts
γ	gyromagnetic ratio
µL	microliter
µs	microsecond
σ	standard deviation
τ	time delay

Chapter 1 – Introduction

1.1 Elastin and Tropoelastin

Elastin is the extracellular matrix protein that confers the ability to stretch and recoil to the elastic fiber in vertebrate tissues. This protein is found in abundance in tissues such as blood vessels and skin that require elasticity to function. Tropoelastin, the soluble, monomeric precursor to elastin, has a molecular weight of ~70 kDa, and is arranged in alternating hydrophobic and crosslinking domains.[1] The hydrophobic domains have an abundance or polypenta- and polyhexapeptide sequences, some of which are believed to give rise to the elastic properties of elastin.[1-3] In contrast, the crosslinking domains contain alanine-rich sequences and lysine residues that facilitate crosslink formation through the activity of lysyl oxidase.[1-2] Overall, elastin's composition is dominated by the presence of small, nonpolar amino acids, such as glycine, alanine, proline, and valine.

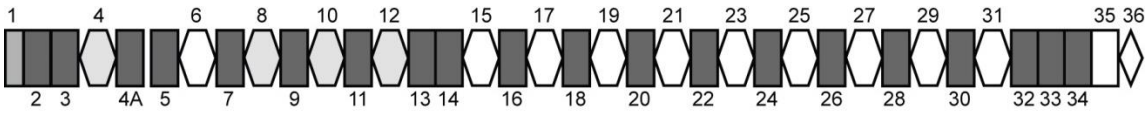

Figure 1.1. Representation of the alternating domains of tropoelastin. Hexagons represent the crosslinking domains, and the dark gray rectangles represent hydrophobic domains. The gray rectangle and white diamond represent the N- and C-terminus domains, respectively. (Figure is adapted from Vrhovski et al. 1998, reference 1).

Mature elastin is a highly crosslinked biopolymer that is insoluble in all but the most harsh conditions. Elastin's insolubility precludes the use of typical protein characterization techniques, such as X-ray crystallography and solution nuclear

magnetic resonance, NMR, spectroscopy. Therefore, solid-state NMR (SSNMR) spectroscopy has been successfully utilized to study this biopolymer. However, due to the complexity of this protein, a detailed three-dimensional structure and the specific structure-function relationship of elastin remain elusive and up to debate.

1.2 Elastin as a Biomaterial

Elastin is an attractive component for the production of biomaterials due to its elasticity, mechanical stability, biocompatibility, and self-assembly properties.[4-5] Furthermore, biomimetic scaffolds containing elastin emulate the physical features of the extraceulluar matrix while also providing the biological prompts needed for cell attachment and incorporation. Depending on the desired function and morphology of the material, elastin can be incorporated in many ways from both native and biosynthetic sources. Elastin from native (natural) sources include decellularized (elastin-rich) tissue, purified insoluble elastin, hydrolyzed elastin (e.g. α-, β-, κ- elastin), etc.[5-7] In contrast, examples of biosynthetic sources are recombinant tropoelastin, elastin-like polypeptides, and hybrid block polymers containing elastin-based sequences.[5]

In general, soluble elastins (tropoelastin, partially hydrolyzed elastin, some elastin-like polypeptides) are easier to manipulate, and therefore, more versatile than insoluble elastin for the purposes of material fabrication. Their solubility allows them to be used for various applications, such as solution casting, spinning, etc. These materials are being studied for their potential application in dermal replacement, wound healing, and vascular tissue fabrication.[5]

In addition to elastin-only constructs, elastin-containing hybrid materials have also been the subject of investigation. These hybrid materials, fabricated by blending elastin with other natural or synthetic polymers, are designed to create a product that has a set of properties that neither homopolymer has on its own. For example, polymers like poly(caprolactone), PCL, have been blended with elastin to produce materials that have the biocompatibility of elastin, with the mechanical stability of PCL.[5, 8] These blended samples have been studied for their application in vascular tissue engineering, where the construct is subjected to stresses that elastin-only materials would not be able to survive.

Two common forms of biomaterials are hydrogels and fibrous scaffolds. Hydrogels are highly absorbent materials comprised of cross-linked polymers. The fabrication of hydrogels usually consists of casting a polymer solution followed by crosslinking through chemical, irradiation, or physical methods. In contrast, fibrous scaffolds can be fabricated using a technique called electrospinning. The resulting non-woven, fibrous constructs have applications in many fields, including materials science, industrial production, etc. Specifically for electrospun elastin-based materials, the fiber-like morphology coupled with elastin's biocompatibility mimic the conditions of the extracellular matrix, ECM.

1.3 Electrospinning

Electrospinning is a process that creates solid micro- to nano-fibers through an electrically charged jet of polymer solution. This technique has potential applications in many different fields, such as materials science, biomaterials, etc., and is theoretically

applicable to any soluble polymer. Electrospinning is a contactless process that forms thinner fibers than comparable methods like mechanical drawing.[9] The resulting fibers have a high surface-to-volume ratio, and if conditions are optimal, sample properties such as fiber porosity and the shape and size of the collected material are controllable.[9]

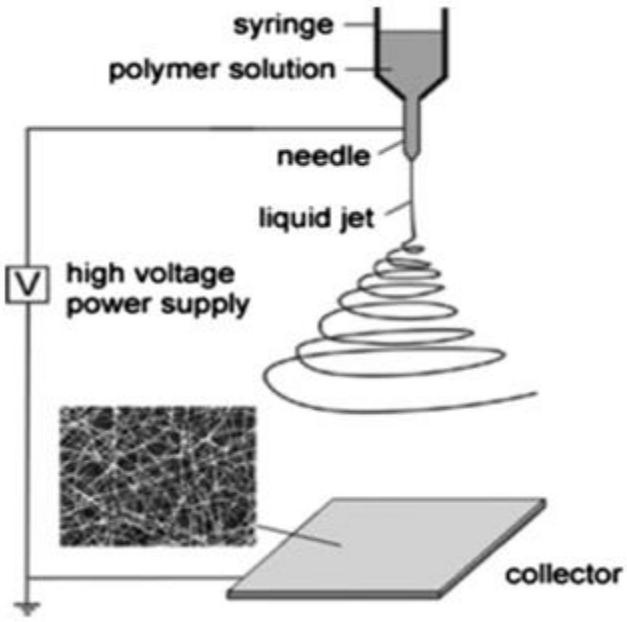

Figure 1.2. A basic electrospinning setup. Polymer solution is loaded into a syringe fitted with an electrically conducting needle. The high voltage supply is connected directly to the needle, and the grounded collector is held at a certain distance from the needle tip. (Figure adapted from Garg et al. 2011, reference 9)

The minimal electrospinning apparatus requires the following components: a high voltage power supply, an electrically conducting needle (for the polymer solution to pass through), a grounded collector held at a defined distance from the needle, and a polymer solution. The power supply should be adjustable and cover a range of at least 0 – 30 kV. The power supply is connected to the needle, and the electrospinning process

initiates once the electrostatic forces overcome the surface tension of the polymer solution. The solution is then ejected from the needle towards the grounded collector. If there is sufficient distance between the needle and collector, all of the solvent should evaporate, resulting in the deposition of dry, randomly oriented, non-woven, nanofibers. This process is continuous only as long as there is polymer solution to spin. The capacity of spinning can be increased by fitting a syringe to the charged needle and using a syringe pump to dispense the polymer solution at a controlled rate. Figure 1.2 illustrates a representation of a basic (minimal) electrospinning setup.

1.4 Characterization Methods

The characterization of electrospun elastin or elastin-containing hybrid materials usually focuses on the morphological features (such as fiber diameter and porosity), mechanical properties (such as tensile strength and water uptake), and cell compatibility to determine viability for tissue engineering. However, very few studies place an emphasis on the molecular-level characterization of these materials. Detailed information about the behavior of these types of biomaterials on the molecular scale should allow for directed tailoring of polymer blends for not only tissue engineering, but for other applications as well. Solid-state NMR spectroscopy provides a means to probe the structure and dynamics of samples in the solid state and thus seems to be a promising tool in the molecular-level characterization of these biomaterials.

1.4.1 High resolution SSNMR techniques

The NMR spectra of solids generally have broad lines due to restricted molecular motion, i.e., the absence of the rapid isotropic tumbling found in solution. Solid samples consist of many molecules with random orientations, and the nuclear spin interactions that affect SSNMR spectra, such as dipolar coupling and chemical shift anisotropy, CSA, are orientation-dependent. Therefore, in SSNMR spectroscopy, certain techniques that address these complications must be implemented to obtain high-resolution spectra.

The chemical shift anisotropy is the result of an asymmetrical distribution of electrons around the nucleus. In liquids, CSA is not apparent in the spectra due to the rapid molecular reorientation that occurs while in solution. For solids, this rapid molecular motion is mimicked by spinning the sample about and angle of 54.74° in relation to the external magnetic field. This technique is called Magic Angle Spinning, MAS, and provided the spinning rate is fast relative to the CSA, the anisotropy is averaged to zero, resulting in narrower lineshapes.

Dipole-dipole coupling arises from the interaction of the nuclear magnetic moments of two spins. In the case of proteins, it is common to observe line broadening due to the heteronuclear dipolar coupling between ^{13}C and ^{1}H. This effect is particularly problematic when observing dilute spins like ^{13}C (1.1% natural abundance). However, the interaction can be decoupled by applying high-power irradiation on the ^{1}H channel during acquisition. The method used in this study is called Two-Pulse Phase Modulation, or TPPM.[10]

1.4.2 Cross-Polarization with Magic Angle Spinning, CPMAS

NMR spectroscopy of ^{1}H and ^{13}C nuclei is widely used for the characterization of biological molecules and polymers. However, due to the low natural abundance of ^{13}C and the long relaxation times in solids, the signal-to-noise for ^{13}C spectra are poor compared to those of more abundant nuclei, like ^{1}H. This sensitivity issue can be partially addressed in solid samples by using cross polarization, CP.

This technique transfers the magnetization of abundant nuclei to more dilute spins, in this case specifically, from ^{1}H to ^{13}C. CP between different spin types can be achieved when the nuclei are irradiated with radiofrequency (rf) fields to achieve the Hartmann-Hahn condition:

$$\gamma^{H} B_1(^{1}H) = \gamma^{C} B_1(^{13}C) \qquad \text{(Eqn. 1.1)}$$

where γ^{H} and γ^{C} are the gyromagnetic ratios of ^{1}H and ^{13}C, respectively, and B_1 correspond to the rf field strengths on the respective channel. At this condition, the energy gaps between the ^{1}H and ^{13}C spin states are equal, i.e. the two types of nuclei precess at the same frequency in their respective rotating frames, allowing for the magnetization transfer.

The pulse sequence for a cross polarization with magic angle spinning (CPMAS) is illustrated in Figure 1.3. First, a 90° pulse brings the ^{1}H magnetization to the xy-plane. Then, a contact pulse is applied to the proton channel, resulting in the spin-lock field, $B_1(^{1}H)$. Simultaneously, the ^{13}C channel is irradiated to induce a $B_1(^{13}C)$ field of adequate power for the Hartmann-Hahn condition to be achieved. Finally, the signals are acquired on the ^{13}C channel while applying high-power ^{1}H decoupling using TPPM. All experiments in this study are based on CPMAS.

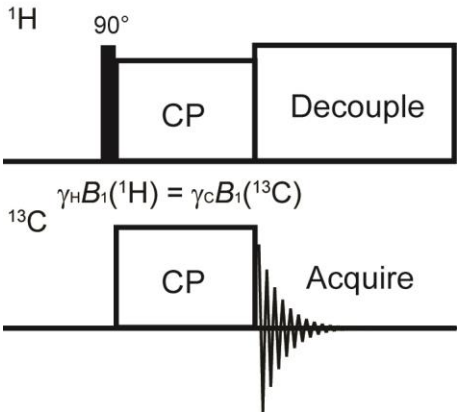

Figure 1.3. Pulse sequence for ^{13}C CPMAS. The ^{1}H to ^{13}C magnetization transfer is accomplished by CP with a Hartmann-Hahn matching condition of $\gamma^H B_1(^1H) = \gamma^C B_1(^{13}C)$. The signals are acquired during high-power ^{1}H decoupling using TPPM.

1.4.3 NMR relaxation experiments

Relaxation time measurements have been used for many years to characterize the molecular motions of solids. In general, relaxation is the process by which the system, or nuclei, returns to equilibrium from a non-equilibrium state. For NMR, this non-equilibrium state is achieved through a series or combination of rf pulses. Using a combination of different relaxation experiments, one is able to probe the dynamics at different time scales as well as the molecular-scale homogeneity of the target samples. Therefore, these types of experiments are powerful tools to investigate the molecular motions, interactions, and compatibility of polymer blends. This study will focus on three types of time constants: spin-lattice relaxation, T_1, spin-lattice relaxation in the rotating frame, $T_{1\rho}$, and the carbon-proton cross-polarization time constant, T_{CH}.

The ^{13}C spin-lattice relaxation times, T_1, were obtained by the method of Torchia (Figure 1.4A).[11] The sequence starts with CP, followed by a 90° pulse that rotates the ^{13}C magnetization to the –z-axis. Now aligned against the external magnetic field, B_0,

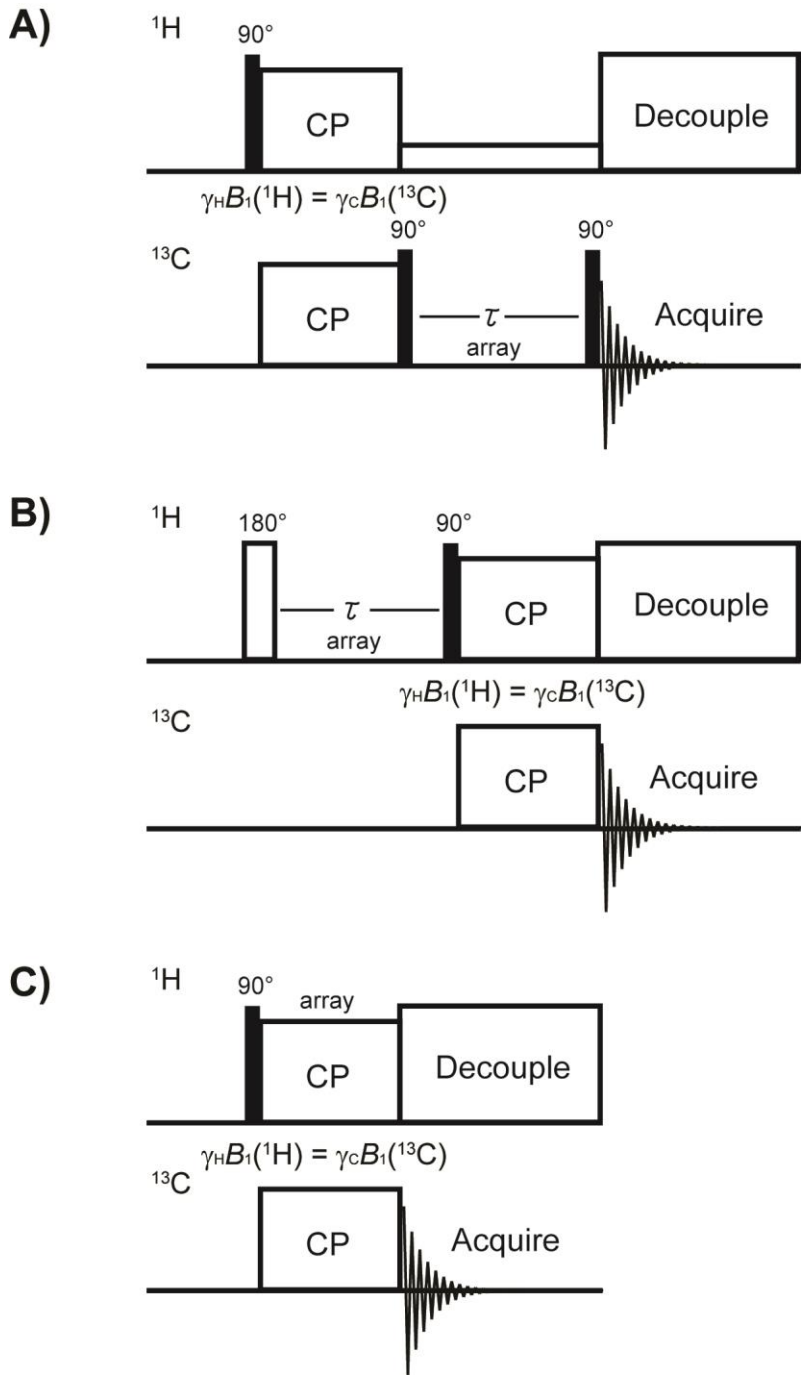

Figure 1.4. CP-based pulse sequences for NMR relaxation experiments. These pulse sequences were used to determine, (A) ^{13}C T_1 by the method of Torchia[11], (B) ^{1}H T_1 using inversion-recovery, (C) ^{1}H $T_{1\rho}$ and T_{CH} through an array of CP-contact times. Detection was on the ^{13}C channel for all experiments. The signals are acquired during high-power ^{1}H decoupling using TPPM[10].

the spins undergo longitudinal relaxation back towards their equilibrium state (alignment along the +z-axis). After variable delay times, τ, the extent of relaxation is monitored by applying another 90° pulse, bringing the magnetization back to the transverse plane before acquisition.

^{1}H T_1 values were determined by inversion recovery with indirect detection through resolved ^{13}C peaks (Figure 1.4B). An initial 180° pulse inverts the proton magnetization (aligned along the –z-axis). The ^{1}H's are allowed to relax (back towards the +z-axis) during the arrayed times, τ. A ^{1}H 90° pulse brings magnetization back to the transverse plane before CP to ^{13}C. The result is reflective of the proton spin-lattice relaxation, but, because the ^{1}H spectra for solids are typically very broad, indirect detection through ^{13}C is utilized to achieve higher spectral resolution.

The ^{1}H $T_{1\rho}$ and T_{CH} time constants were determined simultaneously by an arrayed CP contact-time experiment (Figure 1.4C). The buildup of magnetization during CP is due to T_{CH}, while the decay is governed by the ^{1}H and ^{13}C $T_{1\rho}$'s. For a given contact time, τ, the intensity, I(τ), can be described by:

$$I(\tau) = \frac{M_0\left[1-e^{-\left(1+\frac{T_{CH}}{T_{1\rho(H)}}-\frac{T_{CH}}{T_{1\rho(C)}}\right)}\right]e^{-\tau/T_{CH}}}{1+\frac{T_{CH}}{T_{1\rho(H)}}-\frac{T_{CH}}{T_{1\rho(C)}}} \qquad \text{(Eqn. 1.2)}$$

where τ is the arrayed CP contact time and M_0 is the initial peak intensity. $T_{1\rho}$ values are usually on the order of ms, while T_{CH}'s are usually in μs. Therefore, under the assumption that ^{13}C $T_{1\rho} >> T_{CH}$, the equation can be simplified to:

$$I(\tau) = \left(\frac{M_0}{T_{CH}}\right)\frac{e^{-\tau/T_{1\rho(H)}} - e^{-\tau/T_{CH}}}{1/T_{CH} - 1/T_{1\rho(H)}} \quad \text{(Eqn. 1.3)}$$

where I(τ) is expressed only in terms of ^{1}H $T_{1\rho}$ and T_{CH}. These values are also indirectly detected through ^{13}C.

In this study, NMR relaxation time constants ^{13}C T_1, ^{1}H T_1, ^{1}H $T_{1\rho}$ and T_{CH} were used to probe the motion of polymers at different time scales, and also for ^{1}H T_1 and $T_{1\rho}$, the molecular-scale homogeneity. All experiments were conducted under MAS conditions with high-power proton decoupling during acquisition.

1.5 Objectives and Scope of this Thesis

In this thesis, the preparation of electrospun blends of elastin and a synthetic polymer will be described, and SSNMR data will be presented. Furthermore, NMR relaxation experiments were used to investigate molecular motion (dynamics) in the prepared samples. This study aims to provide information on molecular-scale interactions between elastin and copolymers, as well as insights into the molecular-level behavior of elastin in the context of a biocompatible, ECM-analogous environment.

1.5.1 Chapter 2 – Elastin purification, electrospinning, and characterization

Elastin was purified from bovine nuchal ligament, BNL, using an autoclave-based scheme before subsequent partial hydrolysis using oxalic acid. The resulting soluble elastin was then electrospun and subsequently crosslinked using glutaraldehyde vapors to yield a water-stable product. These electrospun, crosslinked

elastin preparations were studied in their dry and hydrated states using SSNMR spectroscopy. Also, results from the amino acid analyses and SSNMR experiments will be presented and discussed in this chapter.

1.5.2 Chapter 3 – Characterization of poly(vinyl alcohol) and elastin electrospun blends using SSNMR spectroscopy

PVA-only and *PVA-elastin blend* samples were prepared by electrospinning from aqueous solutions. The *PVA-elastin blend* was crosslinked with glutaraldehyde, while the electrospun PVA was treated with water vapor to yield an insoluble product. Both samples were analyzed in their dry and hydrated states using SSNMR spectroscopy.

1.5.3 Chapter 4 – Characterization of poly(caprolactone) and elastin electrospun blends using SSNMR spectroscopy

PCL-only and *PCL-elastin blend* samples were prepared by electrospinning from HFIP only and HFIP-water solvent systems, respectively. PCL alone was not soluble in water so no further processing was necessary after electrospinning. The PCL-elastin blend was crosslinked with glutaraldehyde to stabilize in water. The *PCL- only* was analyzed only in the dry state, and the *PCL-elastin blend* sample was analyzed in their dry and hydrated states using SSNMR spectroscopy.

1.5.4 Chapter 5 – Summary and concluding remarks

This chapter summarizes the results of this study and highlights what is new to the field of elastin research.

1.6 References

1. Vrhovski, B.; Weiss, A. S., Biochemistry of tropoelastin. *European Journal of Biochemistry* **1998,** *258* (1), 1-18.
2. Kumashiro, K. K. In *Solid-state NMR studies of elastin and elastin peptides*, Springer: 2006; pp 89-95.
3. Ohgo, K.; Niemczura, W. P.; Ashida, J.; Okonogi, M.; Asakura, T.; Kumashiro, K. K., Heterogeneity in the conformation of valine in the elastin mimetic (LGGVG)(6) as shown by solid-state C-13 NMR spectroscopy. *Biomacromolecules* **2006,** *7* (12), 3306-3310.
4. Wise, S. G.; Yeo, G. C.; Hiob, M. A.; Rnjak-Kovacina, J.; Kaplan, D. L.; Ng, M. K. C.; Weiss, A. S., Tropoelastin: A versatile, bioactive assembly module. *Acta Biomaterialia* **2014,** *10* (4), 1532-1541.
5. Yeo, G. C.; Aghaei-Ghareh-Bolagh, B.; Brackenreg, E. P.; Hiob, M. A.; Lee, P.; Weiss, A. S., Fabricated Elastin. *Advanced Healthcare Materials* **2015,** *4* (16), 2530-2556.
6. Partridge, S. M.; Davis, H. F.; Adair, G. S., The chemistry of connective tissues. 2. Soluble proteins derived from partial hydrolysis of elastin. *Biochemical Journal* **1955,** *61* (1), 11-21.
7. Robert, L. H., William, *Elastin and Elastases*. CRC Press, Inc.: Boca Raton, Florida, 1989; Vol. 1.
8. Wise, S. G.; Byrom, M. J.; Waterhouse, A.; Bannon, P. G.; Ng, M. K. C.; Weiss, A. S., A multilayered synthetic human elastin/polycaprolactone hybrid vascular graft with tailored mechanical properties. *Acta Biomaterialia* **2011,** *7* (1), 295-303.
9. Garg, K.; Bowlin, G. L., Electrospinning jets and nanofibrous structures. *Biomicrofluidics* **2011,** *5* (1), 013403.
10. Bennett, A. E.; Rienstra, C. M.; Auger, M.; Lakshmi, K. V.; Griffin, R. G., Heteronuclear decoupling in rotating solids. *J. Chem. Phys.* **1995,** *103* (16), 6951-8.
11. Torchia, D. A., The measurement of proton-enhanced carbon-13 T1 values by a method which suppresses artifacts. *J. Magn. Reson.* **1978,** *30* (3), 613-16.

Chapter 2. Elastin purification, electrospinning, and characterization

2.1 Introduction

Elastin is an attractive candidate for the fabrication of biomaterials, due to its unique mechanical and biological properties. This protein provides the ability to stretch and recoil to vertebrate tissues and organs. Therefore, elastin is found in abundance in blood vessels, ligaments, lung, and skin, where elasticity is important for function. Over the years, there have been various methods proposed and implemented for the purification of elastin from native tissues.[1-5] Furthermore, partial hydrolysis after purification yields a soluble product that can be manipulated for the fabrication of biomaterials.[7,14-16]

Electrospinning is a common method for the production of nanofibers, which, in turn, can be used as ECM analogs or support substrates for cells. Many different types of electrospun constructs have been used as biomaterials, and specifically, elastin-based materials have been considered very attractive, due to elastin's unique mechanical and biological properties. Fabricated materials are only useful in physiological conditions, if they are stable in aqueous solutions for extended periods of time. Therefore, post-electrospinning crosslinking methods are usually required to stabilize the samples.

This chapter describes the preparation of electrospun, crosslinked elastin and the analysis that followed. First, the scheme used to purify elastin from bovine nuchal ligament tissue and the subsequent procedure to obtain a soluble elastin will be described. Both insoluble and soluble elastin preparations were assayed by amino acid analysis. Soluble elastin was used to fabricate electrospun samples that were

crosslinked with glutaraldehyde vapors. These electrospun, crosslinked elastin preparations were studied in their dry and hydrated states using SSNMR spectroscopy. Results from the amino acid analyses and SSNMR experiments will be presented and discussed in this chapter.

2.1.1 Purification of elastin from native tissues

Elastin present in native tissues is always found in association with other proteins, such as collagen, and therefore must be isolated from the other elastic fiber components prior to study. There have been many different isolation schemes proposed, but each need to be tailored to the organ or tissue source, as well as the specific application of the purified elastin. Most elastin purification procedures fall into one of three categories: acid or alkaline extraction, a multi-step sequential extraction, or purification by means of physical methods.

Acid- and alkaline-based extraction methods take advantage of the differences between elastin and collagen's susceptibility to acid or alkaline hydrolysis. Acid-based methods usually consist of treatment in either formic acid or trichloroacetic acid following defatting and salt-extraction of the source tissue.[1] Alkaline-based methods also start with defatting and salt-extraction steps, but are followed by treatment with sodium hydroxide.[2] For methods described above, repeated extractions are usually necessary before the desired product is obtained. In general, these procedures are considered to be relatively harsh treatments that show evidence of protein degradation.[3]

Purification methods by sequential extraction usually utilize enzyme digestion, chemical treatment, or a combination of both to isolate elastin. Typical proteases used

are trypsin, which removes non-elastin and non-collagen proteins, and bacterial collagenase, which removes polymeric collagen.[1] Repeated treatment with chemical mixtures of urea-mercaptoethanol or guanidinium chloride-dithiothreitol have also been utilized to remove microfibril components.[1] Similarly, buffered EDTA also removes non-elastin components as well as calcium salts.[1]. Treatment with cyanogen bromide, CNBr, in formic acid has also been used as a step in elastin purification.[4] CNBr cleaves peptide bonds at the C-terminus of methionine residues, and this method takes advantage of the lack of methionine in the primary amino acid sequence of elastin. Multi-step extraction procedures usually utilize a combination of these types of treatments, and are usually tailored to the needs of the research project.

The only example of purification of elastin by means of physical methods is an autoclave-based scheme described by Partridge et al.[5] This method focuses on removing the collagen components of the elastic tissue by a series of repeated autoclave-rinse cycles. Briefly, tissues are cut into small pieces, suspended in water, then autoclaved for 1 hour. The supernatant containing non-elastin proteins such as gelatin (the denatured form of collagen) is then removed, and the remaining insoluble portions are rinsed with clean water before each subsequent autoclaving run. Advantages of this procedure include the fact that it avoids the use of chemicals and harsh acid- or alkaline-treatments, and the sample capacity is essentially only restricted by the size of one's autoclave. An autoclave-based purification scheme was chosen for the purposes of this study, because it can accommodate large sample sizes (gram-scale), and it does not produce any hazardous chemical waste.

2.1.2 Partial hydrolysis of elastin

Partial hydrolysis of elastin using different methods has been traditionally employed to obtain a soluble product that is easier to analyze than native, insoluble elastin.[1, 5] Two common methods to solubilize elastin utilize oxalic acid (α- and β- elastin) or a potassium hydroxide-ethanol aqueous solution (κ-elastin). Both preparations yield a heterogeneous mixture of partially cross-linked peptides with a wide range of molecular weights.[6] The first method produces two distinct protein components with different physical properties and mean molecular weights (α-elastin = 60,000-84,000 Da and β-elastin = 5,500 Da).[7] The second method yields a soluble elastin with mixture of molecular weights up to 70,000 Da, but with a large portion under 50,000 Da.[1, 8]

Products of both oxalic acid- and potassium hydroxide-based methods have been used as models to study elastin. Both types contain similar amino acid compositions to mature elastin (including the presence of crosslinks, desmosine and isodesmosine)[9-10], and have the ability to coacervate [11]. In more recent years, soluble elastin has also been used for the creation of elastin-based biomaterials. α-elastin has previously been used for electrospinning,[12] whereas κ-elastin has not. Although not investigated thoroughly, perhaps the higher average molecular weight of α-elastin allows for better electrospinning conditions than the κ-elastin with a lower average molecular weight. Therefore, for this study, soluble elastin from the oxalic acid treatment was used for electrospinning purposes.

2.1.3 Electrospinning of elastin

Electrospinning has been successfully used to fabricate materials from solutions

of tropoelastin[13-14] and soluble elastin[14-16]. A common solvent used to dissolve elastin is 1,1,1,3,3,3-hexafluoro-2-propanol, HFIP. These materials were subsequently crosslinked and preconditioned before use as cell scaffolds. Elastin retains its biological activity after the electrospinning process, evident by the positive growth and proliferation of cells on these elastin-based scaffolds.[12-13,16] Proposed applications for elastin-based, electrospun biomaterials include use as a dermal replacement and vascular scaffolds.[12] The characterization of these materials usually focuses on the morphological features (such as fiber diameter and porosity), mechanical properties (such as tensile strength and water uptake), and cell compatability to determine viability for tissue engineering. To complement methods that focus on macroscale properties, SSNMR spectroscopy can be used for the molecular-level characterization of these materials.

2.1.4 Crosslinking methods

Crosslinking is an important step in the process of fabricating elastin-based, electrospun biomaterials. Without crosslinking, the electrospun protein will dissolve in aqueous media, rendering it unfit for use as a biomaterial. There have been many chemical crosslinking reagents used to treat elastin-based samples, with common examples being glutaraldehyde, genepin, and hexamethylene diisocyanate, HMDI.[12] These three crosslinking methods involve post-electrospinning sample incubation in vapors (glutaraldehyde), or an ethanol/water solvent system containing the crosslinking reagent (genepin and HMDI). For this study, crosslinking in glutaraldehyde vapors was chosen for its relatively simple procedure, low cost, ease of acquisition, and its general acceptance as a good choice as a crosslinker for electrospun fibers.[17]

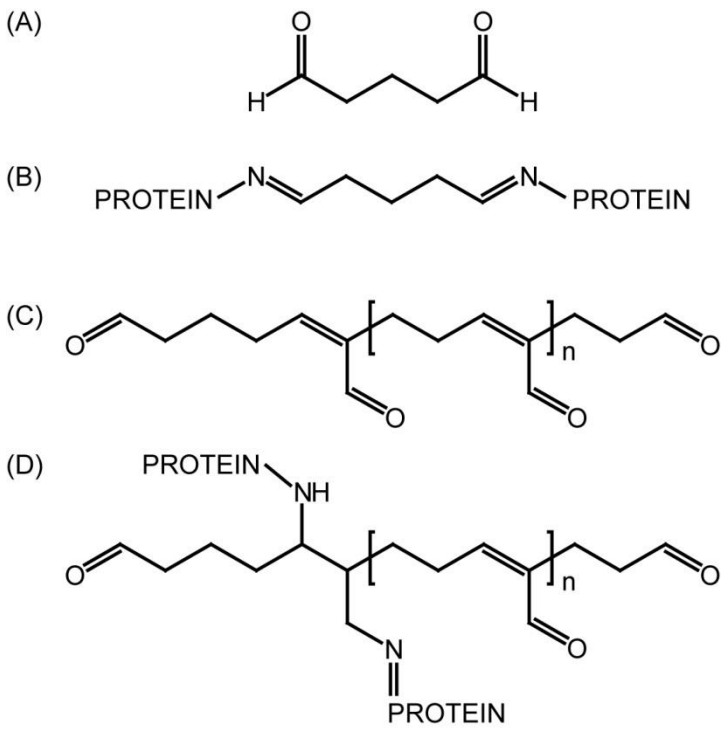

Figure 2.1. Proposed products of glutaraldehyde crosslinking with lysine residues. (A) The structure of monomeric glutaraldehyde, (B) Schiff base formation obtained by crosslinking of lysine residues from two protein molecules by monomeric glutaraldehyde, (C) the structure of polymeric glutaraldehyde, (D) suggested end product obtained from reaction between polymeric glutaraldehyde and lysine residues from the crosslinked proteins. (Figure adapted from Wine et al. 2007, reference 16)

Glutaraldehyde has been used for many years as a protein crosslinking reagent in various applications, including sample fixation for electron microscopy, immobilization of enzymes and whole cells, protein crystal stabilization[18], as well as the aforementioned use with electrospun protein fibers.[12, 17] Despite its widespread use, the detailed mechanism for chemical crosslinking using glutaraldehyde is not completely understood.[18] While it has been proposed that glutaraldehyde has the ability to react with

several functional groups in proteins, its effects as a crosslinker is thought to be dominated by reactions with the ε-amino groups of lysine residues.[18] In the simplest case, monomeric glutaraldehyde is thought to form a Schiff base at each aldehyde group with a lysine reside of a protein (Figure 2B). Possible crosslinking products have also been suggested for the reaction of proteins with polymeric glutaraldehyde (Figure 2D). Upon crosslinking using glutaraldehyde, protein scaffolds have been shown to be stabilized for extended periods of time.[12, 17]

2.2. Materials and Methods

2.2.1 Materials

The 1,1,1,3,3,3-hexafluoro-2-propanol, HFIP, (>99.0%) was purchased from Tokyo Chemical Industry (Tokyo, Japan). Glutaraldehyde solution (Grade II, 25% in H_2O) and dialysis tubing (cellulose, 25-mm average flat diameter, molecular weight cut off = 14,000) were purchased from Sigma Aldrich (Missouri, USA). Syringes (polypropylene, 1-mL slip-tip disposable tuberculin syringe) and needles (stainless steel, 18 G, 1.2 mm x 40 mm) from Becton, Dickinson and Company (New Jersey, USA) were used for electrospinning. Unless otherwise stated, Milli-Q ultrapure water was used for all instances where water was necessary.

2.2.2 Purification of insoluble elastin from bovine nuchal ligament

Elastin was purified from bovine nuchal ligament, BNL, using an adapted autoclaving method.[5, 15] BNL tissue was minced to pieces around 1 mm in diameter and

suspended in a 10 wt% NaCl aqueous solution for 24 h at 4 °C. The NaCl solution was then drained, and the sample was rinsed and then suspended in water before autoclaving for 1 h at 121 °C. Supernatant was removed, and the remaining solids were rinsed again with water. The autoclaving and subsequent rinsing with water were repeated until a negative Biuret test was obtained for the supernatant (no detectable protein in solution). Five to seven autoclave-rinse cycles were typically needed. The insoluble material was then maintained in 90 wt% ethanol for at least 10 h before drying under vacuum. The ethanol incubation aided in the drying process by partially dehydrating the insoluble pieces before vacuum drying. Particle size was broken down further using a blender, followed by two more autoclave-rinse cycles. Finally, the resulting solids were once more suspended in 90 wt% ethanol for 10 h before drying over vacuum. The result of this procedure was a dry, purified, insoluble elastin.

This sample was assayed by amino acid analysis (SPARC Biocentre, The Hospital for Sick Children, Toronto, Canada). The facility uses the Waters Pico-Tag System for analysis which involves hydrolysis, pre-column derivatization of the hydrolysates, followed by reverse-phase HPLC for separation. In addition to commonly screened amino acids, the SPARC Biocentre facility provides the estimated amounts desmosine and isodesmosine.[27]

2.2.3 Solubilization of insoluble elastin from BNL

Purified elastin from BNL was solubilized by a series of extractions with oxalic acid.[7] Insoluble elastin from section 2.2.2 was suspended in aqueous 0.25 M oxalic acid and maintained at 100 °C for 1 h. The mixture was then rapidly cooled over ice and

subsequently centrifuged at 4 °C for usually 30 to 45 min. Centrifugation time was extended if the insoluble material was not sufficiently pelleted. The supernatant was collected and stored at 4 °C. The extraction and collection procedure was repeated with all remaining insoluble material until complete dissolution. The typical initial mixture ratio was ~ 4.5 mL of oxalic acid to 1 g of dry insoluble elastin, and ~ 3 mL oxalic acid was added to the insoluble material for subsequent extractions. The procedure would typically need to be repeated around ten times for complete solubilization. The resulting solutions were dialyzed against deionized water to remove all oxalic acid before drying by lyophilization. The final product was a dry, soluble elastin, suitable for electrospinning. This sample was also assayed by amino acid analysis (SPARC Biocentre, The Hospital for Sick Children, Toronto, Canada).

2.2.4 Electrospinning of soluble elastin and subsequent crosslinking

Solutions were prepared by dissolving soluble elastin in a HFIP/water (9:1 by volume) solvent system, typically to volumes of 0.5 to 1 mL with concentrations of 10-12 wt%. A syringe was filled with the soluble elastin solution, fitted with a blunt steel needle, and connected to a syringe pump (NE-300 Just Infusion Syringe Pump, New Era Pump Systems, New York, USA). The solution was pumped through the syringe at constant speed between 20-30 µL/min. A rectangular aluminum collector plate was placed at a distance of 10 cm from the needle tip in a perpendicular orientation to the syringe. The needle was connected to a positive high voltage power supply, set at about 17 kV (ES30P-10W/DAM HV power supply, Gamma High Voltage Research, Florida, USA). The syringe pump, power source, and collector plate were all externally grounded.

Electrospun material was subsequently crosslinked by glutaraldehyde vapors. Samples were incubated for at least 24 h in a closed, 250-mL glass container containing about 7 mL of glutaraldehyde solution in a 10-mL beaker. Crosslinked material was then rinsed with water to hydrate and remove any remaining soluble portions. The samples were then either directly used (hydrated) or lyophilized (dry) for NMR analysis. Electrospun samples were also collected for observation under microscope (12-560-45 Microscope, Fisher Scientific, Massachusetts, USA).

2.2.5 NMR methods and processing

NMR experiments were conducted on an Agilent DD2 NMR spectrometer (Agilent Technologies, California, USA) equipped with an 89 mm Oxford wide-bore superconducting magnet with a proton resonance frequency of 399.976 MHz. ^{13}C NMR spectra were acquired using a 4.0-mm triple resonance (HXY) T3 MAS probe (ChemMagnetics/Varian NMR, Colorado, USA). Elastin samples were packed into 4.0 mm rotors with typical sample weights of 20-30 mg for dry and 50-60 mg for hydrated preparations. The hydration level was maintained with custom-machined Kel-F spacers (Revolution NMR, Fort Collins, Colorado, USA) fitted with fluorosilicone micro o-rings (Apple Rubber Products, New York, USA). Data for the dry and hydrated samples were acquired at 37 °C and -20 °C.

All SSNMR experiments were CPMAS-based, including 1D CPMAS and determination of the time constants ^{13}C T_1, ^{1}H T_1, ^{1}H $T_{1\rho}$ and T_{CH}. Typically for CPMAS, a 3.8 - 4.6 μs ^{1}H 90° pulse was followed by a 1-ms contact time with a 5-s recycle delay (6-s recycle delay for NMR relaxation measurements). The ^{1}H to ^{13}C magnetization

transfer was accomplished by CP with a Hartmann-Hahn matching condition of $\gamma^H B_1{}^H/2\pi = \gamma^C B_1{}^C/2\pi \sim 50$ kHz. ^{1}H TPPM decoupling[19] was applied during acquisition with $\gamma^H B_1/2\pi \sim 50$ kHz. The spinning speed used in MAS experiments was 8 kHz. Chemical shifts are referenced to the tetramethylsilane scale, using hexamethylbenzene as an external standard ($\delta(^{13}CH_3) = 17.0$ ppm) at room temperature.

^{13}C T_1 measurements were made using the method of Torchia.[20] Briefly, CP was followed by a 4.5 μs ^{13}C 90° pulse, arrayed delay times τ, a second ^{13}C 90° pulse, and finally acquisition with TPPM decoupling. Typical τ times ranged from 0.1 to 20 s. To obtain the relaxation rate constant, ^{13}C peak intensities were fit using single-exponential decay functions (Equation 2.1).

$$I(\tau) = A * e^{-\frac{-\tau}{T_1}} \qquad \text{(Eqn. 2.1)}$$

where τ is the delay time and A is the amplitude.

^{1}H T_1 values were indirectly determined from well-resolved ^{13}C signals from CPMAS following a ^{1}H inversion recovery pulse sequence. Briefly, a 9.2 μs ^{1}H 180° pulse is followed by an array of τ delays (typically 0 to 10 s), a ^{1}H 90° pulse, CP, and finally acquisition with proton decoupling. The ^{1}H T_1 constants were determined by fitting to the equation:

$$I(\tau) = M_0[1 - 2e^{-\frac{\tau}{T_1}}] \qquad \text{(Eqn. 2.2)}$$

where τ is the delay following the initial ^{1}H 180° pulse and M_0 denotes the initial peak intensity.[21]

T_{CH} and ^{1}H $T_{1\rho}$ were obtained from arrayed CP contact time experiments. The pulse sequence was identical to the one used for CPMAS experiments, with CP contact

times typically arrayed from 0.05 to 20 ms. Time constants T_{CH} and ^{1}H $T_{1\rho}$ were determined by fitting to the equation[22]:

$$I(\tau) = \left(\frac{M_0}{T_{CH}}\right)\frac{e^{-\tau/T_{1\rho(H)}} - e^{-\tau/T_{CH}}}{1/T_{CH} - 1/T_{1\rho(H)}} \qquad \text{(Eqn. 2.3)}$$

where τ is the arrayed CP contact time and M_0 is the initial peak intensity. [22]

Relaxation time constants ^{13}C T_1, ^{1}H T_1, ^{1}H $T_{1\rho}$ and T_{CH} were determined using a '3D-fitting' algorithm developed in our lab.[32] Each NMR relaxation data set consists of an array of 1D spectra corresponding to different delay times, τ. One of the most common methods of analyzing experimental relaxation data has three independent steps: obtain peak intensities at a certain chemical shift from each array slice, plot the intensity as a function of time, and then fit to a model describing the decay or build-up of intensity to determine the relaxation time constant. This type of analysis does not provide an accurate determination of time constants when there are overlapping signals present. In contrast, the 3D-fitting procedure incorporates peak separation to address issues with spectral overlap.

As part of the analysis, spectra were deconvolved to separate overlapping signals and obtain the following parameters for each peak: chemical shift, peak amplitude, width, and the fraction of Lorentzian character, α. Initial estimates of these four parameters were obtained through deconvolution of the time point with highest intensity (ex. τ = 0.1 s for the ^{13}C T_1 experiments). Depending on the sample, the peaks were considered as pure Lorentzian (α = 1), pure Gaussian (α = 0), or a linear combination of a Lorentzian and a Gaussian function, *F*:

$$F(\delta;\delta_i,\mathrm{w}_i,\alpha)=(\alpha)\left[\left(\frac{\delta-\delta_\mathrm{i}}{\mathrm{w_i}}\right)^2+1\right]^{-1}+(1-\alpha)\left[\mathrm{e}^{\left(-\frac{-4\ln 2}{\mathrm{w_i}^2}(\delta-\delta_\mathrm{i})^2\right)}\right] \quad \text{(Eqn. 2.4)}$$

where α = fraction Lorentzian, 1 - α = fraction Gaussian, and δ_i and w_i are the peak position and line width, respectively, of the i^{th} component. *F* yields the sum of a Lorentzian lineshape with height = α, and a Gaussian lineshape with height = 1 - α, therefore, the height at the center of the overall lineshape is 1.

For comparison, the SPORT-NMR method[31] also incorporates peak separation into its algorithm to determine NMR relaxation times. Briefly, the spectrum at each time point is independently deconvolved, the resulting intensities are plotted against time, and finally, the curve is fit to the desired model. However, the 3D-fitting algorithm utilized in this study differs from SPORT, because the peaks and time constants are fit simultaneously.

For 3D-fitting, spectral fitting and time constant optimization are simultaneously executed. The relaxation data is considered as a 3D object (S) defined by a function of the chemical shift (δ) and delay time (τ):

$$S^{fit}(\delta,\tau)=\sum_i \mathrm{a}_i * F(\delta;\delta_i,\mathrm{w}_i,\%\mathrm{G/L}) * I(\tau;T_{\mathrm{xi}}) \qquad \text{(Eqn. 2.5)}$$

where a_i is the amplitude of the i^{th} component and $I(\tau;T_{xi})$ corresponds the appropriate model of intensity decay, build-up, or build-up then decay (Equation 2.1, 2,2, or 2.3). T_{xi} is the NMR time constant(s) of the i^{th} component with x = 1, 1ρ, or CH. Then, the difference between the experimentally observed (S^{obs}) and fitted 3D (S^{fit}) surfaces is minimized,

$$\min \| S^{obs}(\delta,\tau)-S^{fit}(\delta,\tau)\| \qquad \text{(Eqn. 2.5)}$$

to obtain a_i and T_{xi} simultaneously. Time constant T_{xi} = T_{1i} for the cases of Eqn. 2.1 and

2.2, and $T_{xi} = T_{CH\,i}$ and $T_{1\rho i}$ for the case of Eqn. 2.3. Chemical shifts, linewidths, and fraction Lorentzian character were held constant for this application of the 3D-fitting procedure.

Monte-Carlo simulations were used to estimate the error of fitting. First, an ideal 3D surface was prepared based on the estimated parameters from 3D-fitting (described above). Then, synthetic, random noise with the same RMS level as the experimental spectra was added to the surface. This procedure was repeated 100 times per relaxation experiment to produce simulated data with different sets of random noise. Monte-Carlo simulations of the 3D-fitting were then performed on these data, and the standard deviation (σ) for each ^{13}C T_1, ^{1}H T_1, ^{1}H $T_{1\rho}$ or T_{CH} value was calculated from the results. Measured time constants are reported with (+/-) values that indicate 2*σ, estimated by this procedure.

MATLAB (R2016b, MathWorks Inc., Massachusetts, USA) programs were utilized for the processing of NMR spectra, deconvolution, and the 3D-fitting analysis. Non-linear fitting was achieved by the Levenberg-Maquardt algorithm[29-30] using the MATLAB-function ”lsqcurvefit” in the Optimization Toolbox. MestReNova software (version 9, Mestrelab Research, Santiago de Compostela, Spain) was used for the processing of 1D spectra, and preliminary analysis.

2.3 Results and Discussion

2.3.1 Prepared samples have amino acid compositions typical of elastin

Autoclave-purification followed by oxalic acid treatment yields a soluble sample that is suitable for electrospinning, with an amino acid composition comparable to mature elastin. The published autoclave-based scheme was customized to our source BNL tissue and instrumentation to obtain a purified elastin (section 2.2.2). Initial attempts to utilize published protocol[15] without changes resulted in an impure product, based on the results of Biuret tests and SDS-PAGE (sodium dodecyl sulfate-polyacrylamide gel electrophoresis). For completely pure elastin, a Biuret test on the supernatant after autoclaving should be negative (indicating no soluble protein), and SDS-PAGE of the insoluble product should not show any bands (elastin is resistant to the routine DTT or mercaptoethanol treatment before SDS-PAGE). However, results of both assays indicated that there were impurities remaining in the sample. To address these issues, additional autoclave-rinse cycles were repeated until a negative Biuret test was obtained. Additionally, after the first purification cycle, samples were further processed in a blender to break down particle size before more autoclave-rinse cycles to ensure removal of non-elastin components. Although not explicitly tested, possible variables may include the autoclave size and cycle pattern, specific solution/water-to-sample ratios, consistency of the source tissue, etc. Once a purified elastin was obtained, the sample needed to be solubilized in preparation for electrospinning.

After purification, the elastin is solubilized in preparation for electrospinning. The partial hydrolysis of elastin by oxalic acid yields a water- and solvent- (HFIP-) soluble product that is adequate for electrospinning (section 2.2.3). Soluble elastin prepared by

this procedure reportedly has an average molecular weight of 65,000 Da (which approaches the molecular weight of tropoelastin) and the ability to coacervate.[5, 7] Briefly, insoluble elastin was suspended in oxalic acid before heating for 1 h. Then, the mixture was rapidly cooled, centrifuged, and the supernatant containing soluble elastin was collected. Extraction and collection were repeated until complete dissolution of the solid. The solubilization scheme was slightly altered from published protocol.[15] After heating for an hour, the suspension of insoluble elastin in oxalic acid was rapidly cooled over ice and subsequently centrifuged at 4 °C to avoid coacervation. Mixtures were typically centrifuged for 30-45 min, but time was extended if the insoluble material was not sufficiently pelleted. Up to ten extraction cycles were usually needed to obtain complete dissolution, which was more than typical number of repetitions in the literature.[6,15] The insoluble and soluble elastin samples were then assayed by amino acid analysis.

For this study, samples were sent to the SPARC Biocentre (The Hospital for Sick Children, Toronto, Canada) for analysis, where they screen for desmosine and isodesmosine crosslinks in addition to standard amino acids. In general, amino acid analysis includes hydrolysis of the sample, separation, and quantification of specific amino acids. Composition profiles of elastin purified and solubilized using a comparable method to this study[5, 7], elastin from CNBr-based purifications[4, 23], and the primary amino acid sequence of bovine tropoelastin (Isoform 1, P04985)[28] are summarized and reported in **Table 1**.

Comparisons of prepared samples with the literature[4,7,23,28] show that the utilized purification procedure yields a product with an amino acid composition typical of mature elastin. The prepared samples have similar relative quantities of key amino acids as the

Table 2.1. Amino acid analysis of purified insoluble elastin and soluble elastin from BNL [a,b]

	Current Work		Literature Values[4, 7, 23, 28]					
Amino Acid	**Insoluble Elastin**	**Soluble Elastin**	Auto (1)[7]	Auto (2)[7]	Soluble Elastin[7]	CNBr (1) [4]	CNBr (2)[23]	Primary Structure[28]
Asx	**11**	**7**	8	8	5	7	6.5	4
Glx	**23**	**24**	15	16	18	17	16	18
Hyp	**10**	**9**	11	11	12	11	13	-
Ser	**11**	**11**	8	9	9	10	9	12
Gly	**327**	**306**	331	332	314	333	332	308
His	**1**	**0**	0	1	0	-	1	0
Arg	**7**	**7**	7	6	7	5	5	11
Thr	**9**	**9**	9	9	10	11	9	9
Ala	**224**	**264**	222	239	279	225	228	207
Pro	**108**	**107**	109	103	109	115	117	119
Tyr	**8**	**9**	8	6	9	10	6	9
Val	**136**	**126**	141	134	134	129	138	123
Met	**1**	**1**	0	0	0	-	1	1
Cys	**1**	**1**	3	0	3	-	-	4
Ile	**24**	**20**	27	26	23	25	25	25
Leu	**60**	**56**	64	63	64	64	60	67
Phe	**28**	**29**	35	35	-	31	29	28
Ides	**4**	**6**	-	-	-	2	1	-
Des	**4**	**5**	-	-	-	2	1	-
Lys	**4**	**4**	3	3	4	3	3	51

[a] Reported as residues per 1000 residues (RPTR).

[b] Hyphen (-) indicates value not reported in literature source.

literature data sets, i.e. high glycine, alanine, proline, valine. Also, the characteristic crosslinks found in mature elastin, desmosine and isodesmosine, are preserved through purification and solubilization. Discrepancies may arise from reporting in terms of RPTR, which only indicates the relative amino acid composition, not absolute quantities. For example, in studies where desmosine and isodesmosine crosslinks were not reported[7], values for other amino acids are more heavily weighted. Also, the primary amino acid sequence[28] shows a high amount of lysine residues due to the absence of desmosine and isodesmosine in tropoelastin (~4 lysines per crosslink).

Analyses of the two prepared samples show strongly similar compositions, indicating no significant degradation after solubilization. Amino acid analysis shows that glycine is the most abundant amino acid, followed by alanine, valine, then proline. The relative amount of these four key amino acids are similar, with Gly+Ala+Val+Pro = 795 and 803 RPTR for the insoluble and soluble sample, respectively. In both samples, most amino acid quantities are either the same, or agreeing within 10 RPTR (~1 %). The exceptions are seen in the glycine and alanine residue counts.

Slight differences in glycine and alanine content are observed in elastin after oxalic acid treatment. Glycine content appears to be lower in the soluble elastin compared to insoluble elastin, 306 and 327 RPTR, respectively. Also, the amount of alanine is 40 RPTR higher in the soluble elastin. The trend to lower glycine and higher alanine content by soluble elastin has been previously reported in the literature for elastin purified and solubilized in a similar method to this study (17-18 RPTR lower for glycine and 40-57 RPTR higher for alanine).[5,7] Partridge and coworkers rectify this discrepancy by stating that a certain amount of the original insoluble protein is lost as

diffusible proteins during the partial hydrolysis, and that the lost fraction would not be expected to have the same composition as the parent protein due to the variation in the hydrolysis rates of the peptide bonds.[5]

Amino acid analysis is useful for determining the relative amounts of peptide residues in a sample, but it does not provide information on the structure, sequence, or dynamics of non-hydrolyzed proteins. SSNMR spectroscopy can provide these types of information for intact protein samples. In the following section, ^{13}C chemical shifts from CPMAS experiments will be used to show similarities between different preparations of elastin.

2.3.2 ^{13}C chemical shifts show similarities between elastin preparations

The autoclave-purified elastin was solubilized, before electrospinning and subsequent crosslinked in glutaraldehyde vapors (Sections 2.2.2-2.2.4). Electrospinning of elastin was initially attempted based on published protocols for elastin.[14-16] However, the described electrospinning parameters and solution conditions did not produce fibers. Therefore, electrospinning parameters (type of collector plate, distance from needle to collector plate, applied voltage, pump speed, etc.) and solution conditions (concentration, solvent-system, etc.) were optimized to produce a soluble elastin that could be successfully electrospun. A few considerations that could possibly explain inadequacies of literature protocols[14-16] for our electrospinning setup include differences in atmospheric humidity, tissue samples, purification methods, etc. Once electrospun elastin fibers were obtained, they were crosslinked in glutaraldehyde vapors, rinsed in water, and lyophilized before NMR analysis.

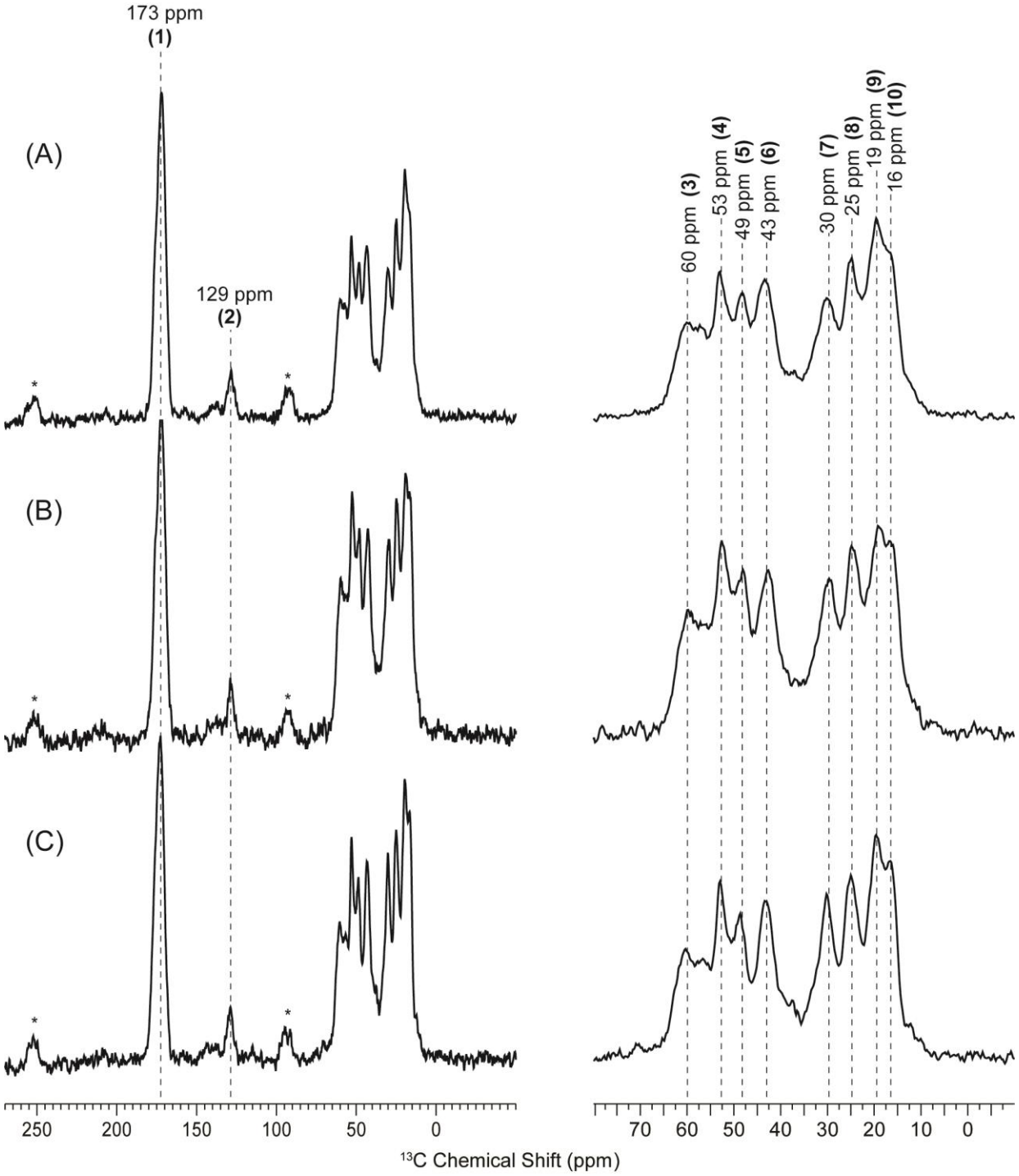

Figure 2.2. ^{13}C CPMAS NMR spectra of dry BNL elastin preparations. (A) Purified insoluble elastin, (B) solubilized elastin, and (C) crosslinked, electrospun elastin. All spectra were taken at 37 °C with 1024 scans, and a 1 ms contact time. Vertical dashed lines indicate chemical shifts of resolved peaks. Spinning side bands are indicated by asterisks (*).

Table 2.2. ^{13}C Chemical shift assignments for major features in the ^{13}C CPMAS NMR spectra of prepared elastin samples.

	^{13}C δ(ppm)	Assignments[8]
1	173	Carbonyl carbons
2	129	Aromatic carbons
3	60	Pro Cα & Val Cα
4	53	Ala Cα
5	49	Pro Cδ
6	43	Gly Cα
7	30	Pro Cβ & Val Cβ
8	25	Pro Cγ
9	19	Val Cγ
10	16	Ala Cβ

General features of the ^{13}C CPMAS spectra of dry samples of insoluble elastin (Figure 3A), soluble elastin (Figure 3B), and crosslinked, electrospun elastin (Figure 3C) show many similarities. The resolved peaks of all preparations have comparable chemical shifts, line widths, and relative intensities. The similar chemical shifts imply that there were no drastic changes in local chemical structure after solubilizing and electrospinning the elastin.

The ^{13}C chemical shifts of all resolved peaks for prepared samples are comparable to each other and with the literature.[24,25] Chemical shifts and assignments of major resolved peaks are summarized in **Table 2**. Assignments were based on previous work on native BNL elastin purified by CNBr.[24] The peak at 173 ppm corresponds to the backbone carbonyl carbons. The carbonyl line widths for all three sample preparations were FWHM ~750 Hz. The aromatic carbons in elastin, phenylalanine and tyrosine, are tentatively assigned to the peak at 129 ppm. Most of the

peaks in the chemical shift range of around 40 to 60 ppm correspond to the backbone Cα carbons, including Pro Cα and Val Cα at 60 ppm, Ala Cα at 53 ppm, and Gly Cα at 43 ppm. The peak at 49 ppm is attributed to Pro Cδ. The features in the 20 to 30 ppm region arise from the aliphatic, nonmethyl, side chain carbons, Pro Cβ and Val Cβ at 30 ppm and Pro Cγ at 25 ppm. Lastly, peaks at 19 and 16 ppm correspond to the Val Cγ and Ala Cβ methyl carbons, respectively.

The comparable chemical shifts and relative intensities imply that the local chemical structures are similar for all mentioned dry preparations of elastin. However, in order to be useful as a biomaterial, electrospun samples must be stable in water for extended periods of time. Therefore, the effect of crosslinking with glutaraldehyde vapors in terms of aqueous stability was investigated.

2.3.3 Crosslinking of electrospun elastin fibers in glutaraldehyde vapors yields a water-stable, insoluble product

Electrospun elastin fibers after glutaraldehyde crosslinking retain their fiber-like morphology and are stable in water for extended periods of time. Electrospinning has been used to create non-woven, nanofiber mats that have potential applications in cell and tissue culture.[13-16] Electrospun scaffolds usually have to be crosslinked prior to use as a biomaterial in order to be functional in physiological conditions.[12] An optimal crosslinker for electrospun samples should produce a water- (buffer-) insoluble product that is stable over extended periods of time, while preserving the sample's fiber-like morphology. The effectiveness of glutaraldehyde as a crosslinker for electrospun elastin was therefore investigated by water-solubility tests and observations under microscope.

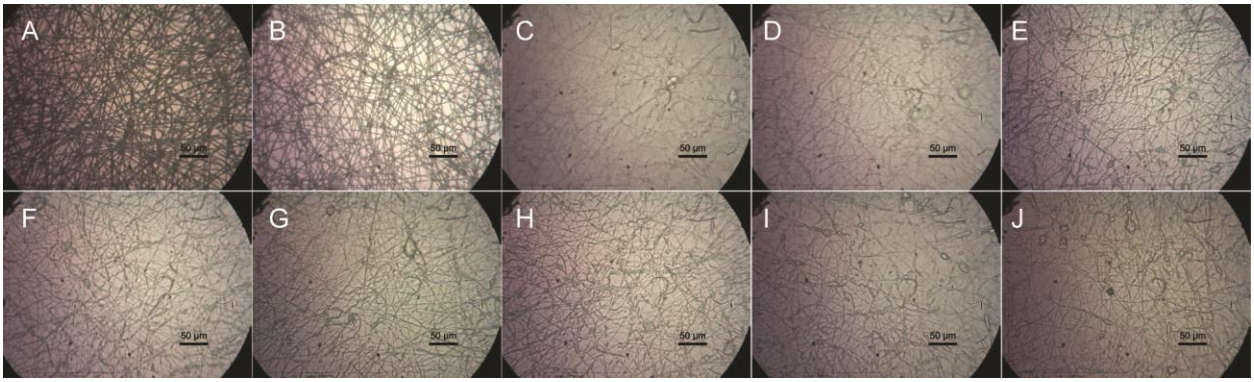

Figure 2.3. Microscope images of electrospun elastin samples at different points of processing: (A) electrospun elastin, dry; (B) crosslinked electrospun elastin, dry; (C)-(J) crosslinked electrospun elastin in water after different incubation times: (C) 0 min , (D) 10 min, (E) 30 min, (F) 1 h, (G) 3 h, (H) 5 h, (I) 7 h, and (J) 24 h. Scale bars represent 50 μm.

Fiber-like morphology of electrospun samples before and after crosslinking was confirmed by observation under microscope. Fiber samples were collected by placing a glass coverslip on the grounded electrospinning collector plate. Electrospun samples were crosslinked by incubating in a closed container with a beaker with aqueous glutaraldehyde solutions. The fiber-like morphology was observed for the electrospun elastin (Figure 3A), and appeared to be mostly retained after crosslinking in glutaraldehyde vapors (Figure 3B). Individual fibers appear to partially fuse together at junctions of contact with other fibers during the crosslinking process, perhaps due to water vapor from the aqueous glutaraldehyde solutions. The electrospun, crosslinked fibers were then subjected to solubility tests by incubating in water.

After incubation in water, the electrospun, crosslinked elastin samples retained their fiber-like morphology and remained stable in water for an extended period of time. Elastin samples were placed in water for different lengths of time to observe the effects

of water on morphology. Upon submersion in water, the fibers immediately appeared to swell, but not dissolve (Figure 3C). In contrast, if the electrospun elastin was not crosslinked prior to incubation, the sample immediately dissolved upon contact with water (picture not shown). Incubation in water was continued for a total of 24 hours, and microscope images were acquired at intermediate time points. The morphology of the fibers did not change significantly throughout the test period (Figure 3, C-J), confirming that the fabricated material appears to remain water-stable for extended periods of time. Based on these observations, it is assumed that the hydrated electrospun, crosslinked elastin samples remain insoluble during SSNMR experiments rather than dissolving into aqueous solutions of soluble elastin.

As discussed previously, the chemical shifts of the electrospun, crosslinked elastin sample are similar to those expected for BNL elastin.[24,25] The observed chemical shifts for the dry sample at 37°C (Figure 4A) and the hydrated sample at -20°C (Figure 4C) were similar. The chemical shifts from these two spectra were comparable to those reported in **Table 2**. The spectrum of hydrated elastin at 37°C (Figure 4B) shows a broad resonance (FWHM ~750 Hz) in the backbone carbonyl region centered at 173 ppm. The Cα region is dominated by a peak at 53 ppm, with less intense peaks around 60 ppm and 43 ppm. Other features were observed at roughly 31, 25, 19, and 17 ppm. Peaks for the hydrated sample at 37°C were not well-resolved due to the relatively low signal-to-noise, but the chemical shifts are similar to values previously reported for fully hydrated BNL elastin.[25]

Differences in the CPMAS spectra of dry (Figure 4A) and hydrated (Figure 4B) crosslinked, electrospun elastin at 37 °C reflect the effect of hydration on the sample.

The dry preparation at high temperature has a CPMAS spectrum that shows good cross-polarization efficiency across the population of carbons in the sample, indicated by the relatively high peak intensities and well-resolved features. Generally, rigid samples cross-polarize well, and the efficiency decreases as relative molecular mobility increases. By comparison, the CPMAS spectrum of the hydrated sample at 37 °C (Figure 4B) has lower signal intensities, and fewer peaks are clearly distinguishable compared to the dry sample at the same temperature. The reduction in overall signal implies that fewer carbons cross-polarize in the hydrated sample which also suggests an increase of relative mobility of the sample in the presence of water.

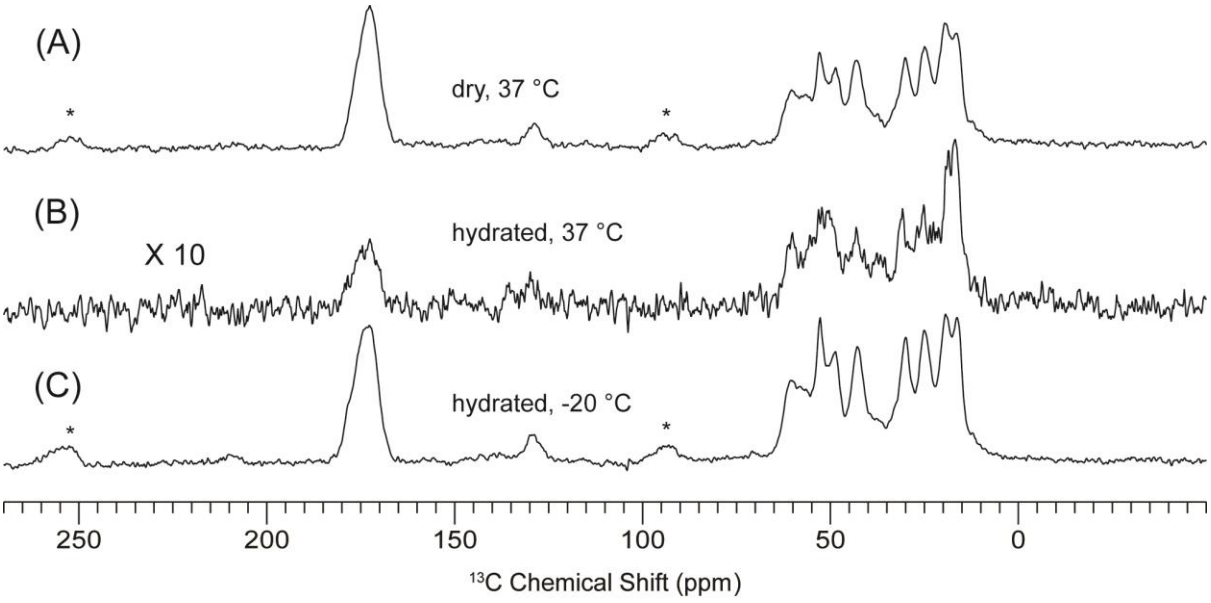

Figure 2.4. ^{13}C CPMAS spectra of electrospun, crosslinked elastin at different hydration states and temperatures: (A) dry (lyophilized) at 37 °C, (B) hydrated at 37 °C, and (C) hydrated at -20 °C. Spectra were taken with 1024 scans and a 1 ms contact time. Spinning side bands are indicated by asterisks (*).

The same sample was then cooled to -20 °C before subsequent acquisition. The resulting spectrum of the hydrated sample at low temperature (Figure 4C) resembles that of the dry sample in terms of overall signal intensity and spectral features. Specifically, the number of resolved peaks corresponding to the backbone carbonyl, aromatic peak, and the aliphatic features and their associated chemical shifts appear to be similar between the dry and frozen states. The observed higher signal intensities suggest an increase in the sample's cross-polarization efficiency due to decreased mobility of the sample after cooling to a temperature below the freezing point of water. These observations are consistent with previous work on the effects of hydration and temperature on insoluble BNL elastin.[25] The effects of hydration on the dynamics of the elastin samples will be further discussed in the next subsection.

2.3.4 NMR relaxation measurements reflect the effects of water on the dynamics of crosslinked, electrospun elastin

NMR relaxation time constants ^{13}C T_1, ^{1}H T_1, ^{1}H $T_{1\rho}$ and T_{CH} were determined for the resolved peaks in the CPMAS spectra of dry and hydrated electrospun, crosslinked elastin at -20 °C. NMR relaxation measurements are useful for probing the motion of polymers at different time scales, and also for ^{1}H T_1 and $T_{1\rho}$, the molecular-scale homogeneity. The hydrated sample is then swelled in water at room temperature before cooling to -20 °C immediately prior to NMR measurements; i.e., these hydrated samples are frozen for characterization by NMR.

The ^{13}C spin-lattice relaxation times, T_1, were obtained by the method of Torchia[20] (**Table 3** and **Figure 5**). Generally, shorter ^{13}C T_1 values are observed in the

frozen, hydrated sample. Time constants associated with the carbonyl carbons have values of 33.6 s for dry and 18.2 s for hydrated. The α-carbons with shifts from roughly 43 to 60 ppm have ^{13}C T_1 values from around 15-26 s and 7-13 s for the dry and hydrated samples, respectively. The peak at 49 ppm corresponding to Pro Cδ has a value of roughly 10 s for the dry case and 7 s for the hydrated condition. Side-chain carbons corresponding to Pro Cγ at 25 ppm, and Pro and Val Cβ's at 30 ppm have values of about 7-8 s for the dry, and 4-6 s for the hydrated states. Finally, as expected, all methyl carbons have very short time constants (< 1 s), due to the methyl rotor; 0.4 and 0.3 s for peaks at 16 and 19 ppm, respectively, for both samples.

Differences in ^{13}C T_1 in imply an effect of water on the sample system. The time constants for the hydrated sample were typically shorter than those measured for the dry sample. This trend indicates that water affects the ^{13}C T_1 relaxation mechanisms, possibly through water-protein interactions or by inducing a change in mobility upon hydration and subsequent freezing, with the former possibly being more probable.

Measured values in this study are generally comparable to previously reported work on BNL elastin,[25] but tend to slightly longer time constants. Spin-lattice relaxation time constants can be used to comment on the relative mobility of samples if all other relaxation mechanisms are considered to be similar. By this interpretation, long ^{13}C T_1's are indicative of carbons in a rigid environment, while short values are reflective of a mobile environment. One might hypothesize that by introducing new covalent bonds to electrospun elastin through crosslinking with glutaraldehyde, the resulting sample would be more rigid than native elastin. The reduced mobility in the electrospun, crosslinked elastin would then be reflected in the observed, longer ^{13}C T_1 values.

Table 2.3. ^{13}C T_1 values (s) for electrospun, crosslinked, elastin samples at -20 °C.

	^{13}C δ (ppm)	'Hydrated'		'Dry'	
		^{13}C T_1 (s)	+/-	^{13}C T_1 (s)	+/-
1	173	18.2	0.8	33.6	0.9
2	129	11.3	4.3	30.8	7.9
3	60	9.9	1.3	25.5	3.4
4	53	12.5	1.1	15.3	1.2
5	49	5.2	0.7	9.9	1.0
6	43	6.7	0.6	20.6	1.3
7	30	5.7	0.5	8.2	0.6
8	25	4.3	0.5	7.0	0.6
9	19	0.3	0.02	0.3	0.03
10	16	0.4	0.1	0.4	0.1

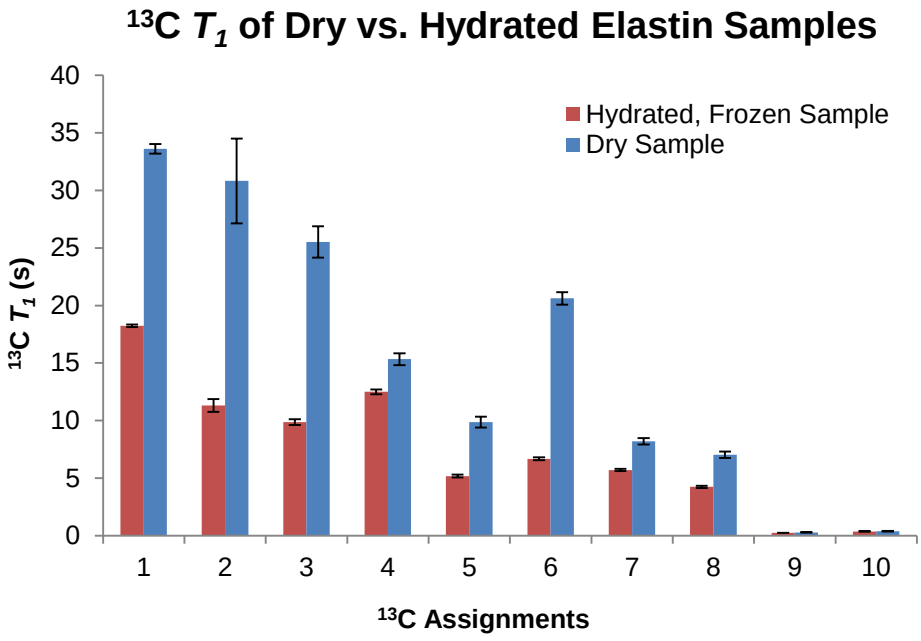

Figure 2.5. ^{13}C T_1 values (s) for electrospun, crosslinked, elastin samples at -20 °C. Blue and red bars correspond to the 'dry' and 'hydrated, frozen' samples, respectively. Error bars correspond to the error determined by the fitting procedure.

The carbon-proton cross-polarization time constant, T_{CH}, and ^{1}H spin-lattice relaxation time in the rotating frame, $T_{1\rho}$, were determined simultaneously by an arrayed CP contact-time experiment. The values were obtained through 3D-fitting with **Equation 2.3**, which describes the carbon magnetization behavior at various CP contact-times.

T_{CH} values are correlated with the initial signal intensity build-up on the CP contact-time plot array and are used to comment on the relative rigidities of the samples. Measured values are summarized in **Table 4** and visualized in **Figure 6**. The carbon magnetization at a given time point is inversely related to the T_{CH} time constant (Equation 2.3). The carbonyl carbons have values of 390 and 499 μs for the dry and hydrated states, respectively. Time constants corresponding to the backbone Cα's range from 13-42 μs for the dry, and 34-83 μs for the hydrated sample. The values for Pro Cδ and Pro Cγ increase upon hydration from 45 to 75 μs and 53 to 123 μs, respectively. However, the T_{CH} from the peak at 30 ppm, Pro and Val Cβ, does not appear to change. Methyl values were 152 and 184 μs for the dry sample, and 175 and 203 μs for the hydrated. Overall, the measured T_{CH} values trended to larger values in the hydrated sample.

In general, T_{CH} values are not interpreted in terms of correlation times (related to molecular motions), but rather, they can be used to comment on the relative rigidity of these samples.[26] Therefore, shorter values of T_{CH} reflect higher CP efficiencies. By this interpretation, carbons with short T_{CH} values reside in domains with reduced motion, compared to those with higher T_{CH}. The higher values for the hydrated state imply that upon the introduction of water to the system, the hydrated elastin is overall less rigid than

Table 2.4. T_{CH} values (μs) for electrospun, crosslinked, elastin samples at -20 °C.

	^{13}C δ (ppm)	'Hydrated' T_{CH} (μs)	+/-	'Dry' T_{CH} (μs)	+/-
1	173	499	22	390	12
2	129	--	--	67	20
3	60	46	13	13	7
4	53	83	8	42	5
5	49	75	12	45	6
6	43	34	12	18	4
7	30	30	13	32	4
8	25	123	14	53	4
9	19	203	11	184	9
10	16	175	14	152	11

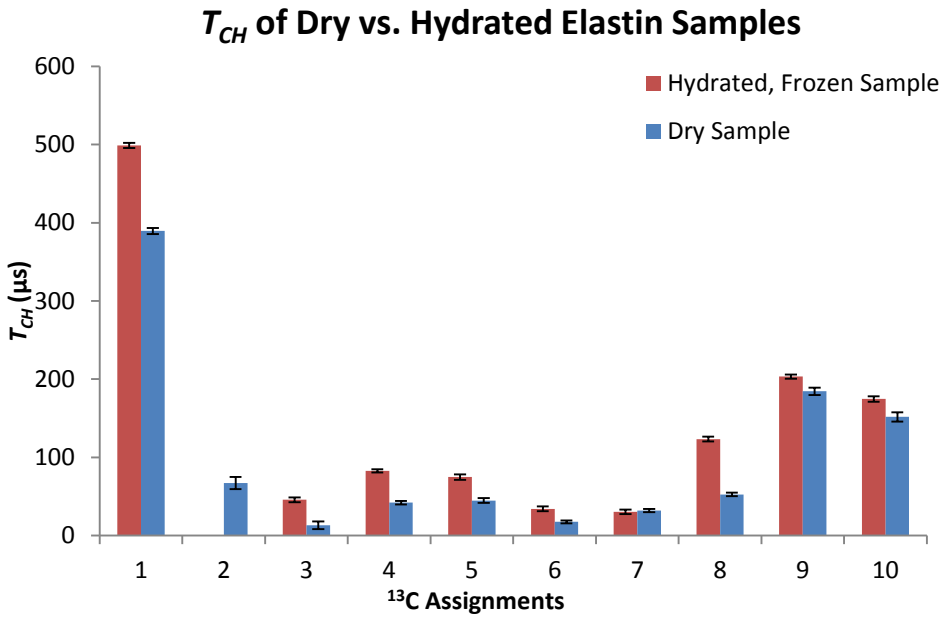

Figure 2.6. T_{CH} values (μs) for electrospun, crosslinked, elastin samples at -20 °C. Blue and red bars correspond to the 'dry' and 'hydrated, frozen' samples, respectively. Error bars correspond to the error determined by the fitting procedure.

the dry sample. This observation is consistent with the interpretation of the ^{13}C T_1 values for the same samples.

^{1}H $T_{1\rho}$ values correspond to the decay portion of the contact-time-arrayed plot (**Table 5** and **Figure 7**). The measured values appeared relatively homogenous for either sample condition, but there is a general trend towards lower values in the hydrated state compared to the dry state. In the dry state, measured ^{1}H $T_{1\rho}$ values were generally in the range of 5.7-7.2 ms, while in the hydrated state they were around 6.2-8.2 ms.

^{1}H inversion recovery with indirect detection through resolved ^{13}C peaks was used to determine ^{1}H T_1 values (**Table 6** and **Figure 8**). Similar to the case of ^{1}H $T_{1\rho}$, measured ^{1}H T_1's were homogenous within each sample and there is a general trend to shorter values in the hydrated condition. Measured time constants were 0.4 s and 0.6-0.7 s for the hydrated and dry states, respectively.

The ^{1}H relaxation time constants $T_{1\rho}$ and T_1 are dominated by proton-proton spin diffusion. Therefore, they provide information that is averaged over a certain domain.[26] For both ^{1}H $T_{1\rho}$ and T_1, each sample data set has similar time constants, implying there are no significant heterogeneities in the structural organization of the electrospun protein. The trend towards shorter values upon hydration indicate that water influences the relaxation mechanisms of the samples in the domain sizes observable by ^{1}H $T_{1\rho}$ and T_1 experiments.

Table 2.5. ^{1}H $T_{1\rho}$ values (ms) for electrospun, crosslinked, elastin samples at -20 °C.

	^{13}C δ (ppm)	'Hydrated' ^{1}H $T_{1\rho}$ (ms)	+/-	'Dry' ^{1}H $T_{1\rho}$ (ms)	+/-
1	173	6.7	0.3	6.7	0.2
2	129	--	--	7.4	1.5
3	60	6.3	0.5	7.1	0.6
4	53	7.2	0.3	8.2	0.5
5	49	6.4	0.7	6.6	0.5
6	43	5.7	0.4	6.3	0.2
7	30	5.7	0.3	6.4	0.3
8	25	5.7	0.3	6.2	0.3
9	19	6.8	0.3	6.9	0.3
10	16	7.4	0.4	7.5	0.4

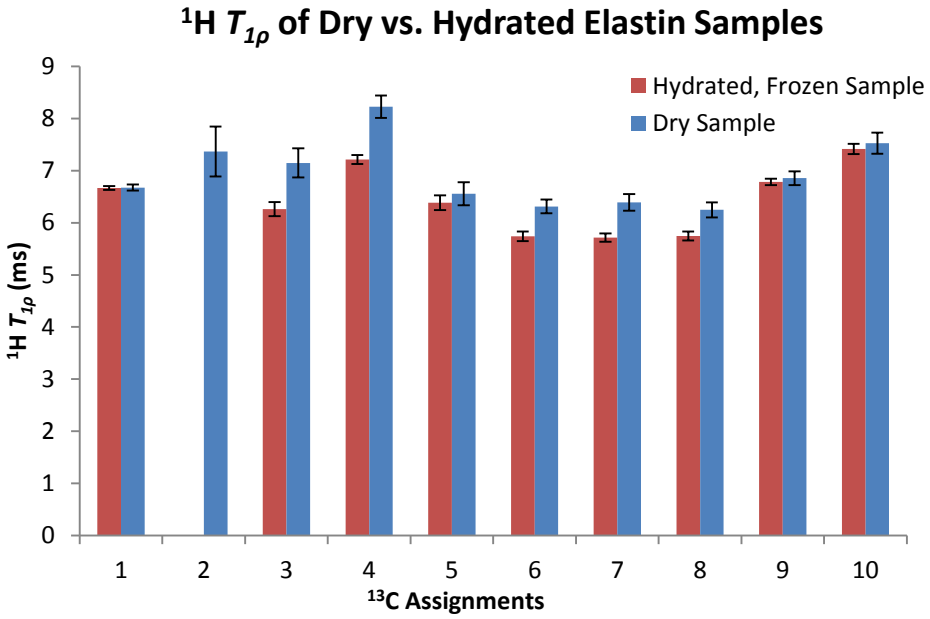

Figure 2.7. ^{1}H $T_{1\rho}$ values (s) for electrospun, crosslinked, elastin samples at -20 °C. Blue and red bars correspond to the 'dry' and 'hydrated, frozen' samples, respectively. Error bars correspond to the error determined by the fitting procedure.

Table 2.6. $^{1}H\ T_1$ values (s) for electrospun, crosslinked, elastin samples at -20 °C.

	δ (ppm)	'Hydrated' $^{1}H\ T_1$ (s)	+/-	'Dry' $^{1}H\ T_1$ (s)	+/-
1	173	0.40	0.01	0.63	0.01
2	129	0.40	0.12	0.58	0.10
3	60	0.41	0.06	0.62	0.05
4	53	0.38	0.03	0.67	0.04
5	49	0.42	0.03	0.65	0.05
6	43	0.41	0.03	0.65	0.03
7	30	0.41	0.02	0.68	0.05
8	25	0.40	0.02	0.65	0.03
9	19	0.38	0.02	0.62	0.02
10	16	0.38	0.02	0.62	0.03

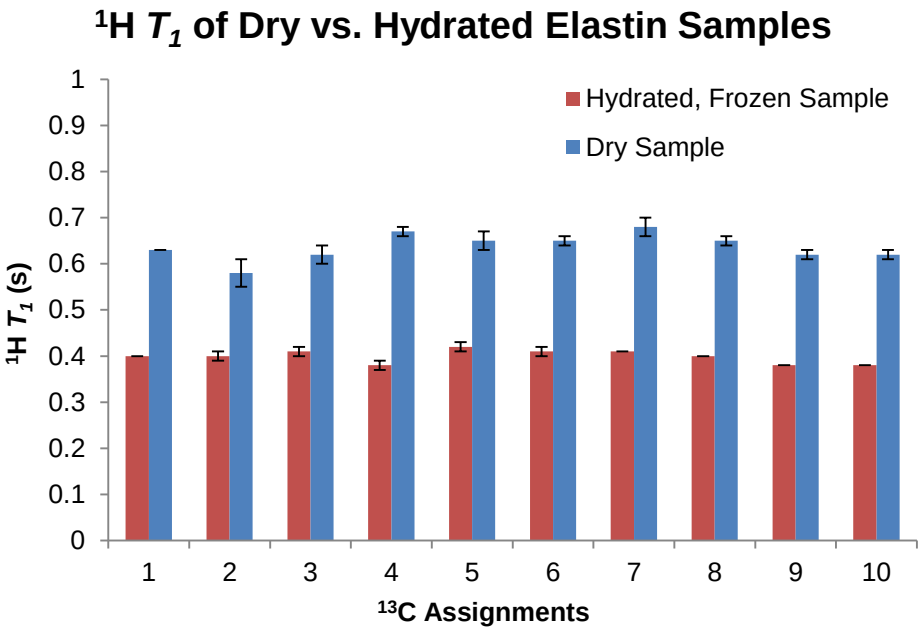

Figure 2.8. $^{1}H\ T_1$ values (s) for electrospun, crosslinked, elastin samples at 20 °C. Blue and red bars correspond to the 'dry' and 'hydrated, frozen' samples, respectively. Error bars correspond to the error determined by the fitting procedure.

2.4 Conclusion

The mechanical and biological properties of elastin make it a highly attractive candidate for the fabrication of various biomaterials. Electrospinning is a common method for the production of nanofibers which can be used as extracellular matrix analogs or support substrates for cells. In this study, electrospun elastin samples were studied using SSNMR spectroscopy.

Elastin was purified from bovine nuchal ligament using an autoclave-based procedure before subsequent partial hydrolysis using oxalic acid. Prepared samples were assayed by amino acid analysis and were found to have composition profiles similar to what is expected for elastin.[4,7,23,28] Soluble elastin was then electrospun and crosslinked using glutaraldehyde vapors. 1D CPMAS NMR spectra of the samples at differing processing points (insoluble, soluble, electrospun and crosslinked) were similar to what has been previously reported for elastin.[24,25] The effects of hydration on the electrospun, crosslinked elastin samples were also investigated using CPMAS and NMR relaxation measurements. Water appeared to influence the dynamics of the protein sample. A similar approach will be used to characterize and probe the molecular-level interactions of electrospun blends of elastin and synthetic polymers in the following chapters.

2.5 References

1. Robert, L. H., William, *Elastin and Elastases*. CRC Press, Inc.: Boca Raton, Florida, 1989; Vol. 1.
2. Lowry, O. H.; Gilligan, D. R.; Katersky, E. M., The determination of collagen and elastin in tissues with results obtained in various normal tissues from different species. *J. Biol. Chem.* **1941,** *139*, 795-804.
3. Mecham, R. P., Methods in elastic tissue biology: Elastin isolation and purification. *Methods (Oxford, U. K.)* **2008,** *45* (1), 32-41.
4. Rasmussen, B. L.; Bruenger, E.; Sandberg, L. B., A new method for purification of mature elastin. *Anal Biochem* **1975,** *64* (1), 255-9.
5. Partridge, S. M.; Davis, H. F.; Adair, G. S., The chemistry of connective tissues. 2. Soluble proteins derived from partial hydrolysis of elastin. *Biochemical Journal* **1955,** *61* (1), 11-21.
6. Vrhovski, B.; Weiss, A. S., Biochemistry of tropoelastin. *European Journal of Biochemistry* **1998,** *258* (1), 1-18.
7. Partridge, S. M.; Davis, H. F., Chemistry of Connectrive Tissues. 3. Composition of the Soluble Proteins Derived from Elastin.. *Biochemical Journal* **1955,** *61* (1), 21-30.
8. Robert, L., The Saga of κ-Elastin or the Promotion of Elastin Degradation Products from 'Garbage' to Receptor Agonists and Pharmacologically Active Principles. *Connective Tissue Research* **2010,** *51* (1), 8-13.
9. Menasche, M.; Jacob, M. P.; Godeau, G.; Robert, A. M.; Robert, L., Pharmacological studies on elastin peptides (kappa-elastin). Blood clearance, percutaneous penetration and tissue distribution. *Pathol. Biol.* **1981,** *29* (9), 548-54.
10. Kumashiro, K. K.; Kim, M. S.; Kaczmarek, S. E.; Sandberg, L. B.; Boyd, C. D., C-13 cross-polarization/magic angle spinning NMR studies of alpha-elastin preparations show retention of overall structure and reduction of mobility with a decreased number of cross-links. *Biopolymers* **2001,** *59* (4), 266-275.
11. Debelle, L.; Tamburro, A. M., Elastin: molecular description and function. *The International Journal of Biochemistry & Cell Biology* **1999,** *31* (2), 261-272.
12. Yeo, G. C.; Aghaei-Ghareh-Bolagh, B.; Brackenreg, E. P.; Hiob, M. A.; Lee, P.; Weiss, A. S., Fabricated Elastin. *Advanced Healthcare Materials* **2015,** *4* (16), 2530-2556.
13. Nivison-Smith, L.; Rnjak, J.; Weiss, A. S., Synthetic human elastin microfibers: Stable cross-linked tropoelastin and cell interactive constructs for tissue engineering

applications. *Acta Biomaterialia* **2010,** *6* (2), 354-359.
14. Li, M. Y.; Mondrinos, M. J.; Gandhi, M. R.; Ko, F. K.; Weiss, A. S.; Lelkes, P. I., Electrospun protein fibers as matrices for tissue engineering. *Biomaterials* **2005,** *26* (30), 5999-6008.
15. Miyamoto, K.; Atarashi, M.; Kadozono, H.; Shibata, M.; Koyama, Y.; Okai, M.; Inakuma, A.; Kitazono, E.; Kaneko, H.; Takebayashi, T.; Horiuchi, T., Creation of cross-linked electrospun isotypic-elastin fibers controlled cell-differentiation with new cross-linker. *International Journal of Biological Macromolecules* **2009,** *45* (1), 33-41.
16. Araujo, J.; Padrão, J.; Silva, J. P.; Dourado, F.; Correia, D. M.; Botelho, G.; Gomez Ribelles, J. L.; Lanceros-Méndez, S.; Sencadas, V., Processing and characterization of α-elastin electrospun membranes. *Appl. Phys. A* **2014,** *115* (4), 1291-1298.
17. Sisson, K.; Zhang, C.; Farach-Carson, M. C.; Chase, D. B.; Rabolt, J. F., Evaluation of Cross-Linking Methods for Electrospun Gelatin on Cell Growth and Viability. *Biomacromolecules* **2009,** *10* (7), 1675-1680.
18. Wine, Y.; Cohen-Hadar, N.; Freeman, A.; Frolow, F., Elucidation of the mechanism and end products of glutaraldehyde crosslinking reaction by X-ray structure analysis. *Biotechnology and Bioengineering* **2007,** *98* (3), 711-718.
19. Bennett, A. E.; Rienstra, C. M.; Auger, M.; Lakshmi, K. V.; Griffin, R. G., Heteronuclear decoupling in rotating solids. *J. Chem. Phys.* **1995,** *103* (16), 6951-8.
20. Torchia, D. A., The measurement of proton-enhanced carbon-13 T1 values by a method which suppresses artifacts. *J. Magn. Reson.* **1978,** *30* (3), 613-16.
21. Keeler, J., *Understanding NMR Spectroscopy*. 2nd ed.; John Wilery & Sons Ltd.: West Sussex, United Kingdom.
22. Saito, H. A., Isao; Naito, Akiro, *Solid State NMR Spectroscopy for Biopolymers*. Springer: Dordrecht, The Netherlands, 2006.
23. Starcher, B. C.; Galione, M. J., Purification and comparison of elastins from different animal species. *Anal. Biochem.* **1976,** *74* (2), 441-7.
24. Ohgo, K.; Niemczura, W. P.; Kumashiro, K. K., Probing the Natural-Abundance C-13 Populations of Insoluble Elastin Using C-13-H-1 Heteronuclear Correlation (HETCOR) NMR Spectroscopy. *Macromolecules* **2009,** *42* (18), 7024-7030.
25. Perry, A.; Stypa, M. P.; Tenn, B. K.; Kumashiro, K. K., Solid-state C-13 NMR reveals effects of temperature and hydration on elastin. *Biophysical Journal* **2002,** *82* (2), 1086-1095.

26. Mirau, P. A., *A Practical Guide to Understanding the NMR of Polymers*. John Wiler & Sons, Inc.: Hoboken, New Jersey, 2005.
27. SPARC BioCentre. Amino Acid Analysis Methods. http://www.sickkids.ca/Research/SPARC/Amino-Acid-Analysis/Methods/index.html (accessed April 2, 2017).
28. UniProt. UniProtKB – P04985 (ELN_BOVIN). http://www.uniprot.org/uniprot/P04985. (accessed April 2, 2017).
29. Levenberg, K., A Method for the Solution of Certain Non-Linear Problems in Least Squares. *Quarterly of Applied Mathematics* **1944,** *2* (2), 164-168.
30. Marquardt, D. W., An Algorithm for Least-Squares Estimation of Nonlinear Parameters. *Journal of the Society for Industrial and Applied Mathematics* **1963,** *11* (2), 431-441.
31. Geppi, M.; Forte, C., The SPORT-NMR software: A tool for determining relaxation times in unresolved NMR spectra. *J. Magn. Reson.* **1999,** *137* (1), 177-185.
32. Ohgo, K; Kumashiro, K. K., **2017,** *to be submitted*.

Chapter 3. Characterization of poly(vinyl alcohol) and elastin electrospun blends using SSNMR spectroscopy

3.1 Introduction

Poly(vinyl alcohol), PVA, is a non-toxic, synthetic polymer that has applications in many different fields due to its water solubility and biodegradability.[1] For example, its mechanical properties and biocompatibility make PVA an attractive candidate for the production of biomaterials.[2] As mentioned in previous chapters, electrospinning is a common method for the production of nanofibers that can be used as biomaterials. Electrospinning can produce fibers of composed of a single polymer, but can also be used for the fabrication of composite materials with two or more components.

In this chapter, the preparation and subsequent analysis of *PVA-only* and *PVA-Elastin blend* samples will be discussed. First, electrospun PVA in both dry and hydrated states were analyzed using SSNMR spectroscopy. Then, results from NMR experiments on the electrospun blend of PVA and elastin will be compared to *PVA-only* and *elastin-only* to probe for differences.

3.1.1 Background information on PVA

PVA is not obtained by direct polymerization because monomeric vinyl alcohol (CH_2=CHOH) is not appreciably stable in solution.[1] Instead, PVA is commonly obtained through the functionalization of poly(vinyl acetate), PVAc. The polymerization of vinyl acetate proceeds through a free-radical mechanism usually in methanol solutions.[1] PVAc is then converted to PVA by alkali-catalyzed methanolysis before isolation and drying.[1, 3]

PVA is semi crystalline with amorphous and crystalline regions that have differing chain conformations. The structure of PVA is presented in **Figure 3.1**. This polymer is known to form both intramolecular and intermolecular hydrogen bonds.[4] PVA's crystalline regions adapt a planar zig-zag conformation with a high packing efficiency, which, in conjunction with the hydrogen bonds, is thought to make these regions more resistant to water.[5] Therefore, molecular-level interactions with water mostly occur in the amorphous segments of PVA.[6]

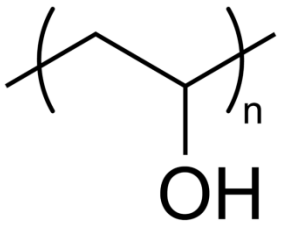

Figure 3.1. The structure of Poly(vinyl alcohol).

The utility of PVA arises from its physical properties such as high heat-resistance (melting point ~200°C), hydrophilic properties, alkali-resistance, etc.[4] Also, it is one of the few vinyl polymers that is soluble in water and also biodegrades.[3] This polymer is an attractive candidate for the production of biomaterials due to its non-toxicity, biocompatibility.

3.1.2 PVA-based materials

PVA is used for biomaterial production due to its abundance, mechanical properties, and biocompatibility.[1-2] PVA-based materials have been successfully

employed in various bio-related fields, with applications for wound dressing, tissue scaffolds, drug release, etc.[2, 7] Diverse methods of fabrication, such as electrospinning, are used to fabricate materials with different forms (fibers, hydrogels, etc.) depending on the intended purpose.

To improve the properties of electrospun PVA, different types of additives, fillers, or other polymers have been incorporated into the fibers.[7] PVA blends have been reported with many synthetic and natural polymers, such as PCL,[8] elastin-like peptides,[9] DNA[10], chitosan[11], starch[11], gelatin[11], cellulose[12], etc. The final properties of polymer blends depend on the miscibility of the two components. Miscibility arises from the inter-polymer interactions such as dipole-dipole forces and hydrogen bonding.[9, 13]

The characterization of these polymer blends usually focus on the morphological features, mechanical properties, and biological functionality. However, few studies place a strong emphasis on molecular-level characterization. SSNMR spectroscopy provides a means to probe the structure and dynamics of these types of blended samples. NMR relaxation experiments are used to probe for interactions between the PVA and elastin, as well as investigate molecular motions and hydration effects on the polymers.

3.2. Materials and Methods

3.2.1 Materials

Polyvinyl alcohol (Mowiol© 10-98, Mw ~ 61,000), glutaraldehyde solution (Grade II, 25% in H_2O), and dialysis tubing (cellulose, 25-mm average flat diameter, molecular weight cut off = 14,000) were also purchased from Sigma Aldrich (Missouri, USA). PVA

was used without further purification. Syringes (polypropylene, 1-mL slip-tip disposable tuberculin syringe) and needles (stainless steel, 18 G, 1.2 mm x 40 mm) from Becton, Dickinson and Company (New Jersey, USA) were used for electrospinning. Unless otherwise stated, Milli-Q ultrapure water was used for all instances where water was necessary.

3.2.2 Electrospinning of PVA and PVA-elastin blends and subsequent crosslinking

PVA solutions were prepared by heating crystals in water at ~80 °C with stirring until complete dissolution. Typical solution batches were ~15-20 mL with concentrations of 17-20 wt% PVA in water. PVA-elastin solutions were prepared by dissolving soluble elastin (from section 2.2.3) in water and mixing with an appropriate amount PVA solution to the desired concentration and composition (total solute concentration ~ 20-27 wt% in water with a 1:1 PVA/elastin mass ratio). A syringe was filled with the *PVA-only* or *PVA-elastin* solution, fitted with a blunt steel needle, and connected to a syringe pump (NE-300 Just Infusion Syringe Pump, New Era Pump Systems, New York, USA). Solutions were pumped through the syringe at constant speed, typically ~ 8-10 µL/min. A rectangular aluminum collector plate was placed at a distance of 10-15 cm from the needle tip in a perpendicular orientation to the syringe. The needle was connected to a positive high voltage power supply, set at ~17-20 kV (ES30P-10W/DAM HV power supply, Gamma High Voltage Research, Florida, USA). The solution pump, power source, and collector plate were all externally grounded.

Electrospun material containing elastin was subsequently crosslinked by glutaraldehyde vapor. Samples were incubated for at least 24 h in a closed, 250-mL

glass container containing about 7 mL of glutaraldehyde solution in a 10-mL beaker. Crosslinked material was then rinsed with water to hydrate and remove any remaining soluble portions. The samples were then either directly used (hydrated) or lyophilized (dry) prior to NMR analysis. Electrospun samples were also collected for observation under microscope (12-560-45 Microscope, Fisher Scientific, Massachusetts, USA).

Dry and hydrated samples were also prepared for PVA. The dry PVA sample was prepared simply by storing PVA in a desiccator for 12-24 h to remove any excess water remaining after electrospinning before packing in a NMR rotor. To prepare the hydrated sample, electrospun PVA was incubated in water vapor using a similar setup used for elastin crosslinking, but with water instead of glutaraldehyde solutions. Fibers were incubated for at least 24 h, resulting in a water-insoluble PVA sample. The sample was then rinsed with water to hydrate and was directly used for NMR analysis. Electrospun PVA samples were also collected for microscope observation.

3.2.3 NMR methods and processing

NMR experiments were conducted on an Agilent DD2 NMR spectrometer (Agilent Technologies, California, USA) equipped with an 89-mm Oxford wide-bore superconducting magnet with a proton resonance frequency of 399.976 MHz. ^{13}C NMR spectra were acquired using a 4.0-mm triple resonance (HXY) T3 MAS probe (ChemMagnetics/Varian NMR, Colorado, USA). Samples were packed into 4.0 mm rotors with typical sample weights of 20-30 mg for dry and 50-60 mg for hydrated preparations. The hydration level was maintained with custom-machined Kel-F spacers (Revolution NMR, Fort Collins, Colorado, USA) fitted with fluorosilicone micro o-rings

(Apple Rubber Products, New York, USA). Data for the dry and hydrated samples were acquired at 37 °C and -20 °C.

All SSNMR experiments were CPMAS-based, including 1D CPMAS and determination of the time constants ^{13}C T_1, ^{1}H T_1, ^{1}H $T_{1\rho}$ and T_{CH}. Typically for CPMAS, a 3.8 - 4.6 μs ^{1}H 90° pulse was followed by a 1-ms contact time with a 5-s recycle delay (6-s recycle delay for NMR relaxation measurements). The ^{1}H to ^{13}C magnetization transfer was accomplished by CP with a Hartmann-Hahn matching condition of $\gamma^H B_1^H/2\pi = \gamma^C B_1^C/2\pi \sim 50$ kHz. ^{1}H TPPM decoupling[14] was applied during acquisition with $\gamma^H B_1/2\pi \sim 50$ kHz. The spinning speed used in MAS experiments was 8 kHz. Chemical shifts are referenced to the tetramethylsilane scale, using hexamethylbenzene as an external standard ($\delta(^{13}CH_3)$ = 17.0 ppm) at room temperature.

^{13}C T_1 measurements were made using the method of Torchia.[20] Briefly, CP was followed by a 4.5 μs ^{13}C 90° pulse, arrayed delay times τ, a second ^{13}C 90° pulse, and finally acquisition with TPPM decoupling. Typical τ times ranged from 0.1 to 20 s. To obtain the relaxation rate constant, ^{13}C peak intensities were fit using single-exponential decay functions (Equation 3.1).

$$I(\tau) = A * e^{-\frac{-\tau}{T_1}} \qquad \text{(Eqn. 3.1)}$$

where τ is the delay time and A is the amplitude.

^{1}H T_1 values were indirectly determined from well-resolved ^{13}C signals from CPMAS following a ^{1}H inversion recovery pulse sequence. Briefly, a 9.2 μs ^{1}H 180° pulse is followed by an array of τ delays (typically 0 to 10 s), a ^{1}H 90° pulse, CP, and finally

acquisition with proton decoupling. The ^{1}H T_1 constants were determined by fitting to the equation:

$$\mathrm{I}(\tau) = \mathrm{M_o}[1 - 2\mathrm{e}^{-\frac{\tau}{T_1}}] \qquad \text{(Eqn. 3.2)}$$

where τ is the delay following the initial ^{1}H 180° pulse and M_o denotes the initial peak intensity.[15]

T_{CH} and ^{1}H $T_{1\rho}$ were obtained from arrayed CP contact time experiments. The pulse sequence was identical to CPMAS experiments, with CP contact times typically arrayed from 0.05 to 20 ms. Time constants T_{CH} and ^{1}H $T_{1\rho}$ were determined by fitting to the equation:

$$\mathrm{I}(\tau) = \left(\frac{M_o}{T_{CH}}\right)\frac{e^{-\tau/T_{1\rho(H)}} - e^{-\tau/T_{CH}}}{1/T_{CH} - 1/T_{1\rho(H)}} \qquad \text{(Eqn. 3.3)}$$

where τ is the arrayed CP contact time and Mo is the initial peak intensity.[16]

Relaxation time constants ^{13}C T_1, ^{1}H T_1, ^{1}H $T_{1\rho}$ and T_{CH} were determined using a '3D-fitting' algorithm developed in our lab.[26] Each NMR relaxation data set consists of an array of 1D spectra corresponding to different delay times, τ. One of the most common methods of analyzing experimental relaxation data has three independent steps: obtain peak intensities at a certain chemical shift from each array slice, plot the intensity as a function of time, and then fit to a model describing the decay or build-up of intensity to determine the relaxation time constant. This type of analysis does not provide an accurate determination of time constants when there are overlapping signals present. In contrast, the 3D-fitting procedure incorporates peak separation to address issues with spectral overlap.

As part of the analysis, spectra were deconvolved to separate overlapping signals and obtain the following parameters for each peak: chemical shift, peak amplitude, width, and the fraction of Lorentzian character, α. Initial estimates of these four parameters were obtained through deconvolution of the time point with highest intensity (ex. τ = 0.1 s for the ^{13}C T_1 experiments). Depending on the sample, the peaks were considered as pure Lorentzian (α = 1), pure Gaussian (α = 0), or a linear combination of a Lorentzian and a Gaussian function, *F*:

$$F(\delta; \delta_i, w_i, \alpha) = (\alpha)\left[\left(\frac{\delta-\delta_i}{w_i}\right)^2 + 1\right]^{-1} + (1-\alpha)\left[e^{\left(-\frac{-4\ln 2}{w_i^2}(\delta-\delta_i)^2\right)}\right] \quad \text{(Eqn. 3.4)}$$

where α = fraction Lorentzian, 1 - α = fraction Gaussian, and δ_i and w_i are the peak position and line width, respectively, of the i^{th} component. *F* yields the sum of a Lorentzian lineshape with height = α, and a Gaussian lineshape with height = 1 - α, therefore, the height at the center of the overall lineshape is 1.

For comparison, the SPORT-NMR method[17] also incorporates peak separation into its algorithm to determine NMR relaxation times. Briefly, the spectrum at each time point is independently deconvolved, the resulting intensities are plotted against time, and finally, the curve is fit to the target equation. However, the 3D-fitting algorithm utilized in this study differs from SPORT because the peaks and time constants are fit simultaneously.

For 3D-fitting, spectral fitting and time constant optimization are simultaneously executed. The relaxation data is considered as a 3D object (S) defined by a function of the chemical shift (δ) and delay time (τ):

$$S^{fit}(\delta,\tau) = \sum_i \mathrm{a}_i * F(\delta;\delta_i,\mathrm{w}_i,\%\mathrm{G/L}) * I(\tau;T_{\mathrm{xi}}) \qquad \text{(Eqn. 3.5)}$$

where a_i is the amplitude of the i^{th} component and $I(\tau;T_{xi})$ corresponds the appropriate model of intensity decay, build-up, or build-up then decay (Equation 3.1, 3,2, or 3.3). T_{xi} is the NMR time constant(s) of the i^{th} component with x = 1, 1ρ, or CH. Then, the difference between the experimentally observed (S^{obs}) and fitted 3D (S^{fit}) surfaces is minimized,

$$\min ||\ S^{obs}(\delta,\tau) - S^{fit}(\delta,\tau)|| \qquad \text{(Eqn. 3.6)}$$

to obtain a_i and T_{xi} simultaneously. Time constant $T_{xi} = T_{1i}$ for the cases of Eqn. 3.1 and 3.2, and $T_{xi} = T_{CH\,i}$ and $T_{1\rho i}$ for the case of Eqn. 3.3. Chemical shifts, linewidths, and fraction Lorentzian character were held constant for this application of the 3D-fitting procedure.

Monte-Carlo simulations were used to estimate the error of fitting. First, an ideal 3D surface was prepared based on the estimated parameters from 3D-fitting (described above). Then, synthetic, random noise with the same RMS level as the experimental spectra was added to the surface. This procedure was repeated 100 times per relaxation experiment to produce simulated data with different sets of random noise. Monte-Carlo simulations of the 3D-fitting were then performed on these data, and the standard deviation (σ) for each ^{13}C T_1, ^{1}H T_1, ^{1}H $T_{1\rho}$ or T_{CH} value was calculated from the results. Measured time constants are reported with (+/-) values that indicate 2*σ, estimated by this procedure.

MATLAB (R2016b, MathWorks Inc., Massachusetts, USA) programs were utilized for the processing of NMR spectra, deconvolution, and the 3D-fitting analysis.

Non-linear fitting was achieved by the Levenberg-Marquardt algorithm[18-19] using the MATLAB-function ”lsqcurvefit” in the Optimization Toolbox. MestReNova software (version 9, Mestrelab Research, Santiago de Compostela, Spain) was used for the processing of 1D spectra, and preliminary analysis.

3.3 Results and Discussion

3.3.1 Electrospinning of PVA only, incubation in water vapor, and CPMAS

Electrospinning conditions (solution concentration, applied voltage, pump speed, etc.) were optimized to produce a stable fiber stream from the needle tip. Hazardous organic solvents were not needed because PVA is soluble in water and was easily electrospun from aqueous solutions. However, due to water’s relatively low vapor pressure, pump speed, needle-to-collector distance, etc. needed to be carefully monitored to ensure that the deposited material was dry fibers. For example, if the distance between the needle and collector plate was not sufficient, the water would not completely evaporate, resulting in deposition of just solution and not fibers. Once adequate conditions were determined, the desired fiber-like morphology after electrospinning was confirmed under microscope (Figure 3.2A). The observed non-woven fibers were continuous and did not show any significant curvature.

As discussed in Chapter 2, electrospun scaffolds usually have to be water-stabilized prior to use as a biomaterial. The electrospun PVA fibers without further processing were readily soluble in water. Incubation in glutaraldehyde vapors was

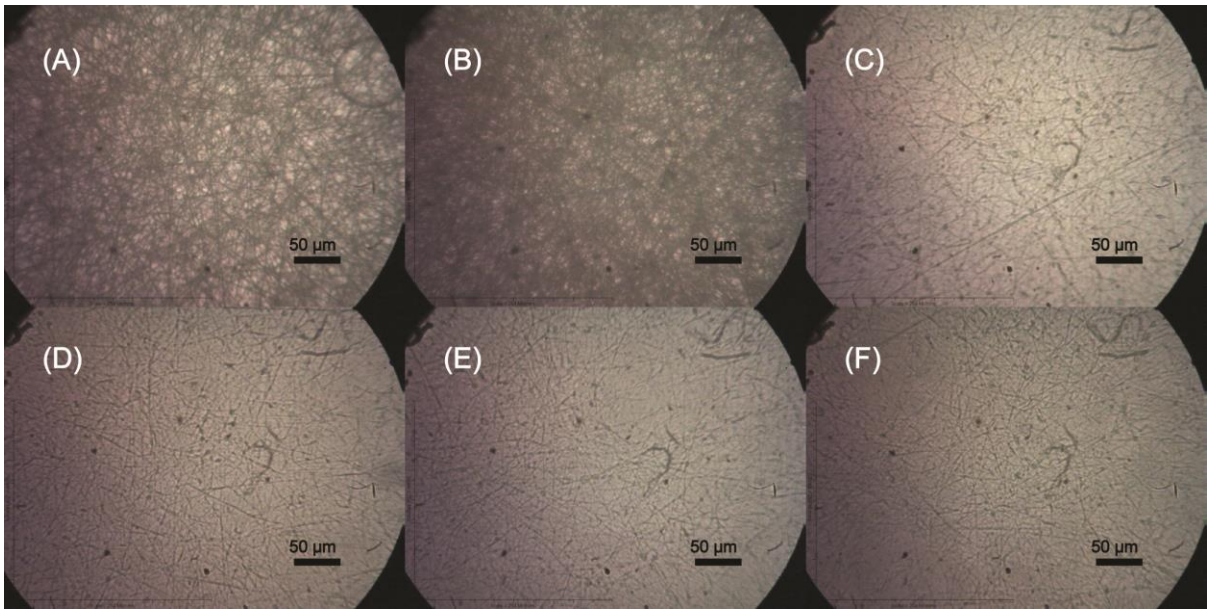

Figure 3.2. Microscope images of electrospun PVA samples at different points of processing: (A) electrospun PVA, dry; (B) electrospun PVA after incubation in water vapor, dry; (C)-(J) water vapor treated electrospun PVA in water after different incubation times: (C) 0 min , (D) 4 h, (E) 6 h, (F) 23 h. Scale bars represent 50 µm.

ineffective in crosslinking the PVA, while incubation in water vapor yielded an insoluble product. Crosslinking of electrospun PVA by glutaraldehyde vapors has been reported in the literature[20], but only when the starting solution was adjusted to a low pH before spinning. Initially, the electrospun samples were incubated in water vapor as a control to test the effectiveness of the aqueous glutaraldehyde vapors for crosslinking. Water vapor treatment of electrospun PVA fibers has been reported in the literature[21]. The authors claim that the fibers are annealed under the humid conditions, which subsequently enhances PVA crystallinity.

Incubation in water vapor after electrospinning produced PVA fibers that retained their fiber-like morphology and were stable in water for extended periods of time. PVA

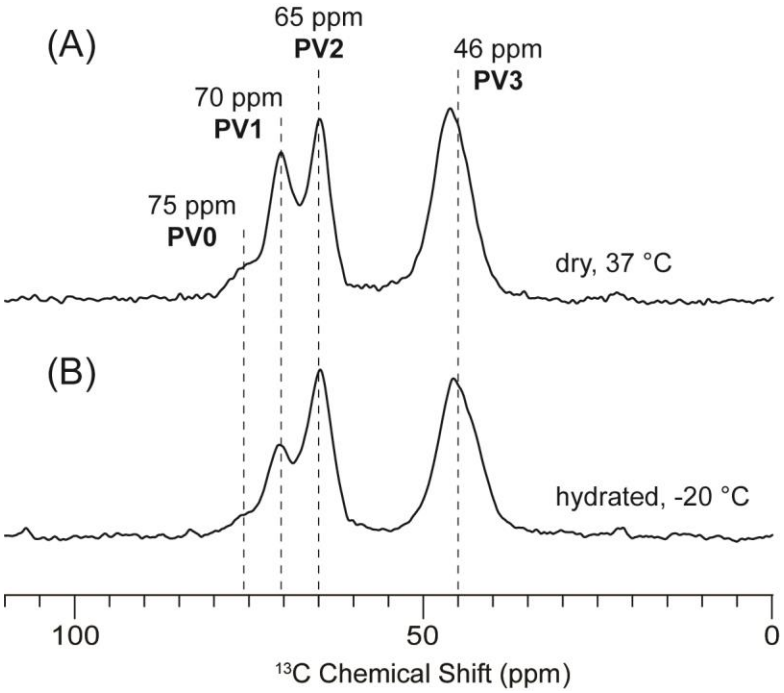

Figure 3.3. ^{13}C CPMAS NMR spectra of electrospun PVA. (A) Electrospun PVA, dry, (B) electrospun PVA after incubation in water vapor, hydrated, frozen. (A) was acquired at 37°C with 512 scans, (B) was acquired at -20 °C with 1024 scans. Both had a 1 ms contact time. Vertical dashed lines indicate chemical shifts of resolved peaks.

after treatment in water vapor were placed in water for different lengths of time to test solubility and observe the effects of water on morphology. Upon submersion in water, the fibers appeared to immediately swell, but not dissolve (Figure 3.2C). Further incubation was continued for a total of 23 hours, and microscope images were acquired at intermediate time points (Figure 3.2, D-F). No significant changes were observed throughout the test period, so it was assumed that the PVA sample remains insoluble for extended periods of time. Once a water-stable product was obtained, 1D NMR spectra were taken to further analyze the dry and hydrated electrospun PVA samples.

Table 3.1. ^{13}C Chemical shift assignments for major features in the CPMAS NMR spectra of PVA.

	^{13}C δ(ppm)	Assignments	# H-bonds
PV0	75	H**C**-OH	Two
PV1	70	H**C**-OH	One
PV2	65	H**C**-OH	None
PV3	46	**C**H_2	--

CPMAS spectra of the electrospun PVA, **Figure 3.3,** have chemical shifts and lineshapes that are comparable to what has been reported in the literature.[4,22] Chemical shifts and assignments of the PVA samples are summarized in **Table 3.1**. The peak at 46 ppm corresponds to the CH_2 carbons. The remaining three peaks at 75, 65, and 60 ppm are assigned to the CH carbons covalently bonded to OH groups. The distribution of the CH chemical shifts is attributed to the formation of two, one, or no intramolecular hydrogen bonds, respectively.[4] In addition to intramolecular hydrogen bonding, conformational effects on the ^{13}C chemical shifts have been previously reported.[22]

The CPMAS spectra for electrospun PVA in the dry (Figure 3.3A) and hydrated/frozen (Figure 3.3B) states have subtle differences. The three CH chemical shifts are similar, but the PVA CH_2 peak is slightly shifted upfield upon the addition of water to the system (Figure 3.3). Masuda and co-workers have reported a distribution of chemical shifts for the CH_2 carbons in PVA arising from the *γ*-gauche effect.[23] Another possible explanation for the chemical shift discrepancy could be a change in the packing arrangement of the PVA in the presence of water.[24] The effects of hydration on the dynamics of the PVA samples will be discussed in the next subsection.

3.3.2 NMR relaxation measurements reflect the effects of water on the dynamics of electrospun PVA

NMR relaxation time constants ^{13}C T_1, T_{CH}, ^{1}H $T_{1\rho}$ and ^{1}H T_1 were determined for the resolved peaks in the CPMAS spectra of dry and hydrated electrospun PVA samples at -20 °C. The dry sample is electrospun PVA without further processing; the hydrated sample is PVA after electrospinning, incubation in water vapors, and rinsing and hydration with water. The hydrated sample is then swelled in water at room temperature before cooling to -20 °C immediately prior to NMR measurements. The peak at 75 ppm (PV0) is excluded from this analysis due to low signal in the hydrated state. In this section, the relaxation times are used to observe the effects of hydration on electrospun PVA.

Table 3.2. ^{13}C T_1 values (s) for electrospun PVA samples at -20 °C.

	^{13}C δ (ppm)	'Hydrated'		'Dry'	
		^{13}C T_1 (s)	+/-	**^{13}C T_1 (s)**	+/-
PV1	70	16.6	5.6	93.1	11.2
PV2	65	10.7	2.0	95.6	11.2
PV3	46	14.8	3.7	81.5	9.8

Table 3.3. T_{CH} values (μs) for electrospun PVA samples at -20 °C.

	^{13}C δ (ppm)	'Hydrated'		'Dry'	
		T_{CH} (μs)	+/-	**T_{CH} (μs)**	+/-
PV1	70	44	12	55	5
PV2	65	43	9	52	2
PV3	46	26	5	37	3

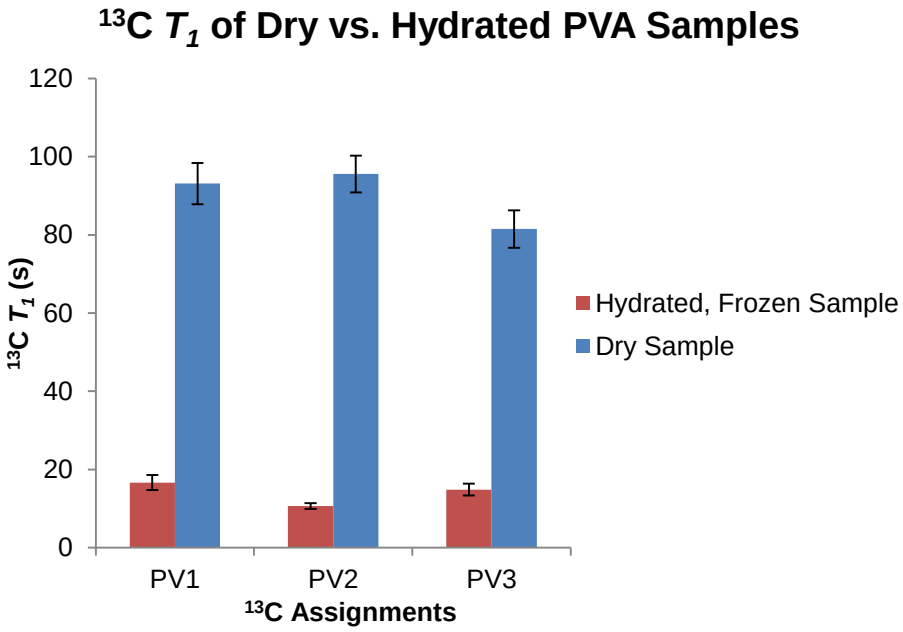

Figure 3.4. ^{13}C T_1 values (s) for resolved peaks in electrospun PVA samples at -20 °C. Blue and red bars correspond to the 'dry' and 'hydrated, frozen' samples, respectively. Error bars correspond to the error determined by the fitting procedure.

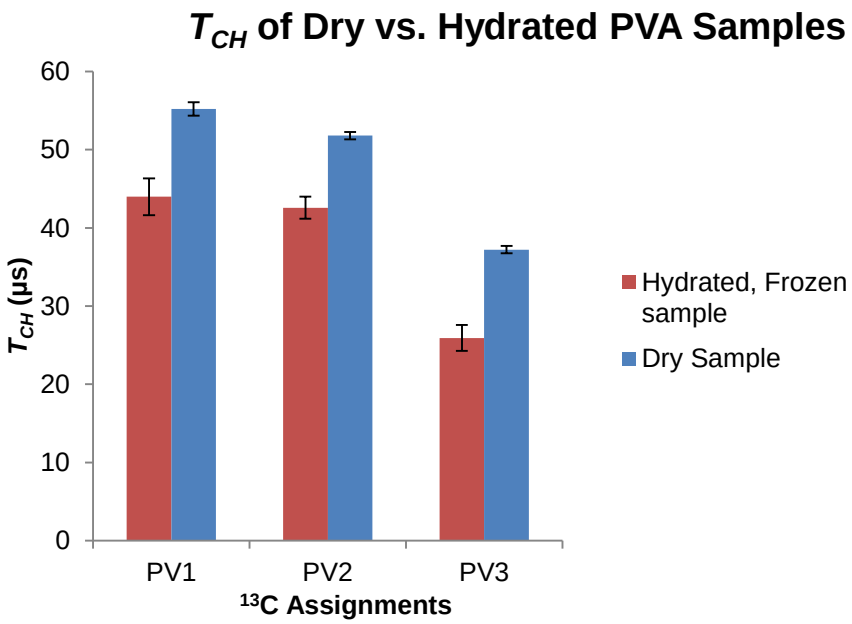

Figure 3.5. T_{CH} values (µs) for resolved peaks in electrospun PVA samples at -20 °C. Blue and red bars correspond to the 'dry' and 'hydrated, frozen' samples, respectively. Error bars correspond to the error determined by the fitting procedure.

The ^{13}C spin-lattice relaxation times, T_1, were obtained by the method of Torchia (Table 3.2 and Figure 3.4). In general, shorter ^{13}C T_1 values are observed in the frozen, hydrated sample. Values for the dry PVA sample are 81.5 s for the CH_2's, and 95.6 s and 93.1 s for the two COH carbons, PV2 and PV1, respectively. The time constants corresponding to the hydrated, frozen PVA are 14.8 s, 10.7 s, and 16.6 s for PV3, PV2, and PV1, respectively. The decrease in ^{13}C T_1 values implies that the relaxation mechanisms on this time scale are influenced by the presence of water through either a change in mobility or PVA-water interactions.

The carbon-proton cross-polarization time constant, T_{CH}, and ^1H spin-lattice relaxation time in the rotating frame, $T_{1\rho}$, were determined simultaneously by an arrayed CP contact-time experiment. As described in Chapter 2, T_{CH} values are used to comment on the relative rigidities of the samples with short values indicating reduced motion and high values corresponding to higher mobility. T_{CH} time constants for PVA are summarized in **Table 3.3** and visualized in **Figure 3.5**. Values corresponding to the two COH carbons were 55 and 52 μs for the dry, and 44 and 43 μs for the hydrated sample. T_{CH}'s of the CH_2's were 37 and 26 μs for the dry and hydrated states, respectively.

The ^{13}C-resolved proton relaxation time constants are measured to probe the homogeneity of the samples. On the contact-time-arrayed plot, ^1H $T_{1\rho}$ values correspond to the decay of intensity after initial buildup from T_{CH} (Table 3.4 and Figure 3.6). The measured values appeared relatively homogenous for either sample condition, but there is a general trend to lower values in the hydrated sample. In the dry state, measured ^1H $T_{1\rho}$ values were generally in the range of 4-5 ms, while in the hydrated state they were around 2-3 ms. Inversion recovery with indirect detection through resolved ^{13}C peaks

was used to determine ^{1}H T_1 values (Table 3.5 and Figure 3.7). Similar to the case of ^{1}H $T_{1\rho}$, measured ^{1}H T_1's were homogenous within each sample, and there is a general trend to shorter values for the hydrated sample. ^{1}H $T_{1\rho}$ time constants were ~0.4-0.5 s and 7-8 s for the hydrated and dry states, respectively. For both ^{1}H $T_{1\rho}$ and T_1, each sample data set has relatively homogeneous time constant values, implying there are no significant heterogeneities in the structural organization of the polymer in the electrospun sample. The trend towards shorter values upon hydration indicate that water uniformly influence the relaxation mechanisms of the samples in the domain sizes probe-able by ^{1}H $T_{1\rho}$ and T_1 experiments.

Table 3.4. ^{1}H $T_{1\rho}$ values (ms) for electrospun PVA samples at -20 °C.

	^{13}C δ (ppm)	'Hydrated'		'Dry'	
		^{1}H $T_{1\rho}$ (ms)	+/-	^{1}H $T_{1\rho}$ (ms)	+/-
PV1	70	3.5	1.1	4.9	0.4
PV2	65	2.3	0.7	4.1	0.2
PV3	46	2.3	0.7	4.6	0.3

Table 3.5. ^{1}H T_1 values (s) for electrospun PVA samples at -20 °C.

	^{13}C δ (ppm)	'Hydrated'		'Dry'	
		^{1}H T_1 (s)	+/-	^{1}H T_1 (s)	+/-
PV1	70	0.48	0.11	8.6	0.6
PV2	65	0.46	0.04	8.3	0.4
PV3	46	0.43	0.04	6.9	0.4

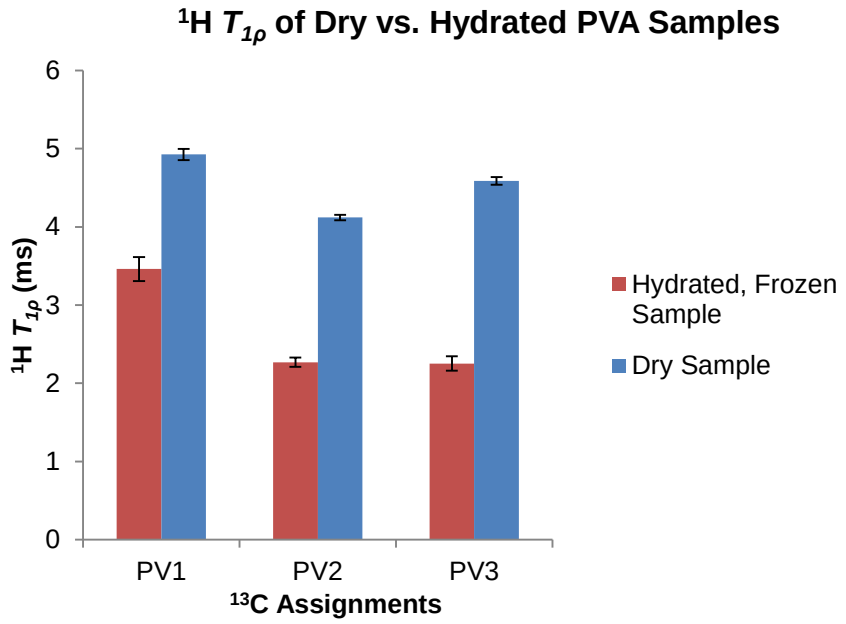

Figure 3.6. ^{1}H $T_{1\rho}$ values (ms) for electrospun PVA samples at -20 °C. Blue and red bars correspond to the 'dry' and 'hydrated, frozen' samples, respectively. Error bars correspond to the error determined by the fitting procedure.

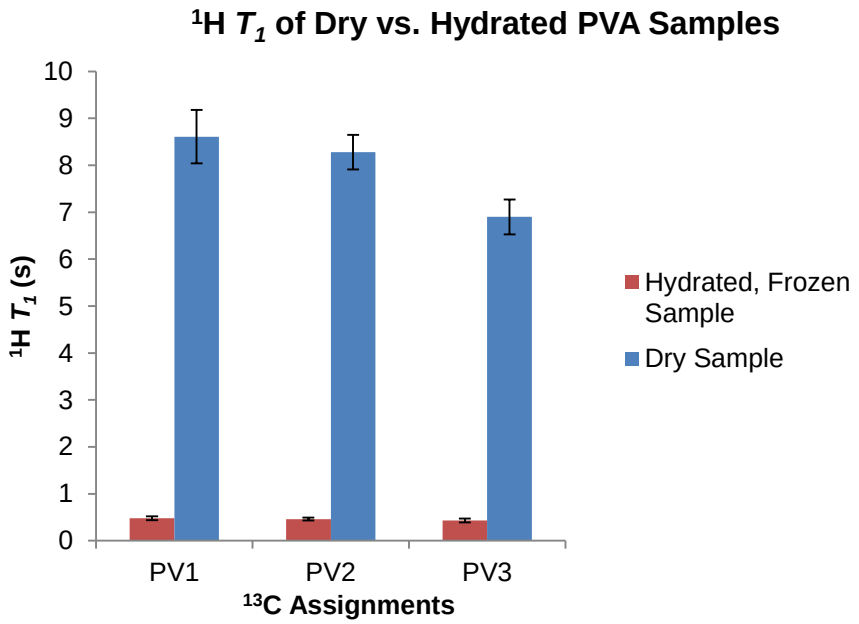

Figure 3.7. ^{1}H T_{1} values (s) for electrospun PVA samples at -20 °C. Blue and red bars correspond to the 'dry' and 'hydrated, frozen' samples, respectively. Error bars correspond to the error determined by the fitting procedure.

The effect of water on the electrospun PVA samples was investigated using NMR relaxation experiments. Shorter ^{13}C T_1 values in the hydrated sample imply that water affects the relaxation mechanisms of PVA through polymer-water interactions, such as dipole-dipole, or possibly motional changes. Comparisons of the T_{CH}'s in the dry and hydrated samples suggest that the PVA is more rigid in the presence of water at -20 °C. Both proton relaxation time constants indicated that there were no significant heterogeneities within either the dry or the hydrated sample on the scales probe-able by the ^{1}H $T_{1\rho}$ and T_1 experiments. In the following sections, a similar approach will be used to characterize electrospun blends of PVA and elastin.

3.3.3 Preparation of PVA-elastin blends and CPMAS

Electrospun blends of PVA and elastin have not been reported in the literature, so optimization of the electrospinning conditions was needed. Different solvent systems were tested, including HFIP, water/ethanol, water/acetone, etc., but, ultimately, 100% water was selected because it was able to readily dissolve both PVA and elastin. Another consideration was that water is a non-toxic alternative to common electrospinning solvents like HFIP, DCM, etc. Once the solvent was selected, different polymer concentrations and ratios were tested before settling on a combination that yielded adequate fibers. Finally, similar to the case of electrospinning PVA only, experimental parameters (pump speed, needle-to-collector distance, etc.) were carefully monitored to ensure that the deposited material was dry fibers and not just solution.

The blend of PVA and soluble elastin was electrospun from an aqueous solution with no organic solvents or other additives (Figure 3.8). PVA-elastin solutions were

prepared by dissolving soluble elastin (from section 2.2.3) in water and adding the appropriate amount PVA solution (section 3.2.2) to obtain the desired concentration and composition. Total solute concentrations were typically ~20-27 wt% in water with a 1:1 ratio of PVA/elastin by mass. Electrospun fibers were observed under microscope to verify fiber-like morphology (Figure 3.8C).

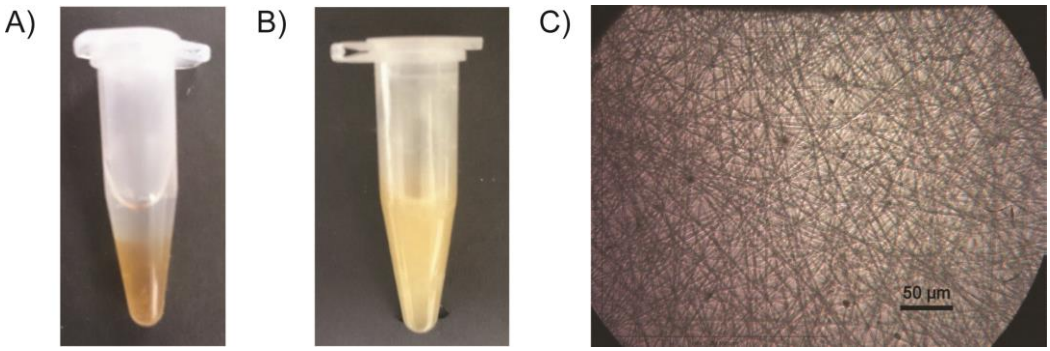

Figure 3.8. PVA-Elastin blend solution (A) before mixing, (B) after mixing, and (C) observed under microscope after electrospinning. Scale bar represents 50 µm.

The electrospun PVA-elastin fiber mats were then crosslinked in glutaraldehyde vapor (section 3.2.2), yielding a water-stable product. The PVA-elastin blends were crosslinked using the same procedure as *elastin-only* (Chapter 2). Both PVA and elastin appeared to be retained in the sample even after multiple rinses in water. In contrast, water-vapor treatment of the blend was not an efficient method of crosslinking, because a large amount of elastin was lost after rinsing. After crosslinking by glutaraldehyde, the PVA-elastin blends were incubated in water for extended periods of time to verify their insolubility (pictures not shown). The water-stable electrospun PVA-elastin sample was then further analyzed by SSNMR spectroscopy.

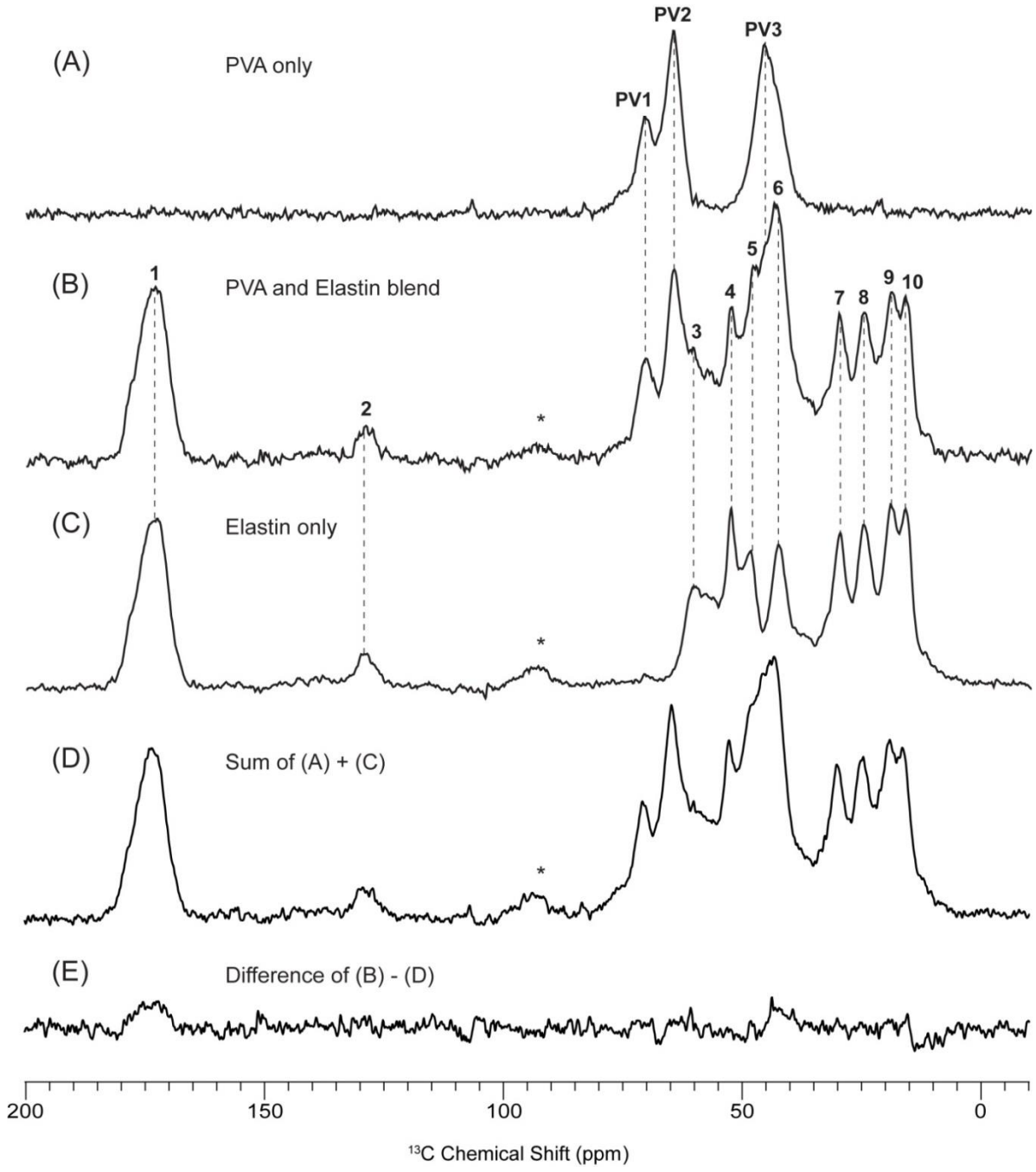

Figure 3.9. ^{13}C CPMAS NMR spectra of electrospun PVA-elastin blend and components. (A) PVA only, (B) PVA-Elastin blend, (C) elastin only, (D) the sum spectrum [(A)+(C)], and (E) the difference spectrum [(B)-(D)]. Elastin-containing samples were crosslinked with glutaraldehyde, and *PVA-only* was incubated in water vapor. Samples were hydrated with water before lowering the temperature and subsequent acquisition. All spectra were taken at -20 °C with 1024 scans, and a 1 ms contact time. Vertical dashed lines indicate chemical shifts of resolved peaks. Spinning side bands are indicated by asterisks (*).

Table 3.6. ^{13}C Chemical shift assignments for major features in the ^{13}C CPMAS NMR spectra of prepared PVA-Elastin blend.

	^{13}C δ(ppm)	Assignments[8]	Polymer
1	173	Carbonyl carbons	Elastin
2	129	Aromatic carbons	Elastin
PV1	70	C-OH	PVA
PV2	65	C-OH	PVA
3	60	Pro Cα & Val Cα	Elastin
4	53	Ala Cα	Elastin
5	49	Pro Cδ	Elastin
PV3	46	CH_2	PVA
6	43	Gly Cα	Elastin
7	30	Pro Cβ & Val Cβ	Elastin
8	25	Pro Cγ	Elastin
9	19	Val Cγ	Elastin
10	16	Ala Cβ	Elastin

The CPMAS spectrum of the electrospun, crosslinked PVA-elastin blend showed evidence that both PVA and elastin components were retained in the sample after rinsing with water (Figure 3.9). Dashed lines originating from the component spectra (Figure 3.9A and 3.9C) trace the chemical shifts of the major resolved peaks to their respective positions in the spectrum of the blend (Figure 3.9B). The chemical shifts and assignments for the blend are summarized in **Table 3.6**. Chemical shifts of elastin and PVA were previously discussed in sections 2.3.2 and 3.4.1, respectively. There appears to be no drastic change of chemical shift or line shapes for elastin and PVA when in the blend.

The sum spectrum of the two individual component spectra (Figure 3.9D) was not significantly different from the spectrum of the blend (Figure 3.9B). The component spectra were scaled by height before addition to minimize the difference between the sum spectrum and the experimentally observed, target spectrum (Figure 3.9B). Subsequently, the difference spectrum (Figure 3.9E) of the sum spectrum and *PVA-Elastin blend* is close to null, indicating that there are no large differences between the sum of intensity of the individual components and the blend as detected by CPMAS experiments. In the next section, NMR relaxation measurements are used to further characterize the electrospun PVA-elastin blend.

3.3.4 NMR relaxation measurements for PVA-Elastin blend

NMR relaxation time constants were measured to probe the effects of water on the blended sample and the compatibility of the two polymers. Specifically, ^{13}C T_1, T_{CH}, ^{1}H $T_{1\rho}$ and ^{1}H T_1 were determined for the resolved peaks in the CPMAS spectra of both dry and hydrated electrospun, PVA-elastin blends at -20 °C. The aromatic carbons in elastin at 129 ppm and are omitted from this analysis due to the low signal-to-noise in the hydrated spectra. Deconvolution results give two peaks for the PVA CH_2, 46 and 43 ppm. The upfield PVA CH_2 peak and Gly Cα both appear at 43 ppm, and therefore, their values are not discussed due to the severe overlap. Consequently, the PVA CH_2 is represented only by the peak at 46 ppm. Comparisons are made for the dry and hydrated blend samples, as well as the elastin and PVA in the blend vs. the components as homopolymers.

^{13}C spin-lattice relaxation times, T_1, were obtained by the method of Torchia[20] (Table 3.7 and Figure 3.10). There was a general trend to shorter ^{13}C T_1 values in the hydrated sample for all of the PVA peaks and all of the elastin peaks besides the methyl carbons. The values corresponding to PV1, PV2, and PV3 were 91.9, 119.8, and 88.1 s for the dry sample and 31.0, 16.8, and 23.5 s in the hydrated sample. ^{13}C T_1 of the carbonyl in elastin was 33.4 s for the dry and 22.6 s for the hydrated state. Values for Pro Cα &Val Cα (60 ppm) and the Ala Cβ (16 ppm) peaks decreased in the presence of water from 20.3 to 16.8 s and 19.0 to 10.5 s, respectively. Pro Cδ (49 ppm) had a value of 17.4 s for the dry and 7.0 s for the hydrated sample. Side-chain carbons Pro Cβ & Val Cβ (30 ppm) and Pro Cγ (25 ppm) decreased from 11.6 to 6.5 s and 8.4 to 3.1 s upon hydration. There was no noticeable difference in the values corresponding to the two methyl peaks at 19 and 16 ppm (either 0.3 or 0.4 s). This trend to shorter ^{13}C T_1 values in the presence of water was also observed for both components, individually.

There were no uniform changes observed from comparisons of the dry component samples with the blend. ^{13}C T_1's for PVA peaks in the dry sample did not appear to differ in the blend compared to the PVA only. There was no overall trend for the values corresponding to elastin. The carbonyl and methyl ^{13}C T_1's did not appear to change, while the value for Pro Cα &Val Cα showed a decrease from 25.5 s to 20.3 s when in the blend. All other elastin peaks trended to slightly longer values when present in the blend with PVA.

In the hydrated samples, values corresponding to PVA all increase when in the blend, but there was no overall trend for the elastin values. ^{13}C T_1's of PVA ranged from 10.7-16.6 s for *PVA-only*, and increased to 16.8-31.0 s in the blend. Assuming that all

Table 3.7. ^{13}C T_1 values (s) for resolved ^{13}C peaks in electrospun, crosslinked, Elastin only, PVA-elastin blend, and PVA only at -20 °C.

		'Hydrated, frozen'						'Dry'					
		Elastin only		PVA-Elastin blend		PVA only		Elastin only		PVA-Elastin blend		PVA only	
	^{13}C δ (ppm)	^{13}C T_1 (s)	+/-	^{13}C T_1 (s)	+/-	^{13}C T_1 (s)	+/-	^{13}C T_1 (s)	+/-	^{13}C T_1 (s)	+/-	^{13}C T_1 (s)	+/-
1	173	18.2	0.8	22.6	3.0			33.6	0.9	33.4	2.5		
PV1	70			31.0	9.9	16.6	5.6			91.9	13.6	93.1	11.1
PV2	65			16.8	3.3	10.7	2.0			119.8	12.3	95.6	11.2
3	60	9.9	1.3	16.8	7.5			25.5	3.4	20.3	3.5		
4	53	12.5	1.1	10.5	2.2			15.3	1.2	19.0	1.7		
5	49	5.2	0.7	7.0	1.6			9.9	1.0	17.4	3.9		
PV3	46			23.5	5.9	14.8	5.1			88.1	32.3	81.5	9.8
7	30	5.7	0.5	6.5	1.4			8.2	0.6	11.6	23.4		
8	25	4.3	0.5	3.1	0.9			7.0	0.6	8.4	1.2		
9	19	0.3	0.02	0.4	0.1			0.3	0.03	0.3	1.5		
10	16	0.4	0.1	0.3	0.1			0.4	0.1	0.4	0.04		

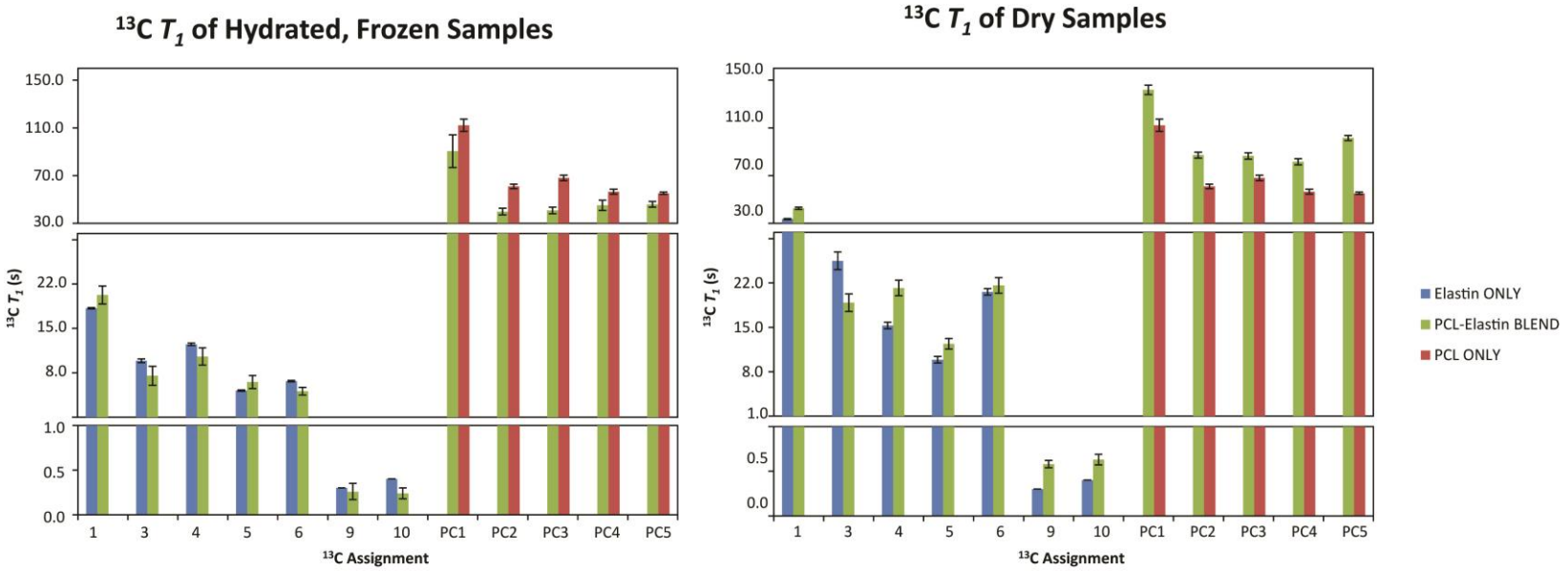

Figure 3.10. ^{13}C T_1 values (s) for select peaks in electrospun, crosslinked, Elastin only (blue), PVA-elastin blend (green), and PVA only (red) at -20 °C. Error bars correspond to the error determined by the fitting procedure.

other factors affecting ^{13}C T_1 are equal, this trend to longer values for PVA may imply that the polymer is more rigid in the hydrated blend. No general trend was observed for elastin in the PVA blend. Time constants for the carbonyl, Pro Cα &Val Cα, and Pro Cδ all increased when in the blend. ^{13}C T_1 for Ala Cα showed a slight decrease when present in the PVA blend. Finally, the side-chain and methyl carbons did not show any significant change in the blend sample compared to *elastin-only*.

T_{CH} values correspond to the intensity build-up on the CP contact-time plot array and are used to comment on the relative rigidities of the samples (Table 3.8 and Figure 3.11). There were no overall trends in T_{CH} when comparing the PVA-elastin blend sample in the dry to hydrated state. The PVA values in the blend all decreased upon hydration. The values corresponding to PV1, PV2, and PV3 were 58, 88, and 57 μs for the dry sample and 49, 47, and 27 μs in the hydrated sample. This trend to shorter time constants in the hydrated state was similar to trend observed for PVA only samples.

For the elastin values in the blend, some T_{CH}'s increased, some decreased, and some remained relatively the same upon hydration. Longer values were observed for the carbonyl (173 ppm), Pro Cα &Val Cα (60 ppm), and the Ala Cβ (16 ppm) peaks in the hydrated state. The values corresponding to carbonyl carbons were 436 and 518 μs for the dry and hydrated states, respectively. T_{CH}'s for the peaks at 60 and 16 ppm increased from 22 to 39 μs and 120 to 166 μs, respectively, upon the introduction of water into the system. Shorter T_{CH}'s were observed in the hydrated state for Pro Cδ (49 ppm), Pro Cγ (25 ppm), and Val Cγ (19 ppm) peaks. Upon the introduction of water, values decreased from 40 to 31 μs for the peak at 49 ppm, 57 to 40 μs for the peak at

Table 3.8. T_{CH} **values (** μ **s) for resolved** ^{13}**C peaks in electrospun, crosslinked, Elastin only, PVA-elastin blend, and PVA only at -20 °C.**

		'Hydrated, frozen'						'Dry'					
		Elastin only		PVA-Elastin blend		PVA only		Elastin only		PVA-Elastin blend		PVA only	
	^{13}C δ (ppm)	T_{CH} (μs)	+/-	T_{CH} (μs)	+/-	T_{CH} (μs)	+/-	T_{CH} (μs)	+/-	T_{CH} (μs)	+/-	T_{CH} (μs)	+/-
1	173	499	22	518	26			390	12	436	19		
PV1	70			49	6	44	12			58	10	55	5
PV2	65			47	4	43	9			88	9	52	2
3	60	46	13	39	6			13	7	22	8		
4	53	83	8	46	4			42	5	45	8		
5	49	75	12	31	4			45	6	40	6		
PV3	46			27	4	26	5			57	7	37	3
7	30	30	13	29	4			32	4	32	6		
8	25	123	14	40	6			53	4	57	10		
9	19	203	11	141	13			184	9	238	21		
10	16	175	14	166	16			152	11	120	15		

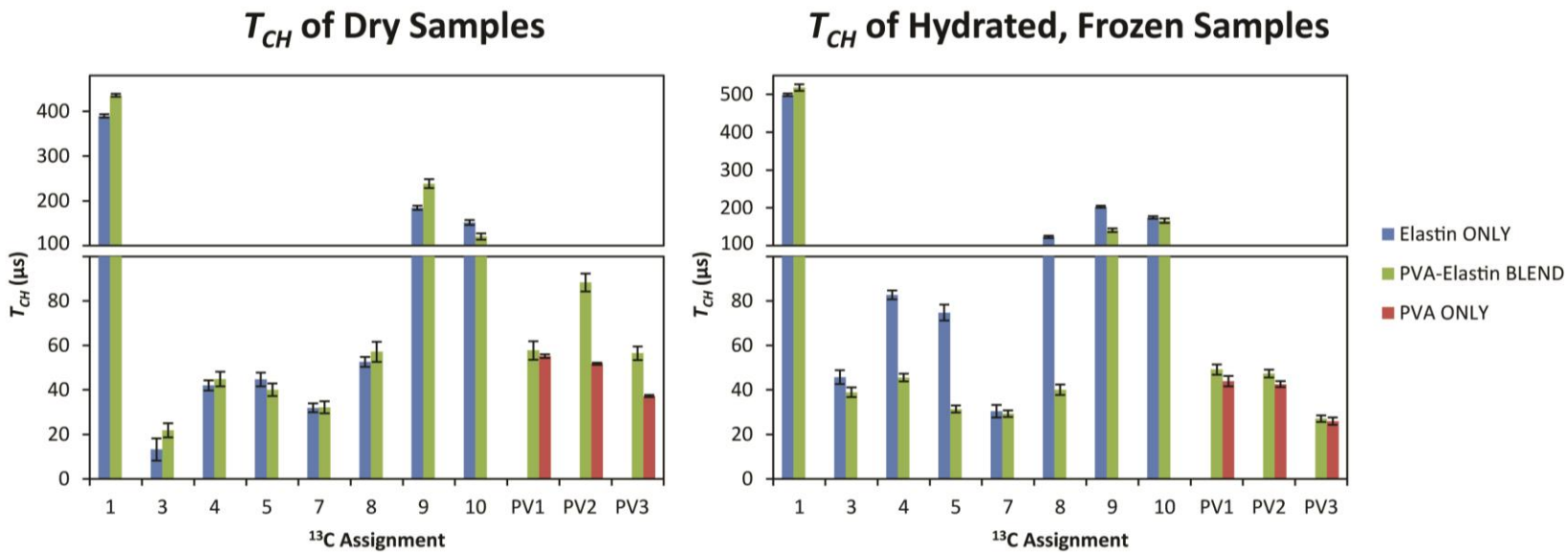

Figure 3.11. T_{CH} values (µs) for select peaks in electrospun, crosslinked, Elastin only (blue), PVA-elastin blend (green), and PVA only (red) at -20 °C. Error bars correspond to the error determined by the fitting procedure.

25 ppm, and 238 to 141 for the peak at 19 ppm. Finally, the peaks corresponding to Ala Cα (53 ppm) and Pro Cβ & Val Cβ (30 ppm) did not appear to drastically change after introducing water to the system. The values corresponding to the dry and hydrated states were 45 and 46 μs for the peak at 53 ppm and 32 and 29 μs for the peak at 30 ppm.

There were no drastic changes in T_{CH} when comparing the values for *PVA-only* and *elastin-only* to values in the blend. Comparisons between the dry samples showed longer T_{CH} values in the blend for the PVA values, but no drastic change for the elastin peaks. There may be a slight increase in the values for the carbonyl, Pro Cα &Val Cα, and Val Cγ peaks and a slight decreased for the Ala Cβ in the blend. In the hydrated samples, PVA values did not appear to change drastically and most elastin values generally showed a decrease when in the blend. There might be a slight increase for the carbonyl (499 to 518 μs), and there appears to be no difference in the T_{CH} for the Pro Cβ and Val Cβ.

^{1}H $T_{1\rho}$ values correspond to the decay portion of the contact-time arrayed plot (Table 3.9 and Figure 3.12). Values for the dry, PVA-blend were all in the range of 5-6 ms, while they were 6-8 ms and 3-4 ms for elastin and PVA peaks, respectfully, in the hydrated, frozen sample. All of the ^{1}H $T_{1\rho}$'s for the PVA-elastin blend in the dry state converged to a value range intermediate to the two component ranges. The similar values imply that the dry PVA-elastin blend is homogenous on the scale probably by ^{1}H $T_{1\rho}$. However, in the hydrated state, the values corresponding with PVA and elastin were relatively homogenous within each of the two components, but not throughout the whole sample. This may imply that water is interfering with the polymer interactions.

Table 3.9. ^{1}H $T_{1\rho}$ values (ms) for resolved ^{13}C peaks in electrospun, crosslinked, Elastin only, PVA-elastin blend, and PVA only at -20 °C.

		'Hydrated, frozen'						'Dry'					
		Elastin only		PVA-Elastin blend		PVA only		Elastin only		PVA-Elastin blend		PVA only	
	^{13}C δ (ppm)	^{1}H $T_{1\rho}$ (ms)	+/-	^{1}H $T_{1\rho}$ (ms)	+/-	^{1}H $T_{1\rho}$ (ms)	+/-	^{1}H $T_{1\rho}$ (ms)	+/-	^{1}H $T_{1\rho}$ (ms)	+/-	^{1}H $T_{1\rho}$ (ms)	+/-
1	173	6.7	0.3	6.9	0.3			6.7	0.2	5.5	0.2		
PV1	70			3.9	0.5	3.5	1.1			5.9	0.5	4.9	0.4
PV2	65			2.6	0.2	2.3	0.7			5.5	0.3	4.1	0.2
3	60	6.3	0.5	7.6	1.0			7.1	0.6	5.9	0.6		
4	53	7.2	0.3	7.9	0.8			8.2	0.5	6.0	0.5		
5	49	6.4	0.7	6.0	0.6			6.6	0.5	6.2	0.4		
PV3	46			3.6	0.3	2.3	0.7			5.8	0.4	4.6	0.3
7	30	5.7	0.3	6.8	0.7			6.4	0.3	5.3	0.4		
8	25	5.7	0.3	6.2	0.9			6.2	0.3	5.5	0.5		
9	19	6.8	0.3	7.2	0.7			6.9	0.3	4.7	0.3		
10	16	7.4	0.4	7.9	0.7			7.5	0.4	6.3	0.5		

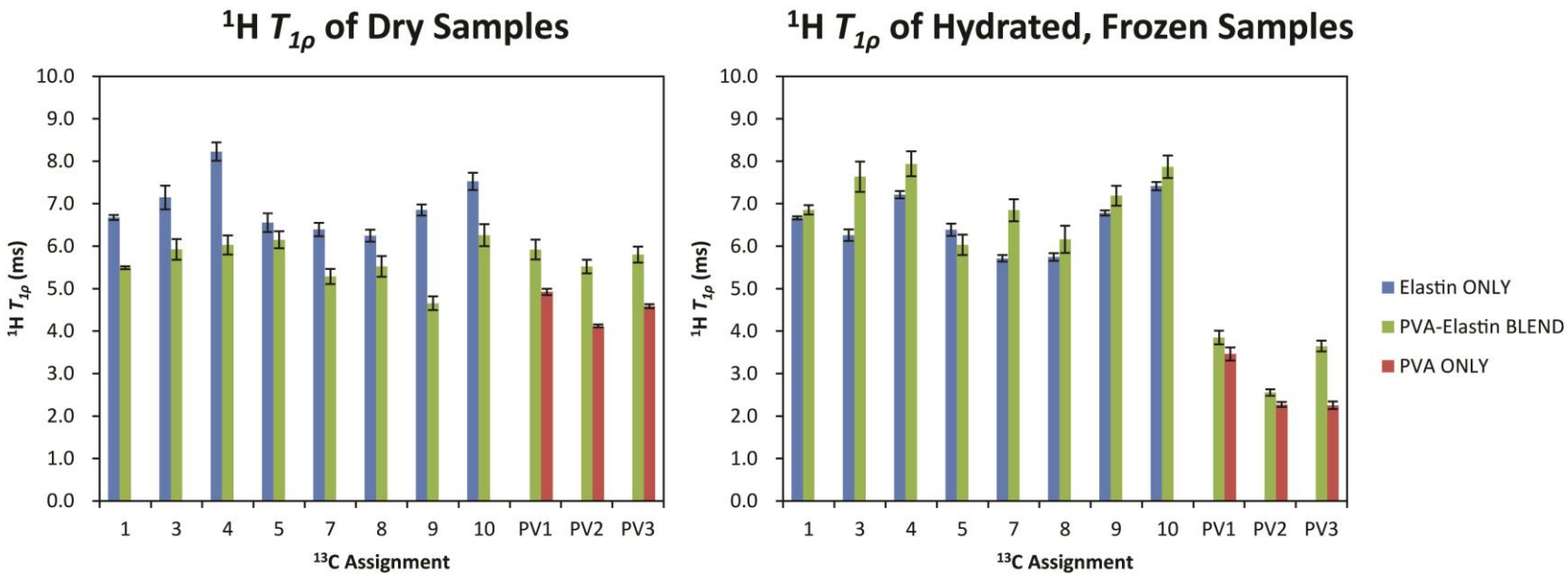

Figure 3.12. ^{1}H $T_{1\rho}$ values (ms) for select peaks in electrospun, crosslinked, Elastin only (blue), PVA-elastin blend (green), and PVA only (red) at -20 °C. Error bars correspond to the error determined by the fitting procedure.

Table 3.10. ^{1}H T_1 values (s) for resolved ^{13}C peaks in electrospun, crosslinked, Elastin only, PVA-elastin blend, and PVA only at -20 °C.

		'Hydrated, frozen'						'Dry'					
		Elastin only		PVA-Elastin blend		PVA only		Elastin only		PVA-Elastin blend		PVA only	
	^{13}C δ (ppm)	^{1}H T_1 (s)	+/-	^{1}H T_1 (s)	+/-	^{1}H T_1 (s)	+/-	^{1}H T_1 (s)	+/-	^{1}H T_1 (s)	+/-	^{1}H T_1 (s)	+/-
1	173	0.40	0.01	0.53	0.02			0.63	0.01	0.8	0.03		
PV1	70			0.67	0.06	0.48	0.11			3.2	0.33	8.6	1.6
PV2	65			0.59	0.03	0.46	0.04			3.0	0.23	8.3	0.8
3	60	0.41	0.06	0.55	0.07			0.62	0.05	1.0	0.12		
4	53	0.38	0.03	0.55	0.05			0.67	0.04	0.9	0.07		
5	49	0.42	0.03	0.59	0.06			0.65	0.05	1.1	0.10		
PV3	46			0.56	0.04	0.43	0.04			2.2	0.14	6.9	0.9
7	30	0.41	0.02	0.56	0.04			0.68	0.05	0.8	0.07		
8	25	0.40	0.02	0.54	0.05			0.65	0.03	0.9	0.08		
9	19	0.38	0.02	0.56	0.05			0.62	0.02	0.8	0.06		
10	16	0.38	0.02	0.50	0.04			0.62	0.03	0.8	0.07		

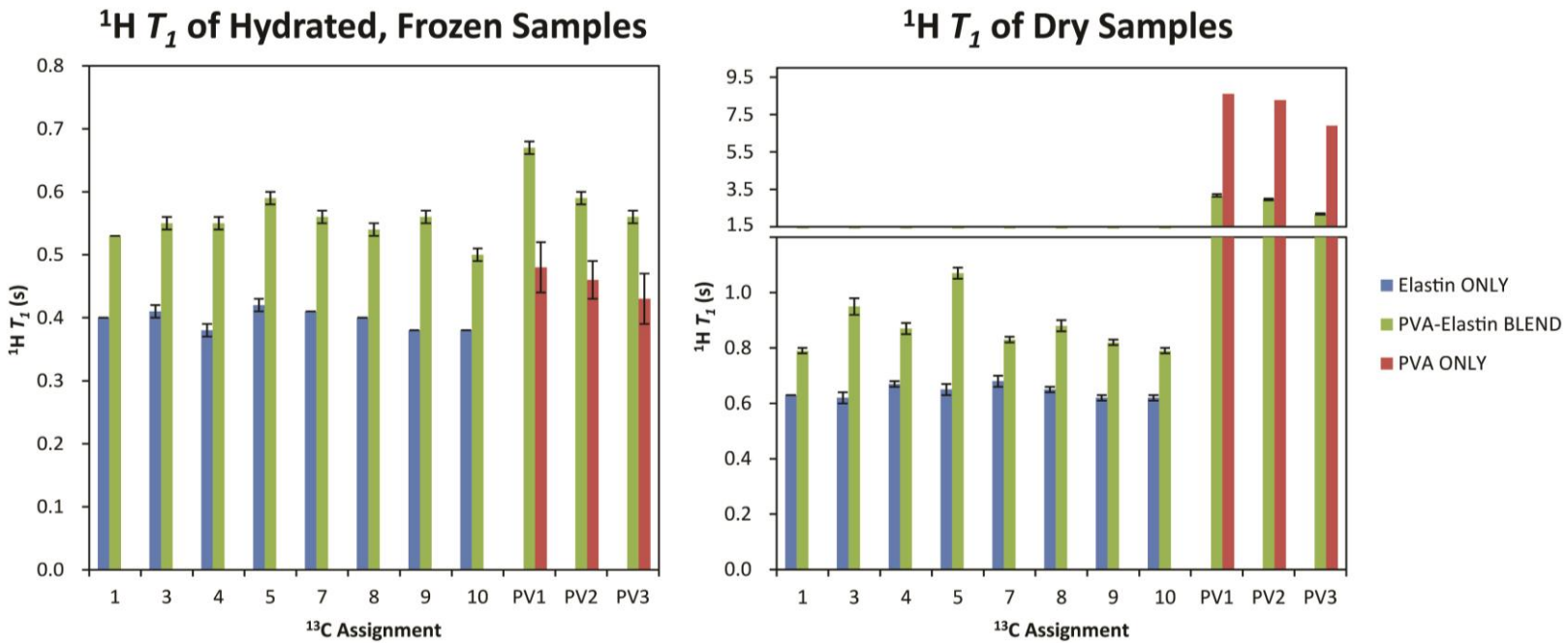

Figure 3.13. ^{1}H T_1 values (s) for select peaks in electrospun, crosslinked, Elastin only (blue), PVA-elastin blend (green), and PVA only (red) at -20 °C. Error bars correspond to the error determined by the fitting procedure.

^{1}H $T_{1\rho}$'s time constants are used to assess the miscibility of the PVA and elastin components in the blended sample. The PVA ^{1}H $T_{1\rho}$ values in the dry state increased when in the blend from 4-5 ms in PVA alone to ~6 ms in the blend. A similar trend of slightly longer values for PVA in the blend was observed for the hydrated sample as well, with 2-3.5 ms for PVA only and 3-4 ms for PVA in the blend. Elastin ^{1}H $T_{1\rho}$'s decreased in the dry PVA-elastin blend from 6-8 ms by itself, to 5-6 ms with the PVA. However, in the hydrated state, the values corresponding to elastin showed a slight increase in the blend, 6-7 ms alone and 6-8 ms in the blend. This is not expected because the values in the blend do not fall intermediate to the two individual components. Perhaps a favored interaction with water is disrupting the interphase between the PVA and elastin domains**.**

^{1}H inversion recovery with indirect detection through resolved ^{13}C peaks was used to determine ^{1}H T_{1} values (Table 3.10 and Figure 3.13). ^{1}H T_{1} values for the blend showed PVA and elastin as two distinct populations when dry, but all values converged in the hydrated sample. In the dry blend, ^{1}H T_{1} values corresponding to elastin are in the range of 0.8-1 s while PVA values are around 2-3 s. In the hydrated PVA-elastin blend, all values from all peaks fell in the range of 0.5-0.7 s. There was an overall trend to shorter times in the hydrated, frozen sample. These observations imply that although PVA and elastin in the dry blend appear to reside in two distinct domains from each other, the sample appears to be more homogenous in the presence of water.

Similar to the ^{1}H $T_{1\rho}$, ^{1}H T_{1} values are used to assess the compatibility of PVA and elastin in the blend. Time constants for the blend in both the dry and hydrated states all lie intermediate to the corresponding values for the components by themselves. For the dry preparations, PVA values all decreased from 7-9 s by itself to 2-3 s for PVA in the

blend. Whereas, values associated with elastin all increased from 0.6-0.7 s in elastin only, to 0.8-1 s in the blend. In the hydrated, frozen state, ^{1}H T_1's corresponding to PVA peaks all increase from ~ 0.4-0.5 s in PVA only, to ~0.6-0.7 s in the blend. Time constants related to elastin peaks all increased from ~0.4 s to ~0.5-0.6 s for *elastin-only* and elastin in the blend, respectively. This 'averaging out' of ^{1}H T_1's observed especially in the dry blend imply intimate interactions between the PVA and elastin components.

3.4 Conclusion

PVA is an attractive candidate for use as a biomaterial due to its abundance, mechanical properties, and biocompatibility. Electrospinning can produce fibers from solutions of a single polymer as well as solutions with more than one component. In this chapter, electrospun *PVA-only* and *PVA-elastin blend* samples were studied using SSNMR spectroscopy.

PVA was electrospun from aqueous solution, and fibers were water-stabilized by treatment with water vapor. CPMAS spectra of the dry and hydrated PVA was similar to what has been reported in the literature.[4, 22-23, 25] The effects of hydration on electrospun PVA was investigated using NMR relaxation measurements. Water appeared to affect the dynamics of the PVA sample.

PVA-elastin blends were prepared by electrospinning from aqueous solutions. Electrospun samples were crosslinked in glutaraldehyde vapors, yielding a water-insoluble product that retained both PVA and elastin components. No drastic

changes were observed on the CPMAS spectra of the blend compared to its components in terms of chemical shift and lineshape. NMR relaxation time constants were determined to investigate the effects of hydration on the blend, in addition to probing for molecular motions and interactions of the component polymers.

Results from the NMR relaxation measurements showed evidence of molecular-level interactions between PVA and elastin in the blend. There were no overall trends for the ^{13}C T_1 and T_{CH} data sets, but the ^{1}H time constants showed changes indicative of polymer-polymer interactions. In the following chapter, blends of PCL and elastin will be discussed and analyzed using a similar strategy.

3.5 References

1. Sakurada, I., *Polyvinyl Alcohol Fibers*. Marcel Dekker, Inc.: New York, New York, 1985.
2. Alves, M. H.; Jensen, B. E. B.; Smith, A. A. A.; Zelikin, A. N., Poly(Vinyl Alcohol) Physical Hydrogels: New Vista on a Long Serving Biomaterial. *Macromol. Biosci.* **2011,** *11* (10), 1293-1313.
3. Chiellini, E.; Corti, A.; D'Antone, S.; Solaro, R., Biodegradation of poly (vinyl alcohol) based materials. *Progress in Polymer Science* **2003,** *28* (6), 963-1014.
4. Masuda, K.; Horii, F., CP/MAS 13C NMR Analyses of the Chain Conformation and Hydrogen Bonding for Frozen Poly(vinyl alcohol) Solutions. *Macromolecules* **1998,** *31* (17), 5810-5817.
5. Hodge, R. M.; Edward, G. H.; Simon, G. P., Water absorption and states of water in semicrystalline poly(vinyl alcohol) films. *Polymer* **1996,** *37* (8), 1371-1376.
6. Hodge, R. M.; Bastow, T. J.; Edward, G. H.; Simon, G. P.; Hill, A. J., Free volume and the mechanism of plasticization in water-swollen poly(vinyl alcohol). *Macromolecules* **1996,** *29* (25), 8137-8143.

7. Huang, C. L.; Peng, S. Y.; Wang, Y. J.; Chen, W. C.; Lin, J. H., Microstructure and characterization of electrospun poly(vinyl alcohol) nanofiber scaffolds filled with graphene nanosheets. *Journal of Applied Polymer Science* **2015,** *132* (17), 11.
8. De Kesel, C.; Lefèvre, C.; Nagy, J. B.; David, C., Blends of polycaprolactone with polyvinylalcohol: a DSC, optical microscopy and solid state NMR study. *Polymer* **1999,** *40* (8), 1969-1978.
9. Mahesh, B.; Nanjundaswamy, G. S.; Gowda, D. C.; Siddaramaiah, Investigation on miscibility behaviors of elastin-like polypentapeptide blends with polyvinyl alcohol in aqueous and solid state. *Journal of Applied Polymer Science* **2017,** *134* (12), 8.
10. Papancea, A.; Valente, A. J. M.; Patachia, S.; Miguel, M. G.; Lindman, B., PVA-DNA cryogel membranes: Characterization, swelling, and transport studies. *Langmuir* **2008,** *24* (1), 273-279.
11. Liu, Y.; Vrana, N. E.; Cahill, P. A.; McGuinness, G. B., Physically Crosslinked Composite Hydrogels of PVA With Natural Macromolecules: Structure, Mechanical Properties, and Endothelial Cell Compatibility. *J. Biomed. Mater. Res. Part B* **2009,** *90B* (2), 492-502.
12. Chang, C.; Lue, A.; Zhang, L., Effects of Crosslinking Methods on Structure and Properties of Cellulose/PVA Hydrogels. *Macromolecular Chemistry and Physics* **2008,** *209* (12), 1266-1273.
13. Asano, A., Polymer Blends. In *Modern Magnetic Resonance*, Webb, G. A., Ed. Springer International Publishing: 2006; pp 631-635.
14. Bennett, A. E.; Rienstra, C. M.; Auger, M.; Lakshmi, K. V.; Griffin, R. G., Heteronuclear decoupling in rotating solids. *J. Chem. Phys.* **1995,** *103* (16), 6951-8.
15. Keeler, J., *Understanding NMR Spectroscopy*. 2nd ed.; John Wilery & Sons Ltd.: West Sussex, United Kingdom.
16. Saito, H. A., Isao; Naito, Akiro, *Solid State NMR Spectroscopy for Biopolymers*. Springer: Dordrecht, The Netherlands, 2006.
17. Geppi, M.; Forte, C., The SPORT-NMR software: A tool for determining relaxation times in unresolved NMR spectra. *J. Magn. Reson.* **1999,** *137* (1), 177-185.
18. Levenberg, K., A Method for the Solution of Certain Non-Linear Problems in Least Squares. *Quarterly of Applied Mathematics* **1944,** *2* (2), 164-168.
19. Marquardt, D. W., An Algorithm for Least-Squares Estimation of Nonlinear Parameters. *Journal of the Society for Industrial and Applied Mathematics* **1963,** *11* (2), 431-441.

20. Destaye, A. G.; Lin, C.-K.; Lee, C.-K., Glutaraldehyde Vapor Cross-linked Nanofibrous PVA Mat with in Situ Formed Silver Nanoparticles. *ACS Applied Materials & Interfaces* **2013,** *5* (11), 4745-4752.
21. Yoshioka, T.; Kawahara, Y.; Tsuji, M.; Schaper, A. K., Structural Modification of PVA Nanofibers by Water Vapor Annealing. *Sen-I Gakkaishi* **2011,** *67* (6), 138-140.
22. Horii, F.; Masuda, K.; Kaji, H., CP/MAS 13C NMR Spectra of Frozen Solutions of Poly(vinyl alcohol) with Different Tacticities. *Macromolecules* **1997,** *30* (8), 2519-2520.
23. Masuda, K.; Kaji, H.; Horii, F., CP/MAS 13C NMR analyses of hydrogen bonding and the chain conformation in the crystalline and noncrystalline regions for poly(vinyl alcohol) films. *Journal of Polymer Science Part B: Polymer Physics* **2000,** *38* (1), 1-9.
24. Tonelli, A. E., Failure of the .gamma.-gauche effect method to predict the stereosequence-dependent carbon-13 NMR spectrum of the disubstituted vinyl polymer atactic poly(methyl methacrylate). *Macromolecules* **1991,** *24* (11), 3065-3068.
25. Masuda, K.; Kaji, H.; Horii, F., Solid-state 13C NMR and 1H CRAMPS investigations of the hydration process and hydrogen bonding for poly(vinyl alcohol) films. *Polym. J. (Tokyo, Jpn.)* **2001,** *33* (4), 356-363.
26. Ohgo, K; Kumashiro, K. K., **2017,** *to be submitted*.

Chapter 4. Characterization of poly(caprolactone) and elastin electrospun blends using SSNMR spectroscopy

4.1 Introduction

Poly(caprolactone), PCL, is a non-toxic, synthetic polymer that has applications in many different fields due to its mechanical properties, biodegradability, and chemical properties.[1] As mentioned in previous chapters, electrospinning is a common method for the production of nanofibers that can be used as biomaterials. Electrospinning can produce fibers of composed of a single polymer, but can also be used for the fabrication of composite materials with two or more components. Composite materials of elastin and PCL and sometimes other polymers have been reported in the literature.[2] However, the characterization of these materials usually focus on more macro-scale properties.

In this chapter, the preparation and subsequent analysis of *PCL-only* and *PCL-Elastin blend* samples will be discussed. First, electrospun PCL in the dry state was analyzed using SSNMR spectroscopy. Then, results from NMR experiments on the electrospun blend of PCL and elastin will be compared to *PCL-only* and *elastin-only* to probe for differences.

4.1.1 Background information on PCL

Poly(caprolactone), PCL, is a semicrystalline, aliphatic polyester with various properties, such as biodegradability, solubility, miscibility with different polymers, etc., that make it a very important and attractive polymer for different applications.[1-3] The mechanical, physical, and thermal properties of PCL are determined by its degree of

crystallinity and molecular weight. Therefore, by manipulating the polymerization and crystallization processes, one can theoretically control the aforementioned properties, as well as the degradability of the polymer.[1]

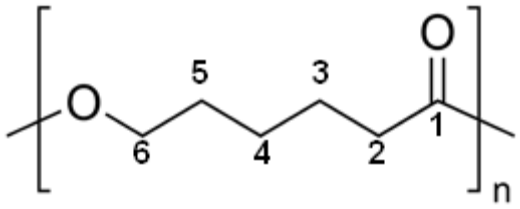

Figure 4.1. Structure of Poly(caprolactone).

The main method of preparing PCL is through a catalyst-driven, ring-opening polymerization of ε-caprolactone.[1] A large number of metal-based, organic, or enzymatic catalytic systems under different conditions have been reported in the literature.[1] The monomer unit of PCL is presented in **Figure 4.1**. Depending on the method of preparation, PCL can have an M_n of 530 to 630,000 g/mol.[1, 4] PCL has a melting point between 59 and 64 °C, and a glass transition temperature, T_g, of -60 °C. Due to its broad range of properties, PCL has many potential uses in various fields such as microelectronics, packaging and adhesives, long-term drug delivery, scaffolds for tissue engineering, etc.[1, 3, 5-6]

3.1.2 PCL-based materials

PCL is an attractive candidate as a biomaterial due to its biodegradability, non-toxicity.[6] PCL has previously been used with elastin and other polymers to create fibrous scaffolds for tissue engineering purposes.[2] Composite materials of

PCL/tropoelastin[7], PCL/collagen/elastin[2], PCL/PGC (poliglecaprone) /elastin/gelatin[2], etc. have been fabricated and investigated as potential vascular replacement engineering applications. Besides vascular repair, combinations of elastin and PCL have also been studied for peripheral nerve regeneration.[1] In all of the mentioned cases, PCL is added to provide mechanical support for the different constructs, which is especially important for the case of vascular grafts where elastin alone would not be able to withstand the high-pressure environment of the blood stream.[7]

As mentioned before, the characterization of these types of polymer blends usually focus on the morphological features, mechanical properties, and biological functionality. However, few studies place an emphasis on molecular-level characterization. SSNMR spectroscopy provides a means to probe the structure and dynamics of these types of blended samples. NMR relaxation experiments are used to probe for interactions between the PCL and elastin, as well as investigate molecular motions and hydration effects on the polymers.

3.2. Materials and Methods

3.2.1 Materials

Polycaprolactone (M_n ~70,000-90,000 by GPC), glutaraldehyde solution (Grade II, 25% in H_2O), and dialysis tubing (cellulose, 25-mm average flat diameter, molecular weight cut off = 14,000) were also purchased from Sigma Aldrich (Missouri, USA). The 1,1,1,3,3,3-hexafluoro-2-propanol, HFIP, (>99.0%) was purchased from Tokyo Chemical Industry (Tokyo, Japan). PCL was used without further processing or purification.

Syringes (polypropylene, 1-mL slip-tip disposable tuberculin syringe) and needles (stainless steel, 18 G, 1.2 mm x 40 mm) from Becton, Dickinson and Company (New Jersey, USA) were used for electrospinning. Unless otherwise stated, Milli-Q ultrapure water was used for all instances where water was necessary.

3.2.2 Electrospinning of PCL and PCL-elastin blends and subsequent crosslinking

PCL solutions in HFIP were prepared by stirring the desired amount of polymer with the appropriate amount of solvent until complete dissolution. Typical solution batches were ~1-1.5 mL with concentrations of 15-20 wt% PCL in HFIP. PCL-elastin solutions were prepared through a step-wise process. First, soluble elastin (from section 2.2.3) is placed in an Eppendorff tube with the target amount of water. Then an equal mass of PCL is added along with enough HFIP to obtain the desired concentrations. The solutions were allowed to stir overnight to ensure a homogenous solution before electrospinning. A typical solution had a total solute concentration ~10 wt% with a 1:1 PCL/elastin mass ratio in 19:1 HFIP/water by volume. A syringe was filled with the *PCL-only* or *PCL-elastin* solution, fitted with a blunt steel needle, and connected to a syringe pump (NE-300 Just Infusion Syringe Pump, New Era Pump Systems, New York, USA). Solutions were pumped through the syringe at constant speed, typically ~17 µL/min. A rectangular aluminum collector plate was placed at a distance of 10-15 cm from the needle tip in a perpendicular orientation to the syringe. The needle was connected to a positive high voltage power supply, set at ~15 kV (ES30P-10W/DAM HV power supply, Gamma High Voltage Research, Florida, USA). The solution pump, power source, and collector plate were all externally grounded.

Electrospun material containing elastin was subsequently crosslinked by glutaraldehyde vapor. Samples were incubated for at least 24 h in a closed, 250-mL glass container containing about 7 mL of glutaraldehyde solution in a 10-mL beaker. Crosslinked material was then rinsed with water to hydrate and remove any remaining soluble portions. The samples were then either directly used (hydrated) or lyophilized (dry) prior to NMR analysis. *PCL-only* does not absorb water so it was only analyzed in the dry state. Electrospun samples were also collected for observation under microscope (12-560-45 Microscope, Fisher Scientific, Massachusetts, USA).

3.2.3 NMR methods and processing

NMR experiments were conducted on an Agilent DD2 NMR spectrometer (Agilent Technologies, California, USA) equipped with an 89-mm Oxford wide-bore superconducting magnet with a proton resonance frequency of 399.976 MHz. ^{13}C NMR spectra were acquired using a 4.0-mm triple resonance (HXY) T3 MAS probe (ChemMagnetics/Varian NMR, Colorado, USA). Samples were packed into 4.0 mm rotors with typical sample weights of 20-30 mg for dry and 50-60 mg for hydrated preparations. The hydration level was maintained with custom-machined Kel-F spacers (Revolution NMR, Fort Collins, Colorado, USA) fitted with fluorosilicone micro o-rings (Apple Rubber Products, New York, USA). Data for the dry and hydrated samples were acquired at 37 °C and -20 °C.

All SSNMR experiments were CPMAS-based, including 1D CPMAS and determination of the time constants ^{13}C T_1, ^{1}H T_1, ^{1}H $T_{1\rho}$ and T_{CH}. Typically for CPMAS, a 3.8 - 4.6 μs ^{1}H 90° pulse was followed by a 1-ms contact time with a 5-s recycle delay

(6-s recycle delay for NMR relaxation measurements). The ^{1}H to ^{13}C magnetization transfer was accomplished by CP with a Hartmann-Hahn matching condition of $\gamma^{H}B_{1}^{H}/2\pi = \gamma^{C}B_{1}^{C}/2\pi \sim 50$ kHz. ^{1}H TPPM decoupling[8] was applied during acquisition with $\gamma^{H}B_{1}/2\pi \sim 50$ kHz. The spinning speed used in MAS experiments was 8 kHz. Chemical shifts are referenced to the tetramethylsilane scale, using hexamethylbenzene as an external standard ($\delta(^{13}CH_3) = 17.0$ ppm) at room temperature.

^{13}C T_1 measurements were made using the method of Torchia.[20] Briefly, CP was followed by a 4.5 μs ^{13}C 90° pulse, arrayed delay times τ, a second ^{13}C 90° pulse, and finally acquisition with TPPM decoupling. Typical τ times ranged from 0.1 to 20 s. To obtain the relaxation rate constant, ^{13}C peak intensities were fit using single-exponential decay functions (Equation 4.1).

$$I(\tau) = A * e^{-\frac{-\tau}{T_1}} \qquad \text{(Eqn. 4.1)}$$

where τ is the delay time and A is the amplitude.

^{1}H T_1 values were indirectly determined from well-resolved ^{13}C signals from CPMAS following a ^{1}H inversion recovery pulse sequence. Briefly, a 9.2 μs ^{1}H 180° pulse is followed by an array of τ delays (typically 0 to 10 s), a ^{1}H 90° pulse, CP, and finally acquisition with proton decoupling. The ^{1}H T_1 constants were determined by fitting to the equation:

$$I(\tau) = M_0[1 - 2e^{-\frac{\tau}{T_1}}] \qquad \text{(Eqn. 4.2)}$$

where τ is the delay following the initial ^{1}H 180° pulse and M_0 denotes the initial peak intensity.[9]

T_{CH} and ^{1}H $T_{1\rho}$ were obtained from arrayed CP contact time experiments. The pulse sequence was identical to the one used for CPMAS experiments, with CP contact times typically arrayed from 0.05 to 20 ms. Time constants T_{CH} and ^{1}H $T_{1\rho}$ were determined by fitting to the equation:

$$\mathrm{I}(\tau) = \left(\frac{M_0}{T_{CH}}\right)\frac{e^{-\tau/T_{1\rho(H)}} - e^{-\tau/T_{CH}}}{1/T_{CH} - 1/T_{1\rho(H)}} \qquad \text{(Eqn. 4.3)}$$

where τ is the arrayed CP contact time and M_0 is the initial peak intensity.[10]

Relaxation time constants ^{13}C T_1, ^{1}H T_1, ^{1}H $T_{1\rho}$ and T_{CH} were determined using a '3D-fitting' algorithm developed in our lab.[16] Each NMR relaxation data set consists of an array of 1D spectra corresponding to different delay times, τ. One of the most common methods of analyzing experimental relaxation data has three independent steps: obtain peak intensities at a certain chemical shift from each array slice, plot the intensity as a function of time, and then fit to a model describing the decay or build-up of intensity to determine the relaxation time constant. This type of analysis does not provide an accurate determination of time constants when there are overlapping signals present. In contrast, the 3D-fitting procedure incorporates peak separation to address issues with spectral overlap.

As part of the analysis, spectra were deconvolved (to separate overlapping signals).The following parameters for each peak: chemical shift, peak amplitude, width, and the fraction of Lorentzian character, α. Initial estimates of these four parameters were obtained through deconvolution of the time point with highest intensity (ex. τ = 0.1 s for the ^{13}C T_1 experiments). Depending on the sample, the peaks were considered as

pure Lorentzian (α = 1), pure Gaussian (α = 0), or a linear combination of a Lorentzian and a Gaussian function, *F*:

$$F(\delta;\delta_i,\mathrm{w}_i,\alpha) = (\alpha)\left[\left(\frac{\delta-\delta_\mathrm{i}}{\mathrm{w}_\mathrm{i}}\right)^2+1\right]^{-1} + (1-\alpha)\left[\mathrm{e}^{\left(-\frac{-4\ln 2}{{\mathrm{w}_\mathrm{i}}^2}(\delta-\delta_\mathrm{i})^2\right)}\right] \quad \text{(Eqn. 4.4)}$$

where α = fraction Lorentzian, 1 - α = fraction Gaussian, and δ_i and w_i are the peak position and line width, respectively, of the i^{th} component. *F* yields the sum of a Lorentzian lineshape with height = α, and a Gaussian lineshape with height = 1 - α, therefore, the height at the center of the overall lineshape is 1.

For comparison, the SPORT method[11] also incorporates peak separation into its algorithm to determine NMR relaxation times. Briefly, the spectrum at each time point is independently deconvolved, the resulting intensities are plotted against time, and finally, the curve is fit to the desired model. However, the 3D-fitting algorithm utilized in this study differs from SPORT, because the peaks and time constants are fit simultaneously.

For 3D-fitting, spectral fitting and time constant optimization are simultaneously executed. The relaxation data is considered as a 3D object (S) defined by a function of the chemical shift (δ) and delay time (τ):

$$S^{fit}(\delta,\tau) = \sum_i \mathrm{a}_i * F(\delta;\delta_i,\mathrm{w}_i,\%\mathrm{G/L}) * I(\tau;T_{\mathrm{xi}}) \qquad \text{(Eqn. 4.5)}$$

where a_i is the amplitude of the i^{th} component and $I(\tau;T_{xi})$ corresponds the appropriate model of intensity decay, build-up, or build-up then decay (Equation 4.1, 4,2, or 4.3). T_{xi} is the NMR time constant(s) of the i^{th} component with x = 1, 1ρ, or CH. Then, the difference between the experimentally observed (S^{obs}) and fitted 3D (S^{fit}) surfaces is minimized,

$$\min \| S^{obs}(\delta,\tau) - S^{fit}(\delta,\tau) \| \qquad \text{(Eqn. 4.6)}$$

to obtain a_i and T_{xi} simultaneously. Time constant $T_{xi} = T_{1i}$ for the cases of Eqn. 4.1 and 4.2, and $T_{xi} = T_{CH\,i}$ and $T_{1\rho i}$ for the case of Eqn. 4.3. Chemical shifts, linewidths, and fraction Lorentzian character were held constant for this application of the 3D-fitting procedure.

Monte-Carlo simulations were used to estimate the error of fitting. First, an ideal 3D surface was prepared based on the estimated parameters from 3D-fitting (described above). Then, synthetic, random noise with the same RMS level as the experimental spectra was added to the surface. This procedure was repeated 100 times per relaxation experiment to produce simulated data with different sets of random noise. Monte-Carlo simulations of the 3D-fitting were then performed on these data, and the standard deviation (σ) for each ^{13}C T_1, ^{1}H T_1, ^{1}H $T_{1\rho}$ or T_{CH} value was calculated from the results. Measured time constants are reported with (+/-) values that indicate 2*σ, estimated by this procedure.

MATLAB (R2016b, MathWorks Inc., Massachusetts, USA) programs were utilized for the processing of NMR spectra, deconvolution, and the 3D-fitting analysis. Non-linear fitting was achieved by the Levenberg-Marquardt algorithm[12-13] using the MATLAB-function ”lsqcurvefit” in the Optimization Toolbox. MestReNova software (version 9, Mestrelab Research, Santiago de Compostela, Spain) was used for the processing of 1D spectra, and preliminary analysis.

4.4 Results and Discussion

4.4.1 *Electrospinning of PCL and CPMAS spectra*

PCL fibers were electrospun from HFIP solutions. PCL is readily soluble in HFIP but not in water and thus, aqueous solutions were not used. After determining adequate electrospinning conditions, the fiber-like morphology was confirmed under microscope (**Figure 4.2**). The fibers were non-woven, continuous, and did not show any significant curvature. Unlike PVA and elastin, the PCL sample was not soluble in water and therefore did not need to be crosslinked prior to further analysis. Furthermore, the polymer fibers do not absorb water so only the dry state was examined.

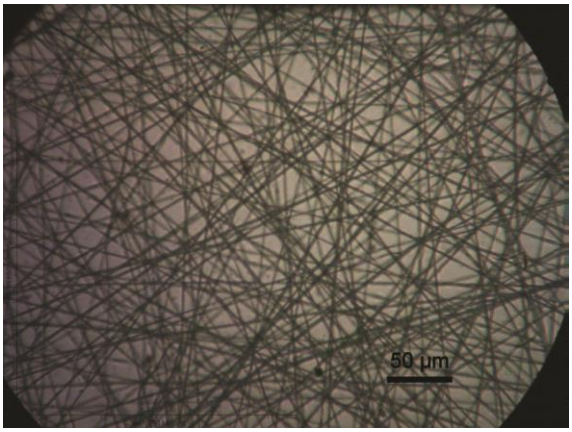

Figure 4.2. Microscope Image of Electrospun PCL Scale bar represents 50 µm.

CPMAS spectra of the electrospun PCL at -20 °C, **Figure 4.3B,** have chemical shifts and lineshapes that are comparable to what has been reported in the literature.[14] Chemical shifts and assignments of the PCL samples are summarized in **Table 4.1**. The peak at 173.8 ppm corresponds to the carbonyl. The remaining four peaks are attributed to the methylene carbons. The distribution of the CH_2 chemical shifts arise mainly from inductive effects caused by the oxygen atoms in the ester group. Therefore, the peak at 66 ppm represents the CH_2 directly bonded to the main chain oxygen and the peak at

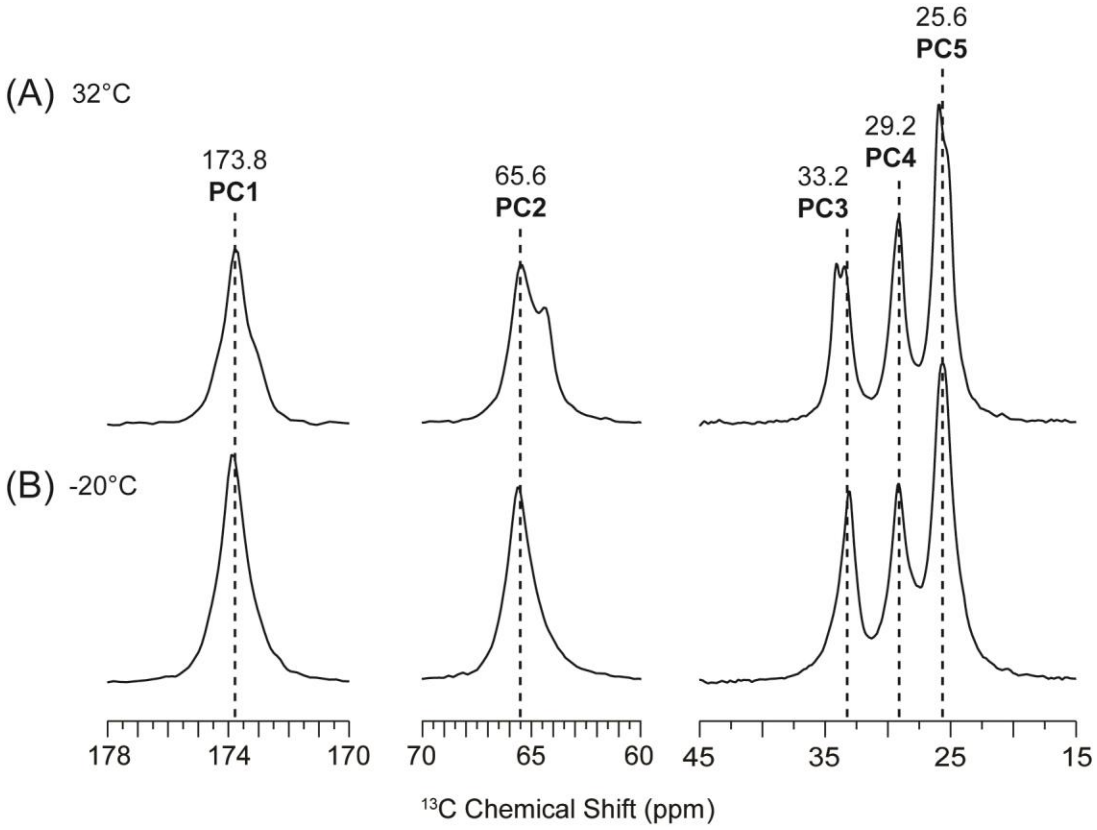

Figure 4.3. ^{13}C CPMAS NMR spectra of electrospun PCL. Electrospun PCL at (A) 37°C and (B) -20°C. (A) was acquired with 1024 scans, (B) was acquired with 512 scans. Both had a 1 ms contact time. Vertical dashed lines indicate chemical shifts of resolved peaks corresponding to the rigid regions in PCL.

Table 4.1. ^{13}C Chemical shift assignments for major features in the CPMAS NMR spectra of electrospun PCL at -20°C.[a]

	^{13}C δ(ppm)	Assignments	C#
PC1	174	O-CH_2-CH_2-CH_2-CH_2-CH_2-**[C]**O	1
PC2	66	O-**[C]**H_2-CH_2-CH_2-CH_2-CH_2-CO	6
PC3	33	O-CH_2-CH_2-CH_2-CH_2-**[C]**H_2-CO	2
PC4	29	O-CH_2-**[C]**H_2-CH_2-CH_2-CH_2-CO	5
PC5	26	O-CH_2-CH_2-**[C]**H_2-**[C]**H_2-CH_2-CO	3,4

[a.] Refer to Figure 1 for C# assignments.

33 ppm is correlated to the CH_2 adjacent to the carbonyl. The peak corresponding to carbon 5 is at 29 ppm and the remaining resonance assigned to carbons 3 and 4 is located at 26 ppm.

The CPMAS for electrospun PCL at 37 °C (Figure 4.3A) and -20 °C (Figure 4.3B) have subtle differences. PCL is a semicrystalline polymer with amorphous segments as well as regions with varying degrees of crystallinity.[14-15] CPMAS spectrum at 37 °C show features that are attributed to the crystalline and amorphous segments of PCL. Dashed lines in **Figure 4.3** indicate the chemical shifts of the rigid portion of PCL. When comparing the chemical shifts of crystalline and amorphous PCL, Tonelli and co-workers report Δδ's of around 0.5-0.9 ppm for most peaks in the PCL spectrum.[14] The upfield shoulders present on the PC1, PC2, and PC5 peaks, as well as the downfield shoulder on PC3 have chemical shifts indicative of amorphous PCL.[14] The peak at 29.2 ppm (PC4) does not have any obvious secondary features. Upon cooling the sample, the amorphous features become less pronounced and the centers of mass appear to converge to the chemical shifts corresponding to crystalline PCL.

4.4.2 *NMR relaxation measurements of electrospun PCL*

NMR relaxation time constants ^{13}C T_1, T_{CH}, ^{1}H $T_{1\rho}$ and ^{1}H T_1 were determined for the resolved peaks in the CPMAS spectra of electrospun PCL at -20 °C. As mentioned previously, PCL is insoluble and does not absorb appreciable amounts of water. Therefore, the analyzed sample is dry, electrospun PCL without further processing. All measurements were taken at -20 °C, and each peak was considered as one component for the 3D-fitting.

Table 4.2. ^{13}C and ^{1}H T_1 values (s) for electrospun PCL at -20 °C.

	^{13}C δ (ppm)	**^{13}C T_1 (s)**	+/-	**^{1}H T_1 (s)**	+/-
PC1	173.8	112.1	9.9	1.56	0.04
PC2	65.6	61.0	3.6	1.47	0.04
PC3	33.2	68.1	4.5	1.49	0.04
PC4	29.2	56.5	2.8	1.46	0.04
PC5	25.6	55.2	1.7	1.44	0.02

Table 4.3. T_{CH} (μs) and ^{1}H $T_{1\rho}$ (ms) values for electrospun PCL at -20 °C.

	^{13}C δ (ppm)	**T_{CH} (μs)**	+/-	**^{1}H $T_{1\rho}$ (ms)**	+/-
PC1	173.8	532	15	19.5	0.5
PC2	65.6	42	5	18.5	0.7
PC3	33.2	47	5	15.6	0.5
PC4	29.2	40	5	13.2	0.4
PC5	25.6	49	3	14.3	0.2

All measured time constants for electrospun PCL are summarized in **Table 4.2 and 4.3**. The ^{13}C T_1 value for PC1 was 112.1 s and the values CH_2's were in the range of 55-68 s. The T_{CH} for the carbonyl in PCL was 532 μs, while the time constants for the methylene carbons ranged from 40-49 μs. For both the ^{13}C T_1's and T_{CH}'s, the values corresponding to the CH_2's appeared to be similar to each other, but not to the carbonyl. Measured ^{1}H T_1 values ranged from 1.44 to 1.56 s and ^{1}H $T_{1\rho}$ values from 13.2 to 19.5 ms. The small variation in the ^{1}H T_1's indicates relative homogeneity in the PCL sample. However, the larger discrepancy in the ^{1}H $T_{1\rho}$'s imply that either the electrospun PCL is not completely homogenous at the scale probe-able by ^{1}H $T_{1\rho}$ experiments, or there are

other factors (difference in mobility, molecular interactions, etc.) that may be affecting the values. The time constant values reported in this subsection will be used as a point of comparison to characterize the electrospun blends of PCL and elastin.

4.4.3 *Preparation of PCL-Elastin blends and CPMAS spectra*

Electrospun blends of PCL and elastin from native tissues have not been reported in the literature, so the electrospinning conditions needed to be optimized. However, PCL-tropoelastin fibers from electrospinning have been reported in the literature, so initial parameters were taken from this source.[7] As in previous chapters, different solvents and solution conditions were considered. PCL is not soluble in water, so HFIP was selected as the majority solvent for this system, with a small amount of water to help with the electrospinning of the elastin component (see Chapter 2). Once adequate solution conditions and apparatus parameters were determined, electrospun fibers were observed under microscope to verify fiber-like morphology (Figure 4.4).

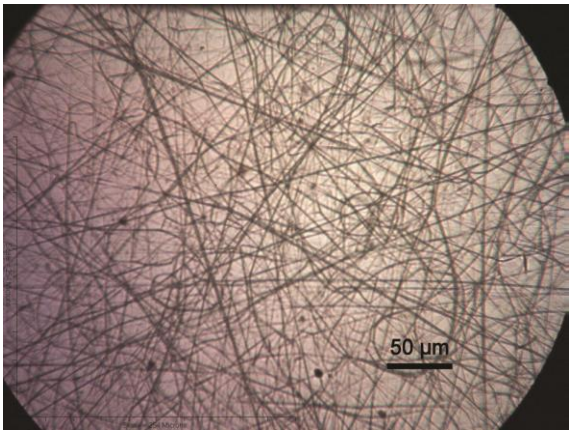

Figure 4.4. Microscope Image of Electrospun PCL-Elastin Blend Scale bar represents 50 µm.

The electrospun PCL-elastin fiber mats were then crosslinked in glutaraldehyde vapor (section 4.2.2), yielding a water-stable product. The PCL-elastin blends were crosslinked using the same procedure as *elastin-only* (Chapter 2). Both PCL and elastin appeared to be retained in the sample even after multiple rinses in water. In contrast, if the material was not crosslinked in glutaraldehyde vapors prior to rinsing, a majority of the elastin would wash out of the sample. After crosslinking by glutaraldehyde, the PCL-elastin blends were incubated in water for extended periods of time to verify their insolubility (pictures not shown). The water-stable electrospun PCL-elastin sample was then further analyzed by SSNMR spectroscopy.

The CPMAS spectrum of the electrospun, crosslinked PCL-elastin blend showed that both PCL and elastin components were retained in the sample after rinsing with water (Figure 4.5). Dashed lines originating from the component spectra (Figure 4.5A and 4.5C) trace the chemical shifts of the major resolved peaks to their respective positions in the spectrum of the blend (Figure 4.5B). The chemical shifts and assignments for the blend are summarized in **Table 4.4**. Chemical shifts of elastin and PCL were previously discussed in sections 2.3.2 and 4.4.1, respectively. There appears to be no drastic change of chemical shift or line shapes between the PCL- and elastin-only spectra and their corresponding positions in the blend spectrum.

The sum spectrum of the two individual component spectra (Figure 4.5D) was not significantly different from the spectrum of the blend (Figure 4.5B). The component spectra were scaled by height before addition to minimize the difference between the sum spectrum and the experimentally observed, target spectrum (Figure 4.5B). Subsequently, the difference spectrum (Figure 4.5E) of the sum spectrum and

PCL-Elastin blend is close to null, indicating that there are no large differences between the sum of intensity of the individual components and the blend as detected by CPMAS experiments. In the next section, NMR relaxation measurements are used to further characterize the electrospun PCL-elastin blend.

Table 4.4. ^{13}C Chemical shift assignments for major features in the ^{13}C CPMAS NMR spectra of prepared PCL-Elastin blend.

	^{13}C δ(ppm)	Assignments[8]	Polymer
PC1	174	CO (#1)	PCL
1	173	Carbonyl carbons	Elastin
2	129	Aromatic carbons	Elastin
PC2	66	CH_2 (#6)	PCL
3	60	Pro Cα & Val Cα	Elastin
4	53	Ala Cα	Elastin
5	49	Pro Cδ	Elastin
6	43	Gly Cα	Elastin
PC3	33	CH_2 (#2)	PCL
7	30	Pro Cβ & Val Cβ	Elastin
PC4	29	CH_2 (#5)	PCL
PC5	26	CH_2 (#3,4)	PCL
8	25	Pro Cγ	Elastin
9	19	Val Cγ	Elastin
10	16	Ala Cβ	Elastin

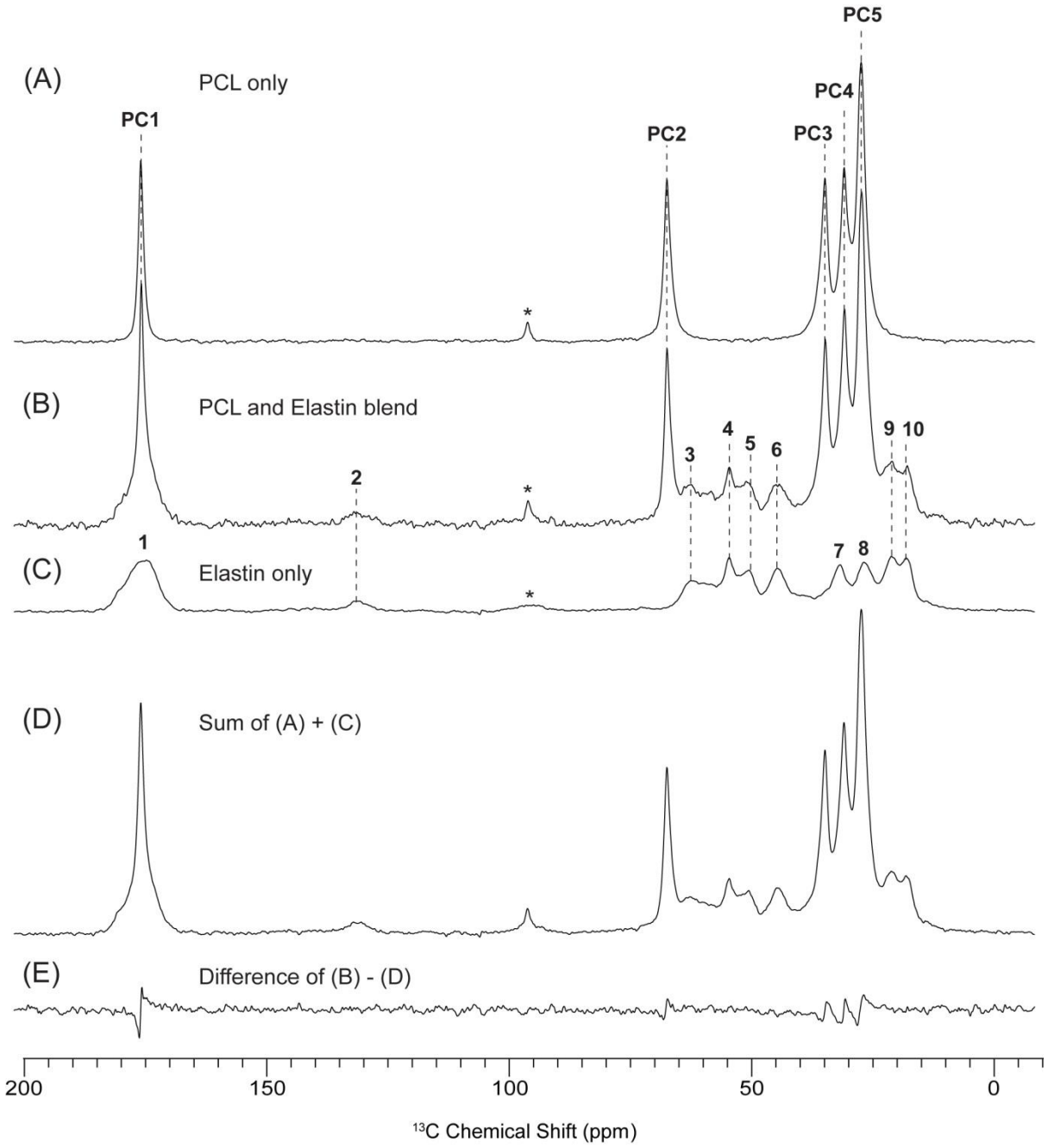

Figure 4.5. ^{13}C CPMAS NMR spectra of electrospun PCL-Elastin blend and components. (A) PCL only, (B) PCL-Elastin blend, (C) elastin only, (D) the sum spectrum [(A)+(C)], and (E) the difference spectrum [(B)-(D)]. Elastin-containing samples were crosslinked with glutaraldehyde. *PCL-only* did not need to be crosslinked. Samples were hydrated with water before lowering the temperature and subsequent acquisition. All spectra were taken at -20 °C with a 1 ms CP contact time. (A) was acquired with 512 scans, (B) and (C) were acquired with 1024 scans. Vertical dashed lines indicate chemical shifts of resolved peaks. Spinning side bands are indicated by asterisks (*).

4.4.4 Relaxation measurements of the PCL-Elastin blend

NMR relaxation time constants were measured to probe the effects of water on the blended sample and the compatibility of the two polymers. Specifically, ^{13}C T_1, T_{CH}, ^{1}H $T_{1\rho}$ and ^{1}H T_1 were determined for the resolved peaks in the CPMAS spectra of both dry and hydrated electrospun, PCL-elastin blends at -20 °C. The aromatic carbons in elastin at 129 ppm and are omitted from this analysis due to the low signal-to-noise in the hydrated spectra. In addition, carbons 7 and 8 in elastin are excluded from discussion due to severe overlap with PC4 and PC5, respectively. In this section, comparisons between the blend and PCL- and elastin-only are made for both dry and hydrated samples, where applicable.

^{13}C spin-lattice relaxation times, T_1, were obtained by the method of Torchia[20] (Table 4.5 and Figure 4.5). There was a general trend to shorter ^{13}C T_1 values in the hydrated sample for all peaks in the PCL-elastin blend. The values corresponding to PC1 were 141.9 and 90.5 s for the dry and hydrated states, respectively. The PCL CH_2's had time constants ranging from around 80 to 100 s in the dry sample, and 40 to 46 s in the hydrated sample. ^{13}C T_1 of the carbonyl in elastin was 42.7 s for the dry and 20.3 s for the hydrated state. The Cα's and Pro Cδ in elastin had time constants ranging from 12.4 to 21.2 s when dry and 5.1 to 10.6 s in the presence of water. There was a slight decrease in T_1 for the two methyl peaks at 19 and 16 ppm from 0.6 s to 0.2-0.3 s in the dry and hydrated samples, respectively. This trend to shorter ^{13}C T_1 values in the presence of water was also observed for the *elastin-only* sample.

There was an overall trend to longer ^{13}C T_1's in the blend for most of the peaks in the dry samples. The values for PCL all increased by around 20 to 50 s when in the

Table 4.5. ^{13}C T_1 values (s) for resolved ^{13}C peaks in electrospun, crosslinked, Elastin only, PCL-elastin blend, and PCL only at -20 °C.

		'Hydrated, frozen'						'Dry'					
		Elastin only		PCL-Elastin blend		PCL only		Elastin only		PCL-Elastin blend		PCL only	
	^{13}C δ (ppm)	^{13}C T_1 (s)	+/-	^{13}C T_1 (s)	+/-	^{13}C T_1 (s)	+/-	^{13}C T_1 (s)	+/-	^{13}C T_1 (s)	+/-	^{13}C T_1 (s)	+/-
PC1	174			90.5	23.9	112.1	9.9			141.9	9.6	112.1	9.9
1	173	18.2	0.8	20.3	3.3			33.6	0.9	42.7	2.4		
PC2	66			39.8	5.5	61.0	3.6			87.2	4.9	61.0	3.6
3	60	9.9	1.3	7.5	3.5			25.5	3.4	18.9	4.2		
4	53	12.5	1.1	10.6	3.5			15.3	1.2	21.2	3.1		
5	49	5.2	0.7	6.6	2.5			9.9	1.0	12.4	1.9		
6	43	6.7	0.6	5.1	1.6			20.6	1.3	21.6	3.3		
PC3	33			40.8	7.0	68.1	4.5			86.5	5.6	68.1	4.5
PC4	29			45.1	9.4	56.5	2.8			81.6	4.9	56.5	2.8
PC5	26			45.9	5.2	55.2	1.7			101.5	5.5	55.2	1.7
9	19	0.3	0.02	0.3	0.1			0.3	0.03	0.6	0.1		
10	16	0.4	0.1	0.2	0.1			0.4	0.1	0.6	0.2		

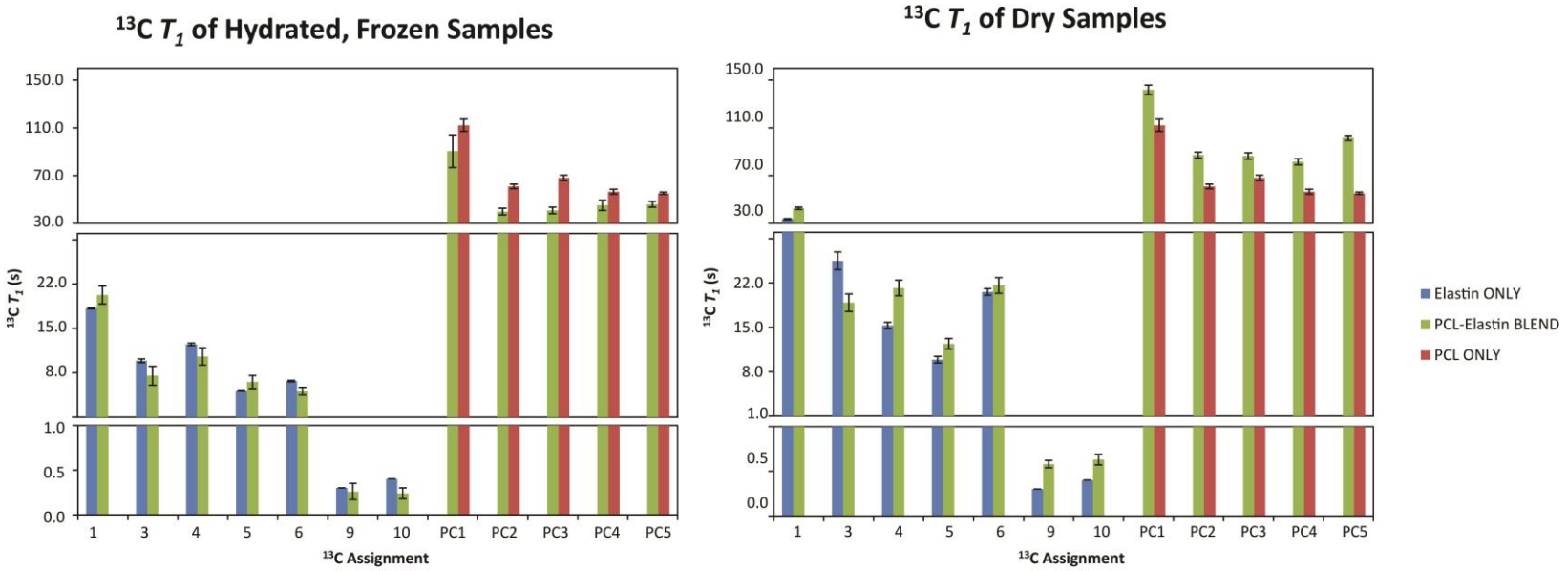

Figure 4.6. ^{13}C T_1 values (s) for select peaks in electrospun, crosslinked, Elastin only (blue), PCL-elastin blend (green), and PCL only (red) at -20 °C. Error bars correspond to the error determined by the fitting procedure.

blend. This increase was more subtle for the elastin peaks with values around 1 to 9 s longer in the blend. The one exception to this trend was the peak at 60 ppm (elastin Pro Cα&Val Cα) which showed a decrease from 25.5 to 18.9 s when in the blend.

In the hydrated samples, ^{13}C T_1 values corresponding to PCL all decrease when in the blend, but there was no overall trend for the elastin values. ^{13}C T_1's of PCL ranged from 55 - 112 s for *PCL-only* and decreased to 41 - 91 s in the blend. No general trend was observed for elastin in the PCL blend. Time constants for the carbonyl and Pro Cδ increased when in the blend. ^{13}C T_1 for Pro Cα &Val Cα, Ala Cα, and Gly Cα showed a slight decrease when present in the PCL blend. Finally, the side-chain and methyl carbons did not show any significant change in the blend sample compared to *elastin-only*.

T_{CH} values correspond to the intensity build-up on the CP contact-time plot array and are used to comment on the relative rigidities of the samples (Table 4.6 and Figure 4.7). In general, *c*arbons with short T_{CH} values reside in domains with reduced motion compared to those with higher T_{CH}. There was and overall trend to longer T_{CH} values for most peaks of the PCL-elastin blend sample in the dry to hydrated state. The PCL values in the blend, except for the carbonyl, all increased upon hydration. The values corresponding to the CH_2's ranged from 35 to 66 μs for the dry sample and 52 to 99 μs in the hydrated sample. The time constant corresponding to PC1 was 659 μs when dry and 639 μs in the presence of water. For the elastin values, some T_{CH}'s increased, some decreased, and some remained relatively the same. The values corresponding to carbonyl carbons were 464 and 494 μs for the dry and hydrated states, respectively.

Table 4.6. T_{CH} values (μs) for resolved ^{13}C peaks in electrospun, crosslinked, Elastin only, PCL-elastin blend, and PCL only at -20 °C.

		'Hydrated, frozen'						'Dry'					
		Elastin only		PCL-Elastin blend		PCL only		Elastin only		PCL-Elastin blend		PCL only	
	^{13}C δ (ppm)	T_{CH} (μs)	+/-	T_{CH} (μs)	+/-	T_{CH} (μs)	+/-	T_{CH} (μs)	+/-	T_{CH} (μs)	+/-	T_{CH} (μs)	+/-
PC1	174			639	41	532	15			659	17	532	15
1	173	499	22	494	42			390	12	464	19		
PC2	66			52	8	42	5			35	2	42	5
3	60	46	13	84	31			13	7	60	14		
4	53	83	8	91	27			42	5	79	12		
5	49	75	12	51	29			45	6	30	8		
6	43	34	12	72	26			18	4	24	6		
PC3	33			58	12	47	5			43	3	47	5
PC4	29			99	18	40	5			59	5	40	5
PC5	26			60	6	49	3			66	3	49	3
9	19	203	11	186	27			184	9	201	13		
10	16	175	14	135	30			152	11	156	22		

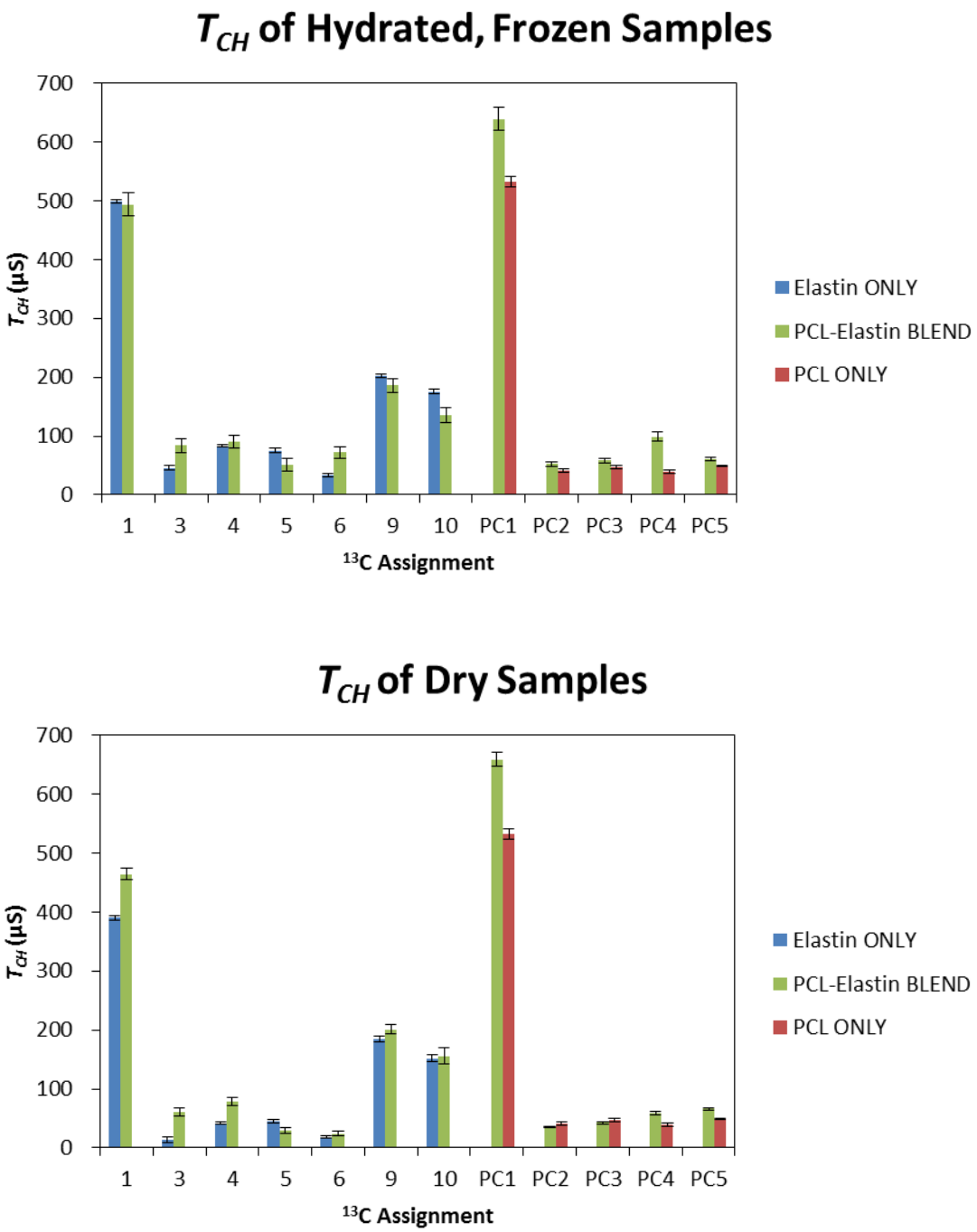

Figure 4.7. T_{CH} values (µs) for select peaks in electrospun, crosslinked, Elastin only (blue), PCL-elastin blend (green), and PCL only (red) at -20 °C. Error bars correspond to the error determined by the fitting procedure.

Longer values were observed for the Cα peaks (60, 53, and 43 ppm) and the Pro Cδ (49 ppm) in the presence of water. Time constants for these peaks ranged from 24 to 79 μs in the dry and 51 to 91 μs in the hydrated state. T_{CH}'s for the peaks at 19 and 16 ppm decreased from 201 to 186 μs and 156 to 135 μs, respectively, upon the introduction of water into the system.

There were no overall trends upon comparing the T_{CH} values for PCL- and elastin-only to the blend. In the dry samples, PCL did not show any overall trends and most elastin peaks had an increase when in the blend. The carbonyl of PCL and PC4 and PC5 had longer values while PC2 showed a decrease when in the blend. The value corresponding to PC3 did not appear to change. Most of the peaks from elastin show longer time constants in the blend. The two exceptions were Pro Cδ (49 ppm) that decreased in the blend and Ala Cβ (16 ppm) that appeared unchanged. In the hydrated samples, PCL values all trended to longer values in the blend and elastin appeared to be non-uniformly affected. There appears to be no difference for the carbonyl peak from elastin. All of the Cα values showed an increase when in the blend. The remaining peaks, Pro Cδ (49 ppm) and the two methyl peaks (19 and 16 ppm) showed decreased values in the blend with PCL.

^{1}H $T_{1\rho}$ values correspond to the decay portion of the contact-time-arrayed plot (Table 4.7 and Figure 4.8). ^{1}H $T_{1\rho}$'s corresponding to PCL in the blend all were in the range of 19 to 24 ms for the dry state and 18 to 22 ms for the hydrated state. Values corresponding to elastin in the blend were 4 to 7 ms and 5 to 8 ms when dry and hydrated, respectively. The two components appeared to be relatively independent from each other as indicated by the discrepancy in ^{1}H $T_{1\rho}$ values. Upon the introduction of

water to the blend, elastin values slightly increase and PCL values slightly decrease. These differences could perhaps imply that water helps to facilitate polymer interactions.

^{1}H $T_{1\rho}$'s time constants are used to assess the miscibility (compatibility) of the PCL and elastin components in the blended sample. In the dry state, PCL shows a trend to longer values when in the blend while elastin trends to shorter values. In the presence of water, PCL has the same trend to longer time constants while the values for elastin do not appear to be significantly affected. The value sets imply that there is some interaction between the elastin and PCL that cause the changes in ^{1}H $T_{1\rho}$. However, in both cases, the values do not fall intermediate to the two individual components, which would be expected for intimately mixed polymers. In this study each PCL peak is fit with only one peak and therefore, the representative lineshape may contain multiple components (rigid, mobile, intermediate) that were not accounted for in the 3D-fitting procedure. Perhaps the elastin is interacting with the amorphous portions of PCL while the crystalline regions remain unchanged. This may account for the only slight changes in ^{1}H $T_{1\rho}$ when comparing the PCL- and elastin-only to the blended sample because we are observing an averaging of all PCL regions rather than just the sections that interact with elastin.

^{1}H inversion recovery with indirect detection through resolved ^{13}C peaks was used to determine ^{1}H T_{1} values (Table 4.8 and Figure 4.9). ^{1}H T_{1} values for the blend showed PCL and elastin as two distinct populations when dry and hydrated samples. In the dry blend, ^{1}H T_{1} values corresponding to elastin are in the range of 0.8-1.3 s while PCL values are around 1.8-2.5 s. In the hydrated PCL-elastin blend, elastin values were around 0.4-0.5 s and PCL time constants were around 0.7-0.9 s. There was an overall trend to shorter times in the hydrated, frozen sample. The discrepancy between the

Table 4.7. ^{1}H $T_{1\rho}$ values (ms) for resolved ^{13}C peaks in electrospun, crosslinked, Elastin only, PCL-elastin blend, and PCL only at -20 °C.

		'Hydrated, frozen'						'Dry'					
		Elastin only		PCL-Elastin blend		PCL only		Elastin only		PCL-Elastin blend		PCL only	
	^{13}C δ (ppm)	^{1}H $T_{1\rho}$ (ms)	+/-	^{1}H $T_{1\rho}$ (ms)	+/-	^{1}H $T_{1\rho}$ (ms)	+/-	^{1}H $T_{1\rho}$ (ms)	+/-	^{1}H $T_{1\rho}$ (ms)	+/-	^{1}H $T_{1\rho}$ (ms)	+/-
PC1	174			24.1	1.5	19.5	0.5			23.5	0.7	19.5	0.5
1	173	6.7	0.3	5.6	0.4			6.7	0.2	5.1	0.2		
PC2	66			21.9	1.7	18.5	0.7			21.7	0.7	18.5	0.7
3	60	6.3	0.5	5.1	1.1			7.1	0.6	4.1	0.4		
4	53	7.2	0.3	7.2	1.2			8.2	0.5	5.8	0.5		
5	49	6.4	0.7	6.1	1.1			6.6	0.5	5.4	0.6		
6	43	5.7	0.4	4.8	0.7			6.3	0.2	5.1	0.4		
PC3	33			18.0	1.4	15.6	0.5			20.9	0.8	15.6	0.5
PC4	29			20.0	1.7	13.2	0.4			18.9	0.9	13.2	0.4
PC5	26			18.6	0.9	14.3	0.2			20.0	0.5	14.3	0.2
9	19	6.8	0.3	7.5	0.8			6.9	0.3	5.4	0.3		
10	16	7.4	0.4	8.2	1.2			7.5	0.4	7.1	0.8		

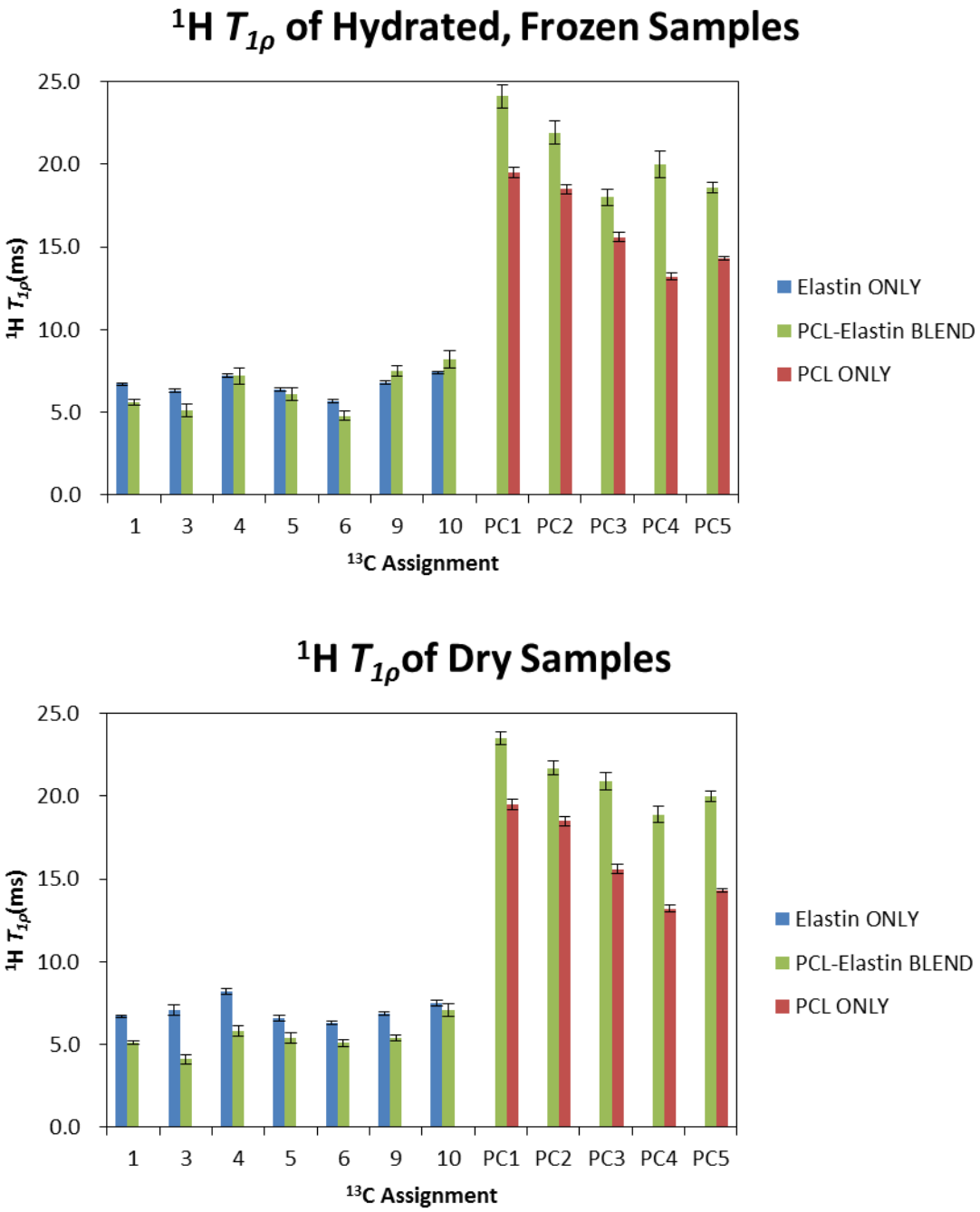

Figure 4.8. ^{1}H $T_{1\rho}$ values (ms) for select peaks in electrospun, crosslinked, Elastin only (blue), PCL-elastin blend (green), and PCL only (red) at -20 °C. Error bars correspond to the standard error from the fitting procedure.

Table 4.8. ^{1}H T_1 values (s) for resolved ^{13}C peaks in electrospun, crosslinked, Elastin only, PCL-elastin blend, and PCL only at -20 °C.

		'Hydrated, frozen'						'Dry'					
		Elastin only		PCL-Elastin blend		PCL only		Elastin only		PCL-Elastin blend		PCL only	
	^{13}C δ (ppm)	^{1}H T_1 (s)	+/-	^{1}H T_1 (s)	+/-	^{1}H T_1 (s)	+/-	^{1}H T_1 (s)	+/-	^{1}H T_1 (s)	+/-	^{1}H T_1 (s)	+/-
PC1	174			0.87	0.05	1.56	0.04			2.02	0.05	1.56	0.04
1	173	0.40	0.01	0.41	0.09			0.63	0.01	0.92	0.03		
PC2	66			0.85	0.04	1.47	0.04			2.03	0.05	1.47	0.04
3	60	0.41	0.06	0.41	0.08			0.62	0.05	1.29	0.15		
4	53	0.38	0.03	0.51	0.10			0.67	0.04	0.98	0.11		
5	49	0.42	0.03	0.40	0.08			0.65	0.05	0.77	0.08		
6	43	0.41	0.03	0.49	0.07			0.65	0.03	0.92	0.06		
PC3	33			0.74	0.04	1.49	0.04			1.76	0.06	1.49	0.04
PC4	29			0.81	0.08	1.46	0.04			1.76	0.05	1.46	0.04
PC5	26			0.76	0.03	1.44	0.02			1.79	0.05	1.44	0.02
9	19	0.38	0.02	0.41	0.05			0.62	0.02	0.76	0.05		
10	16	0.38	0.02	0.47	0.07			0.62	0.03	0.89	0.09		

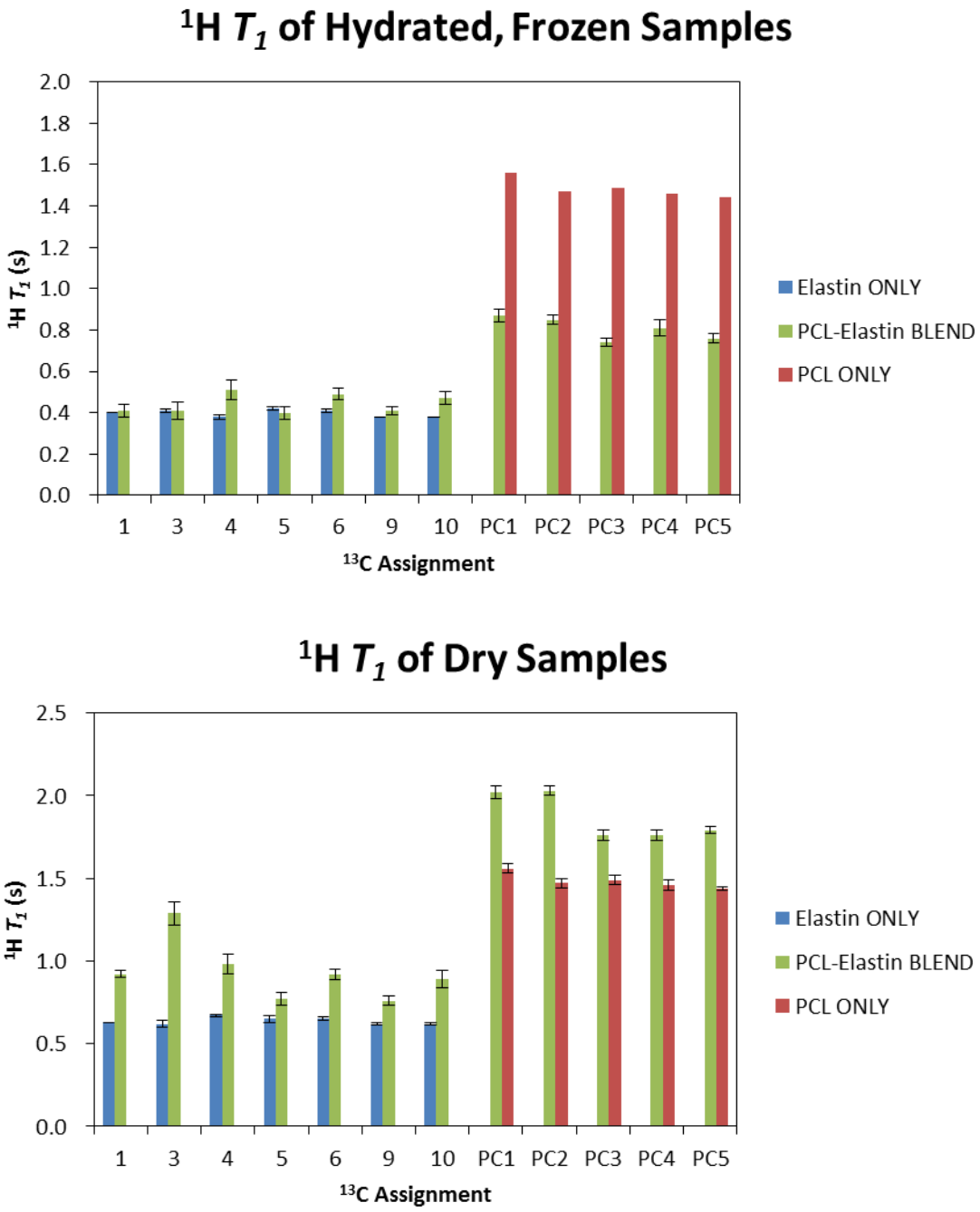

Figure 4.9. ^{1}H T_1 values (s) for select peaks in electrospun, crosslinked, Elastin only (blue), PCL-elastin blend (green), and PCL only (red) at -20 °C. Error bars correspond to the error determined by the fitting procedure.

elastin and PCL populations appears to be reduced in the hydrated sample. These observations imply that although PCL and elastin are not homogenously mixed throughout the whole sample, but it appears that the presence of water helps to improve homogeneity or facilitates further averaging of the ^{1}H T_1 values through polymer-water interactions or another process.

Similar to the ^{1}H $T_{1\rho}$, ^{1}H T_1 values are used to assess the compatibility of PCL and elastin in the blend. In the dry state, ^{1}H T_1's for the blend do not all lie intermediate to the component values. Both the values for PCL and elastin show an increase when in the blend (1.4-1.6 s to 1.8-2.5 s for PCL and 0.6-0.7 s to 0.8-1.3 s for elastin). The increase in ^{1}H T_1 for elastin could be explained by averaging with the PCL values, but, the longer time constants for PCL in the blend is not expected if the two polymers are intimately mixed. However, once water is introduced to the blended sample, ^{1}H T_1's corresponding to PCL peaks all decrease from 1.4-1.6 s in PCL only, to ~0.7-0.9 s in the blend. Time constants related to elastin peaks all increased slightly from ~0.4 s to ~0.4-0.5 s for *elastin-only* and elastin in the blend, respectively. This 'averaging out' of ^{1}H T_1's in the blend imply intimate interactions between the PCL and elastin components and also, that the interactions are either facilitated or aided by the presence of water

4.5 Conclusion

PCL is an attractive candidate for use as a biomaterial due to its abundance, mechanical properties, and biocompatibility. Electrospinning can produce fibers from solutions of a single polymer as well as solutions with more than one component. In this

chapter, electrospun *PCL-only* and *PCL-elastin blend* samples were studied using SSNMR spectroscopy.

PCL was electrospun from HFIP solutions and fibers did not require any further processing to be water-stabilized. CPMAS spectra and NMR relaxation measurements were reported and discussed for *PCL-only*. Subsequently, *PCL-elastin blends* were prepared by electrospinning from HFIP/aqueous solutions. Electrospun samples were crosslinked in glutaraldehyde vapors, yielding a water-insoluble product that retained both PCL and elastin components. No drastic changes were observed on the CPMAS spectra of the blend compared to its components in terms of chemical shift and lineshape. NMR relaxation time constants were determined to investigate the effects of hydration on the blend in addition to probing for molecular motions and interactions of the component polymers.

Results from the NMR relaxation measurements showed evidence of molecular-level interactions between PCL and elastin in the blend. There were no overall trends for the ^{13}C T_1 and T_{CH} data sets, but the ^{1}H time constants showed changes indicative of component interactions. In the following chapter, the PCL-elastin blend and PVA-elastin blends will be compared and contrasted.

4.6 References

1. Labet, M.; Thielemans, W., Synthesis of polycaprolactone: a review. *Chem. Soc. Rev.* **2009,** *38* (12), 3484-3504.

2. Yeo, G. C.; Aghaei-Ghareh-Bolagh, B.; Brackenreg, E. P.; Hiob, M. A.; Lee, P.; Weiss, A. S., Fabricated Elastin. *Advanced Healthcare Materials* **2015**, n/a-n/a.

3. Spěváček, J.; Brus, J.; Divers, T.; Grohens, Y., Solid-state NMR study of biodegradable starch/polycaprolactone blends. *European Polymer Journal* **2007,** *43* (5), 1866-1875.
4. Sinha, V. R.; Bansal, K.; Kaushik, R.; Kumria, R.; Trehan, A., Poly-ϵ-caprolactone microspheres and nanospheres: an overview. *International Journal of Pharmaceutics* **2004,** *278* (1), 1-23.
5. Wang, L.; Ma, W.; Gross, R. A.; McCarthy, S. P., Reactive compatibilization of biodegradable blends of poly(lactic acid) and poly(ε-caprolactone). *Polym. Degrad. Stab.* **1998,** *59* (1-3), 161-168.
6. Coombes, A. G. A.; Verderio, E.; Shaw, B.; Li, X.; Griffin, M.; Downes, S., Biocomposites of non-crosslinked natural and synthetic polymers. *Biomaterials* **2002,** *23* (10), 2113-2118.
7. Wise, S. G.; Byrom, M. J.; Waterhouse, A.; Bannon, P. G.; Ng, M. K. C.; Weiss, A. S., A multilayered synthetic human elastin/polycaprolactone hybrid vascular graft with tailored mechanical properties. *Acta Biomaterialia* **2011,** *7* (1), 295-303.
8. Bennett, A. E.; Rienstra, C. M.; Auger, M.; Lakshmi, K. V.; Griffin, R. G., Heteronuclear decoupling in rotating solids. *J. Chem. Phys.* **1995,** *103* (16), 6951-8.
9. Keeler, J., *Understanding NMR Spectroscopy*. 2nd ed.; John Wilery & Sons Ltd.: West Sussex, United Kingdom.
10. Saito, H. A., Isao; Naito, Akiro, *Solid State NMR Spectroscopy for Biopolymers*. Springer: Dordrecht, The Netherlands, 2006.
11. Geppi, M.; Forte, C., The SPORT-NMR software: A tool for determining relaxation times in unresolved NMR spectra. *J. Magn. Reson.* **1999,** *137* (1), 177-185.
12. Levenberg, K., A Method for the Solution of Certain Non-Linear Problems in Least Squares. *Quarterly of Applied Mathematics* **1944,** *2* (2), 164-168.
13. Marquardt, D. W., An Algorithm for Least-Squares Estimation of Nonlinear Parameters. *Journal of the Society for Industrial and Applied Mathematics* **1963,** *11* (2), 431-441.
14. Vasanthan, N.; Shin, I. D.; Tonelli, A. E., Conformational and Motional Characterization of Isolated Poly(.epsilon.-caprolactone) Chains in Their Inclusion Compound Formed with Urea. *Macromolecules* **1994,** *27* (22), 6515-6519.
15. Monteiro, M. S. S. B.; Chávez, F. V.; Sebastião, P. J.; Tavares, M. I. B., 1H NMR relaxometry and X-ray study of PCL/nevirapine hybrids. *Polymer Testing* **2013,** *32* (3), 553-566.
16. Ohgo, K; Kumashiro, K. K., **2017,** *to be submitted*.

Chapter 5. Summary and Conclusion

This study focused on the characterization of elastin-containing, electrospun materials using SSNMR spectroscopy. Conventional methods to analyze electrospun biomaterials focus mainly on the morphological features, mechanical properties, bio-viability, etc., without much emphasis on characterization at the molecular level. SSNMR spectroscopy provides a means to probe the structure and dynamics of samples in the solid state, and in this case, also the frozen state of the hydrated electrospun materials.

SSNMR spectroscopy is commonly used for the analyses of polymer blends to assess the miscibility of the components using a variety of experiments, including the measurement of different NMR time constants. These NMR relaxation experiments should provide information on the interactions between the components, as well as on the molecular motions of the sample. This NMR relaxation-based approach was used in this study to analyze the prepared electrospun samples. The time constants used in this discussion include ^{13}C T_1, ^{1}H T_1, ^{1}H $T_{1\rho}$, and T_{CH}. This is the first time SSNMR spectroscopy has been used to study elastin-containing electrospun materials (*elastin-only*, *PVA-elastin blend*, and *PCL-elastin blend*) in both dry and hydrated states. The aim of this investigation was to show that SSNMR spectroscopy is a useful tool in the characterization of biomaterials that should complement information obtained from methods that focus more on macro-scale properties.

5.1 Summary of results for *elastin-only*

Elastin was purified from bovine nuchal ligament using an autoclave-based procedure before subsequent partial hydrolysis using oxalic acid. Prepared samples were assayed by amino acid analysis and were found to have composition profiles similar to what is expected for elastin. Soluble elastin was then electrospun and crosslinked using glutaraldehyde vapors.

1D CPMAS NMR spectra of the samples at differing processing points (insoluble, soluble, electrospun and crosslinked) were similar to what has been previously reported for elastin with subtle differences.[1-2] The effects of hydration on the electrospun, crosslinked elastin samples were also investigated using CPMAS and NMR relaxation measurements. Water appeared to influence the dynamics of the protein sample, possibly through water-protein interactions or mobility change. Based on the NMR measurements, the electrospun elastin samples was similar to native elastin implying that the protein was not significantly degraded or denatured after processing (partial hydrolysis, electrospinning, crosslinking), i.e., even after solubilization, the resulting fragments were still large enough to be reflective of elastin. These results for *elastin-only* were used as a comparison point for the analysis of the polymer-elastin blends.

5.2 Summary of results for PVA and elastin blends

PVA is an attractive candidate for use as a biomaterial due to its abundance, mechanical properties, and biocompatibility. Electrospun *PVA-only* and *PVA-elastin blend* samples were studied using SSNMR spectroscopy. In addition to the electrospun

PVA-elastin, this was the first study to report NMR data on hydrated, water-vapor treated, electrospun PVA.

PVA was electrospun from aqueous solution and fibers were water-stabilized by treatment with water vapor. CPMAS spectra of the dry and hydrated PVA had similar features to what has been reported in the literature.[3-5] Based on the NMR relaxation measurements of the dry and hydrated PVA, water appeared to affect the dynamics of the PVA sample, possibly through water-polymer interactions such as dipole-dipole or hydrogen bonding.

PVA-elastin blends were prepared by electrospinning from aqueous solutions. Electrospun samples were crosslinked in glutaraldehyde vapors, yielding a water-insoluble product that retained both PVA and elastin components. No drastic differences were observed on the CPMAS spectra of the blend compared to its components in terms of chemical shift and lineshape, implying that there were no significant changes to the local structure of elastin or PVA. Results from the NMR relaxation measurements showed evidence of molecular-level interactions, most likely due to proton spin diffusion, between PVA and elastin in the blend. There were no overall trends for the ^{13}C T_1 and T_{CH} data sets, but the ^{1}H time constants showed changes indicative of intimate mixing of the two polymers.

5.3 Summary of results for PCL and elastin blends

PCL is also an attractive candidate for use as a biomaterial due to its abundance, mechanical properties, and biocompatibility. This chapter focused on electrospun

PCL-only and *PCL-elastin blend* samples. Electrospun constructs containing PCL and elastin have been fabricated and investigated for their application to vascular tissue engineering.[6-8]

PCL was electrospun from HFIP solutions and fibers did not require any further processing to be water-stabilized (PCL is insoluble in water). CPMAS spectra and NMR relaxation measurements were reported and discussed for *PCL-only*. Subsequently, *PCL-elastin blends* were prepared by electrospinning from HFIP/aqueous solutions. Electrospun samples were crosslinked in glutaraldehyde vapors, yielding a water-insoluble product that retained both PCL and elastin components. No drastic differences were observed on the CPMAS spectra of the blend compared to its components in terms of chemical shift and lineshape, implying that there were no significant changes to the local structure of elastin or PCL. NMR relaxation time constants were determined to investigate the effects of hydration on the blend in addition to probing for molecular motions and interactions of the component polymers.

Results from the NMR relaxation measurements showed evidence of molecular-level interactions between PCL and elastin in the blend. There were no overall trends for the ^{13}C T_1 and T_{CH} data sets. However, the ^{1}H time constants showed changes indicative of the protons of each component interacting through spin diffusion processes. Based on the trends observed for the proton relaxation times, it appears that the elastin is intimately mixed with PCL, but most likely with the amorphous regions rather than the crystalline regions.

5.4 Concluding Remarks

This study highlights the application of SSNMR spectroscopy to the characterization of electrospun polymer blends in both dry and hydrated states. The absence of any overall trends with respect to the ^{13}C T_1 and T_{CH} values, do not necessarily imply that there is no change upon blending or hydration, but rather, that the effects are most likely localized to certain domains or residue types in elastin or the synthetic polymers. Due to the use of natural abundance samples in this study and the resulting spectral overlap, it is difficult to identify, with confidence, any site-specific interactions between the polymers. Perhaps by using isotopically labeled samples, one could investigate what is happening at specific residues in elastin, or specific carbons or functional groups in the synthetic polymers.

In contrast, results from the NMR proton relaxation measurements show evidence of intimate interactions between elastin and each synthetic polymer is observed almost uniformly across the entire each sample. The ^{1}H relaxation time constants $T_{1\rho}$ and T_1 are dominated by proton-proton spin diffusion, and therefore, the effective range observable by these experiments are much larger that the ^{13}C T_1 and T_{CH} values. Therefore, the relative uniformity of the proton time constants across samples imply that the polymer components are intimately mixing (PVA-elastin or PCL-elastin) and are at least partially miscible with each other in the blends. The miscibility of the components is an important consideration when designing materials based on polymer blends and these proton relaxation experiments give us a means to probe for the polymer compatibility.

In addition to the polymer-polymer interactions, from comparisons of the hydrated and dry samples, it appears that water affects the dynamics of the electrospun samples. The change might be due to hydrogen bonding or other interactions between water and the sample, or possibly an implicit mobility change of the polymers.

This study takes into account not only the polymer-polymer interactions in the blends, but also attempts to address the effects of hydration on the samples. Depending on the specific SSNMR experiment, one is able to probe different time scales of motion, molecular-level interactions, homogeneity of samples, etc. The combination of these measurements provides different perspectives for understanding the structure and dynamics in the blends. The results from this study provide the framework for more detailed characterization of elastin-containing biomaterials and electrospun samples.

5.5 References

1. Perry, A.; Stypa, M. P.; Tenn, B. K.; Kumashiro, K. K., Solid-state C-13 NMR reveals effects of temperature and hydration on elastin. *Biophysical Journal* **2002,** *82* (2), 1086-1095.
2. Kumashiro, K. K.; Kim, M. S.; Kaczmarek, S. E.; Sandberg, L. B.; Boyd, C. D., C-13 cross-polarization/magic angle spinning NMR studies of alpha-elastin preparations show retention of overall structure and reduction of mobility with a decreased number of cross-links. *Biopolymers* **2001,** *59* (4), 266-275.
3. Masuda, K.; Kaji, H.; Horii, F., Solid-state 13C NMR and 1H CRAMPS investigations of the hydration process and hydrogen bonding for poly(vinyl alcohol) films. *Polym. J. (Tokyo, Jpn.)* **2001,** *33* (4), 356-363.
4. Masuda, K.; Horii, F., CP/MAS 13C NMR Analyses of the Chain Conformation and Hydrogen Bonding for Frozen Poly(vinyl alcohol) Solutions. *Macromolecules* **1998,** *31* (17), 5810-5817.
5. Horii, F.; Masuda, K.; Kaji, H., CP/MAS 13C NMR Spectra of Frozen Solutions of Poly(vinyl alcohol) with Different Tacticities. *Macromolecules* **1997,** *30* (8), 2519-2520.
6. Yeo, G. C.; Aghaei-Ghareh-Bolagh, B.; Brackenreg, E. P.; Hiob, M. A.; Lee, P.; Weiss, A. S., Fabricated Elastin. *Advanced Healthcare Materials* **2015,** *4* (16), 2530-2556.
7. Annabi, N.; Fathi, A.; Mithieux, S. M.; Martens, P.; Weiss, A. S.; Dehghani, F., The effect of elastin on chondrocyte adhesion and proliferation on poly (ε-caprolactone)/elastin composites. *Biomaterials* **2011,** *32* (6), 1517-1525.
8. Rnjak-Kovacina, J.; Wise, S. G.; Li, Z.; Maitz, P. K. M.; Young, C. J.; Wang, Y.; Weiss, A. S., Tailoring the porosity and pore size of electrospun synthetic human elastin scaffolds for dermal tissue engineering. *Biomaterials* **2011,** *32* (28), 6729-6736.